Nuclear Reactor Reload Pattern Optimization by Application of Heuristic Search and Perturbation Theoretical Methods

Nuclear Reactor Reload Pattern Optimization by Application of Heuristic Search and Perturbation Theoretical Methods

PROEFSCHRIFT

ter verkrijging van de graad van doctor
aan de Technische Universiteit Delft,
op gezag van de Rector Magnificus prof.ir. K.F. Wakker,
in het openbaar te verdedigen ten overstaan van een commissie,
door het College voor Promoties aangewezen,
op maandag 28 juni 1999 te 13:30 uur
door

René VAN GEEMERT

natuurkundig ingenieur
geboren te Zwijndrecht

Printed in the Netherlands

To my parents,
for their encouragements

Contents

Chapter 1

Introduction

1.1 Introduction to reload pattern design

More than five decades ago, in 1942, the first nuclear reactor built by Enrico Fermi achieved a critical fission chain reaction beneath the old Stagg Field football stadium at the University of Chicago. Since that time, nuclear reactors have evolved from research tools into large electricity generating units which are generally capable of producing over 1000 MWe of electrical power and satisfy a significant part (approximately 17%) of the global demand for electrical energy. Basically, a nuclear reactor is a device in which controlled nuclear fission chain reactions can be maintained. In such a device, neutrons are used to induce nuclear fission reactions in heavy nuclei. A significant fraction of these nuclei fission into lighter nuclei (fission products), accompanied by the release of energy (about 200 MeV per event) plus several additional neutrons, thereby inducing a chain of fission events.

An essential difference between nuclear power plants and power plants operating on fossil fuel is that, in a nuclear power plant, the nuclear fuel cannot be fully 'burnt' since at least a critical mass of fissile material is required for sustaining the neutron chain reaction. During the burnup process, the material composition of the nuclear fuel changes such that the reactor core would eventually become subcritical (unable to further sustain the controlled chain reaction) if the reactor operation is continued without adding fresh fissile material. This is why nuclear reactors are periodically partly refuelled with fresh, unburnt fuel, with the cycle length dictated by the criticality requirement.

With a predetermined desired cycle length and a predetermined target power level for the nuclear reactor core, one is not absolutely free in configuring the core such that its economy is maximized. Generally, there are certain safety requirements such as the existence of an upper limit for the total power peaking factor (which is the maximum power density in the core divided by the core-averaged power density). This power peaking factor restricts the degrees of freedom in choosing a refuelling scheme to be implemented, thus reducing the total solution space to a (still very large) subspace of reloading patterns satisfying this power peaking constraint. Other examples of safety constraints that restrict the degrees of freedom are the shutdown margin constraint, the maximum critical heat flux ratio (MCHFR) constraint and the maximum critical power ratio (MCPR) constraint.

This thesis focusses basically on calculational optimization techniques for maximizing nuclear fuel utilization as far as allowed within this constrained solution space.

1.1.1 Nuclear fission reactors

Nuclear reactors have been used for over 40 years in a variety of applications. They are particularly valuable tools for nuclear research since they produce copious amounts of

radiation, primarily in the form of neutrons and gamma rays. Such radiation can be used to probe the microscopic structure and dynamics of matter (neutron or gamma spectroscopy). The radiation produced by reactors can also be used to transmute nuclei into artificial isotopes that can then be used, for example, as radioactive tracers in industrial or medical applications. An example of a typical research reactor is the Hoger Onderwijs Reactor at Delft University of Technology, which is a small $2MW_{th}$ pool-type light water cooled reactor used primarily to produce neutrons for materials research and activation analysis. Further, small, compact reactors have been used for propulsion in submarines and ships, and as compact sources of long-term power in orbiting satellites.

However, yet by far the most significant application of nuclear fission reactors is in large *power plants*. The majority of the nuclear power reactors are operated with approximately 3 % enriched uranium fuel (i.e. 3 % ^{235}U and 97% ^{238}U) and with light water (H_2O, in contrast to heavy water or D_2O) as the coolant material. These reactors are generally referred to as Light Water Cooled Reactors (LWCRs). In this introduction, the LWCR system characteristics will be only briefly discussed. More detailed technological and theoretical information can be acquired from various textbooks [Duderstadt 1976].

Generally, an LWCR core is a cylindrically shaped lattice roughly 3 or 4 m in diameter by 3 or 4 m in height consisting of a large number (100-400) of long fuel assemblies or bundles. These assemblies consist of a large number of long, narrow fuel pins (typically 17x17), which are generally Zirconium alloy tubes containing the nuclear fuel in the form of small UO_2 pellets. The height of a fuel pin and so, the height of a fuel bundle, is about 3 or 4 m. In spite of the presence of the necessary spacing material for keeping the fuel pins in their proper lattice positions, water can flow more or less freely along the fuel pins to carry the nuclear fission heat. The diameter of a fuel pin is about 1 cm. In the reactor core, the nuclear fission chain reaction, producing the desired heat, is maintained. The core itself is enclosed in a much larger container, a reactor pressure vessel, designed to withstand the enormous pressures of the coolant (up to 155 bar). Naturally, the core is linked to several coolant loops that circulate the coolant through the reactor to extract the fission heat energy, and heat exchangers or steam generators that use the heated primary coolant to turn feedwater into steam.

Two basic types of LWCRs can be distinguished : Pressurized Water Reactors (PWRs) and Boiling Water Reactors (BWRs). In a PWR, the primary coolant is water maintained under high temperature and high pressure, allowing high coolant temperatures without steam formation within the reactor. The heat transported out of the reactor core by the primary coolant is then transferred to a secondary loop containing the "working fluid" by a steam generator. In a BWR, the primary coolant water is maintained at a lower pressure (approximately 70 bar) for appreciable boiling and steam formation to occur within the reactor core itself. In this sense the reactor itself serves as the steam generator, thereby eliminating the need for a secondary loop and heat exchanger. Although the BWR seems simpler, the PWR has advantages with regard to fuel utilization and power density, and the two concepts have been economically competitive since the 1960s. The BWR fuel is slightly less enriched, but the PWR fuel produces more energy before being discharged, so these two properties cancel one another economically. In figure 1-1, the configuration of fuel and coolant in a typical PWR core is illustrated.
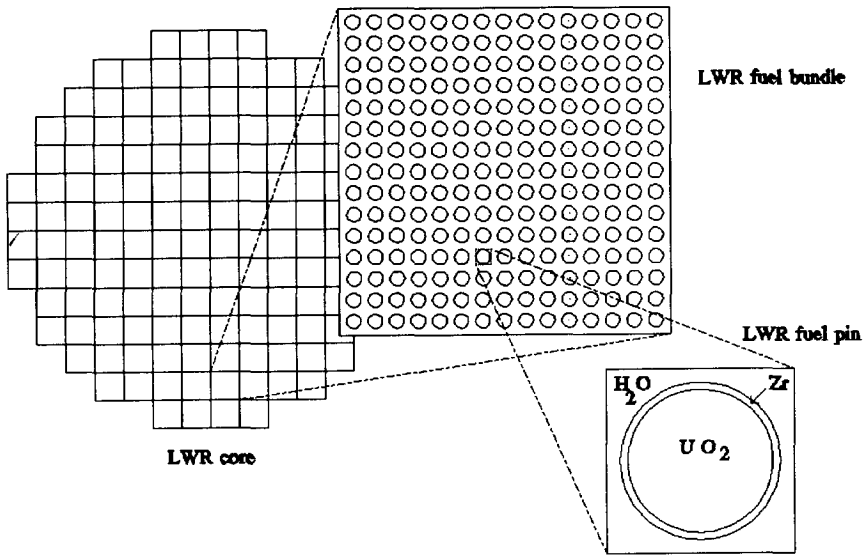
Fig. 1-1. Cross section of a typical PWR fuel bundle

1.1.2 LWCR refuelling

We recall that the interesting difference between nuclear power plants and power plants operating on fossil fuels is that for nuclear power plants the 'fuel' cannot be burnt completely (typically only approximately 60 % of the fissionable nuclides). This is because, in a nuclear reactor, the energy production requires at least a critical mass for maintaining the chain reaction of neutrons. An important quantity to be defined here is the *burnup*. The burnup is basically proportional to the number of fission reactions that have occurred and can be specified both for an entire core and for an individual fuel assembly. The physical unit generally used for burnup is MWdays/kg, in which case the exact definition of the burnup B of a fuel bundle is the amount of energy delivered by the fuel bundle divided by the initial mass of all heavy element isotopes in the fuel bundle (in case of LWCR fuel). A generally known rule of thumb is that two fuel bundles of the same type with the same burnup have the same material composition. Hence, the burnup can be used to characterize the material composition of a fuel bundle.

In the core of the reactor, the power distribution is generally not uniform. When, for example, the entire core is filled with fuel bundles of identical burnup, the radial power distribution will be approximately umbrella-shaped if the core is roughly cylindrical (which, mostly, it is). The nonuniformity of the power distribution induces the presence of variations in the burnup rates of the fuel bundles. During a fuel cycle, less and less control (control rods in a BWR, soluble boron in a PWR) is required to maintain the reactor's criticality, due to increasing burnup for each fuel bundle. When the fuel has been burnt to the extent that the controlled chain reaction of neutrons cannot be further maintai-

3

ned, the reactor core needs to be partly refuelled. It is apparent that because of the burnup differences, only the fraction of bundles featuring the highest burnup need to be replaced by new, "fresh" fuel bundles when the reactor core is reloaded for the next fuel cycle. Generally, one third or one fourth of the fuel bundles is discharged from the core, and the remaining bundles are shuffled to other positions in the core, after which the vacant positions are filled with "fresh" fuel bundles. When, at each reload operation, a fraction $1/n$ of the fuel bundles is replaced by fresh fuel, the burnup distribution will be such that one can distinguish between n different age groups of fuel bundles that will roughly have the same burnup.

In Fig. 1-2, a possible reload operation is illustrated graphically. Fig. 1-2 reveals some of the important aspects of the work described in this thesis. It shows a two-dimensional graphical representation of a nuclear reactor core, partitioned into square, homogenized nodes that contain the different fuel bundles. In the right bottom quadrant the concept of enforcing octant symmetry is illustrated by the octant symmetric numbering of the nodes in this quadrant. The left part of the figure shows the fuel bundle age distribution corresponding to the reload scheme. This age distribution follows from knowledge about the trajectories as depicted in the right top quadrant along which the fuel assemblies travel during their lifetime for the case of a repeated application of a 4-batch reload operation.
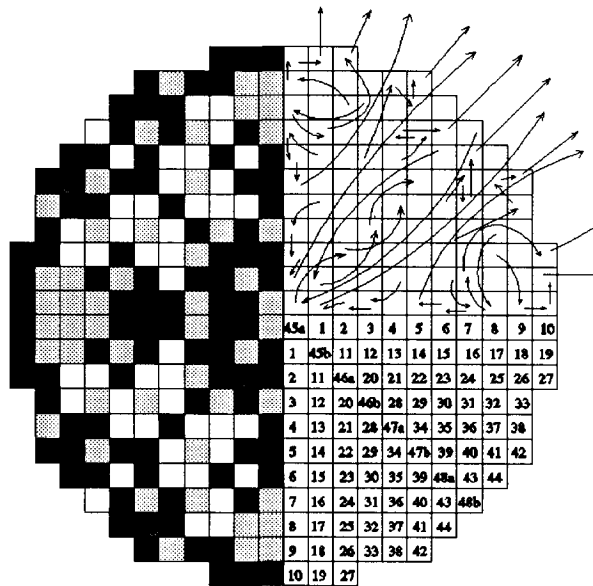
Fig. 1-2. Illustration of a possible reload operation ; the darker the fuel assemblies, the higher their burnup.

A very important advantage of a partial replacement of the nuclear fuel in the core is that a more flat power distribution is realizable, because of the availability of fuel bundles with different burnup levels. When the power shape is flatter, a higher total power output

could be achieved while satisfying the maximum bundle power limit, which is basically an engineering constraint kept for avoiding possible melting of fuel bundles. Another important advantage of batch refuelling with more batches is that the burnup of discharged fuel bundles increases with the number of fuel batches n. Several authors have argued by general analytical methods that the discharge burnup increases roughly with $2n/(n+1)$ [Reilly 1970, Silvennoinen 1976, Strawbridge 1979, Parks 1988, De Jong 1995]. Simultaneously, however, the cycle length (the maximum time at full power) decreases roughly with $2/(n+1)$. For LWCRs, the initial fuel enrichment, the total fuel mass of the core, the total core power and the number of fuel batches are generally such that the reactor core can be refuelled once a year, though for some present-day reactors reloading only occurs every 1½ or 2 years.

1.2 Reload pattern design

One can exert influence on the time-dependent reactor physical characteristics of the core by making a particular choice for the discharge-and-shuffling scheme to be implemented at the reloading operation. Optimization of such schemes with respect to certain target properties of the core during a fuel cycle is called *reload pattern optimization*, or *core loading pattern design*. In many cases, the *objective function* depending on the variable reload pattern is a combination of several relevant quantities, such as for example the burnup of an average fuel bundle at the end of its lifetime, or the neutron leakage. Obviously, in reload pattern optimization the optimal reload pattern associated with a maximal or minimal value of the objective function should be found, subject to the problem constraints.

It should be noted here that, in general nuclear fuel management for LWCRs, a clear distinction exists between *out-of-core fuel management* and *in-core fuel management*. Out-of-core fuel management optimization focusses on optimizing the general behaviour of a nuclear power plant, and addresses issues related to, for example, the choice of the amount of fissile material to be purchased, and the desired material properties (fissile enrichment, etc.) of the fissile material. In-core nuclear fuel management optimization involves optimizing the design of the actual core configuration, so the *actual positioning* of the different fuel elements in the reactor core. Further, in-core fuel management is concerned with the Burnable Poison distribution design and, in the case of BWRs, with the control rod program design. Burnable poisons are materials (such as Gadolinium) that are characterized by very high neutron capture cross sections, especially in the thermal energy range, but are not fissionable. These are generally added to fresh, unburnt fuel elements to condition the power distribution during the first months of a reactor cycle. The purpose of this is twofold : by adding burnable poisons to flatten the power distribution, the power peaking factor is made smaller and the multi-cycle fuel economy for the reactor can be enhanced (in accordance with the arguments presented in section 2.4 of this thesis). Because of burnable poisons have high neutron capture cross sections, they are transmuted rather rapidly, so that their effect becomes smaller and smaller as the operation cycle proceeds. By then the power distribution will already be flatter due to the burnup effect.

The subject of this thesis is a study of heuristic search and perturbation theoretical methods for use in in-core fuel management optimization. In the remainder of this chapter, it

will be indicated that this optimization problem is a very difficult kind of optimization problem from a mathematical point of view, followed by a discussion about the different possible objective functions and the discrete optimization nature of this problem. Further, different optimization approaches applied currently and in the past will be briefly described. Finally, the specific in-core fuel management optimization problems and approaches studied in this work will be introduced.

1.2.1 The factorially large design space

The number of different possible choices for the way in which to reload the core is generally *almost astronomically large*. If, for example, we consider the core depicted in Fig.1.2, and enforce octant symmetry, we have in the case of a reload fraction 1/4, assuming that all unburnt fuel assemblies are similar, the following number of different reload operations : $48 \cdot 47 \cdot ... \cdot 14 \cdot 13 = 48!/12! \cong 2.6 \cdot 10^{52}$. When a system containing N fuel nodes is reloaded in an *n*-batchwise fashion, there are $U_1 = N!/(N/n)!$ possibilities for the choice of the reload scheme. In some optimization studies, the fuel assemblies are classified in n different age groups with the (rather rough) assumption that within one age group, the physical properties of the fuel assemblies (notably, the degree of burnup) are approximately the same. Hence these studies make use of simplified models in which batch properties are considered instead of properties of individual fuel bundles. These models lack information about variations of burnup properties within the batches. However, because of the simpler nature of the reload scheme representation, which reduces from a $N \times N$ node-to-node assignment matrix to a $N \times n$ batch-to-node assignment matrix, the number of possible reload schemes reduces from U_1 to $U_2 = N!/[(N/n)!]^n$.

The majority of standard scientific school calculators are incapable of calculating N! for $N \geq 70$, since for $N \geq 70$, $N! \geq 10^{100}$ and the largest power of ten that can be handled by these devices is 10^{99}. However, for $N \geq 70$ it is justified to apply the *Stirling approximation* :

$$N! \approx \sqrt{2\pi N}\,(N/e)^N \quad , \quad \text{for large N} \tag{1.1}$$

By applying Eq. (1.1), it can be derived that

$$U_1 \sim 10^{\left\{ \log\sqrt{n} + N\log\frac{N}{e} - \frac{N}{n}\log\frac{N}{ne} \right\}} \tag{1.2}$$

and

$$U_2 \sim 10^{\left\{ \left(N + \frac{n}{2}\right)\log n - \frac{1}{2}(n-1)\log[2\pi N] \right\}} \tag{1.3}$$

Table 1.1 lists a number of total reload pattern space sizes for $n=4$. The largest value of 96 for N listed in table 1.1 is representative of a core containing a total of approximately 800 fuel elements, which is quite normal in present-day BWRs. It should be noted here that if one explicitly considers rotational degrees of freedom (that is, accounting for the fact that each individual fuel burnt element can still have four different orientations when

its position in the core lattice is fixed), the size of the solution space is further enhanced by a factor of $4^{(1-1/n)N}$.

TABLE 1.1

N	16	24	32	40	96
U_1	$8.7178 \cdot 10^{11}$	$8.617 \cdot 10^{20}$	$6.526 \cdot 10^{30}$	$2.2484 \cdot 10^{41}$	$1.6 \cdot 10^{126}$
U_2	63063000	$2.31 \cdot 10^{12}$	$9.956 \cdot 10^{16}$	$4.705 \cdot 10^{21}$	$6.78 \cdot 10^{54}$

In most reload pattern optimization studies, one resorts to the consideration of an *octant* reactor core, assuming octant symmetry for the optimal solution. In this case one has to bear in mind that the diagonal nodes contain half as much volume as the non-diagonal nodes, which complicates the calculation of the total number of possibilities. Nevertheless, the consideration of octant cores results in a very significant reduction of the number of different reload patterns. It is, however, important to realize that octant symmetry can never be exactly achieved, except in the case where each fresh fuel bundle that is placed on a diagonal position remains on the diagonal during the rest of its entire lifetime. Therefore, in some studies, the occurence of the last-mentioned situation is defined as a constraint for core geometries in which this is necessary to obtain n-batch reloadings. For present-day modern PWRs, a total number of 400-600 fuel elements is normal, so the octant contains approximately 50-75 fuel elements. Thus, when no rotational freedom is taken into account, solution spaces containing $10^{60}-10^{80}$ octant-symmetric candidate reload schemes are common.

1.2.2 Objectives and constraints

For the core loading pattern optimization problem, different objectives and constraints can be formulated. These depend on the type of reactor one is dealing with and on the specific restrictions imposed by safety and operational requirements. For commercial power plants, one is mostly interested in optimizing fuel economy while satisfying safety limits. This means that, on average, one wants to extract as much energy as possible from the fuel assemblies before they are finally discharged from the core, while satisfying the safety and operational constraints. This objective is quite understandable if one considers the average price of one fuel assembly : approximately $ 700,000 (in the year 1997). However, in most optimization studies, a flat power distribution is also highly valued, and hence sometimes the *total power peaking factor* is included in the objective function, which then becomes a composite objective function. The total power peaking factor can be defined as the maximum power density in the core divided by the average power density. For the case in which one works with node-averaged power densities p_I, with a total of N nodes, the power peaking factor p can be mathematically defined as :

$$p = N \frac{\max\{P_I, I = 1,\ldots,N\}}{\sum_{I=1}^{N} P_I} \qquad (1.4)$$

7

Basically, the total power in the reactor core can be increased until the fuel bundle with the highest power contribution reaches the maximum bundle power limit. So when the power shape is as flat as possible, i.e. when the power peaking factor p is minimal (the theoretical minimum is 1, corresponding to a fully flat power distribution), the total power output of the reactor core can be increased maximally. Nowadays, the total power output of the reactor core is usually constrained to the desired nominal power that can already be reached with a non-minimal power peaking factor f_{lim}, which is called the power peaking limit. So when the power peaking peaking constraint $p \leq f_{lim}$ is satisfied, the nominal power output of the reactor can be achieved.

While satisfying the power peaking constraint, a reasonable objective to be chosen is to maximize the fuel utilization for a given initial enrichment. In practise this is often translated in maximization of the effective multiplication factor [Duderstadt 1976] of the uncontrolled core at the start of the operations cycle for a given number of fuel assemblies, subject to the safety constraints [Galperin 1989, Mahlers 1991, Šmuc 1994, Parks 1996a, Van Geemert 1996]. 'Uncontrolled' means that one considers the core in a fictitious state without external control such as control rods or soluble boron. Optimization of the core result in a design in which a smaller number of fresh fuel assemblies is needed for operation during the forthcoming cycle. Examples of optimization results for large PWRs have indicated that fuel cycle savings of several million US dollars can be realized by application of sophisticated optimization methods [Hager 1997]. Another fuel economy optimization approach, which is focussed on in this thesis, is to minimize the required feed enrichment of a predetermined number of fresh fuel assemblies, subject to the operational and safety constraints [Maldonado 1995, Van Geemert 1997].

1.2.3 Mathematical classification of the in-core fuel management problem

The reload pattern optimization problem can be mathematically classified as an *assignment problem*, which is a general term for all problems in which basically one is interested in an optimal sequence or ordering of different objects. Specifically, the reload optimization problem is concerned with the question of how to optimally distribute N fuel elements over N different core locations such that the utilization of the fuel is maximized. A classical example of a more famous assignment problem is the *travelling salesman problem*, which is concerned with the quest for the optimal visiting sequence of a fixed, predetermined collection of cities such that the associated travelling time is minimized. A solution can generally be presented by a vector $\underline{x}$ containing N different integers $x_1,...,x_N$ indicating the sequential or positional ordering of the elements $1,...,N$. For the travelling salesman problem, $\underline{x}$ represents the travelling sequence and for the reload optimization problem $\underline{x}$ represents the assignment of the different fuel elements over the various core locations.

The very heart of the complexity of both problems is the fact that no *ordering principle* exists for the discrete variables. The purpose of an ordering principle is basically to map the solution space such that it eventually consists of mathematically identifiable regions of approximately the same performance with respect to the objective. An ordering law as described here should, implicitly, contain a lot of the actual physics of the problem in order to even approximately reconstruct the genuine ordering in objective function values. If one is interested in top performance solutions, so solutions associated with objective

function values embedded in a narrow top range, the ordering law should be capable of indicating directly the whereabouts of the region of these solutions in the mapped solution space. So basically, the ordering law should for this narrow range of function values correctly dictate the corresponding ordering properties for the top performance solutions in terms of solution characteristics that are directly and explicitly related to the discrete variables. For example, for reload optimization the ordering law should provide a unique indication for the approximate fuel age distribution of the best reload pattern candidates.

It is obvious that such an ordering principle cannot exist if the actual physics of the problem is characterized by a total lack of fuel age distribution uniformity in the collection of patterns corresponding to the same narrow range of function values. For the travelling salesman problem, this can be illustrated graphically in terms of the visual heterogeneity of the different travelling paths (having about the same length) along the different cities on a two-dimensional map of the travelling region. For the reload pattern optimization problem, this can be illustrated analogously by showing the visual heterogeneity of fuel age distributions corresponding to virtually the same objective function value.

An important difference between the objective functions of both examples is that, for the travelling salesman problem, an explicit functional form exists that is perfectly linear, whereas for the reload optimization problem, the objective function is known only in a very implicit and difficult, and nonlinear form. In order to eventually determine the objective function value, a lot of iterations must be done in which matrix eigenvalue equations of rather high dimensions must be solved. Naturally and unfortunately, these iterative procedures cannot be captured in an explicit functional form. The same applies to the constraint function for reload optimization (i.e. the power peaking factor).

So, from a mathematical optimization point of view, the properties mentioned here cause the reload pattern design problem to be characterized by a number of very inconvenient and unpleasant features [Stevens 1995] :

-   It is well-known in reload pattern optimization that the objective function is generally non-convex (fluctuatory), which means that the solution space features a very large number of local extrema (instead of only one extremum in case of convexity). This property is called *multi-modality*. It is obvious that the global optimum is the best of the local optima. However, there is no method to predict which local optimum is the best for multi-modal functions without identifying and comparing all local optima.

-   The constraint function is usually non-convex (and thus multi-modal) as well, which gives rise to the existence of *disjoint* feasible regions in the solution space. Furthermore, the mere presence of inequality constraints introduces discontinuity and nondifferentiability, so that local optima of the constrained problem are unlikely to occur at an extremum of the objective function.

-   Since the basic variable, the reload scheme or assigment operator, is required to be *integer* valued, the simple calculus of analytic optimization breaks even further down since the concept of the infinitesimal necessary for differentiation does not even exist.

9

- In many cases, the objective function is composed of a number of possibly conflicting objectives (*multi-commodity*). The different components of the objective function are generally weighted in some manner, and the global optimum depends on the ratios of these weightings.

- The solution space is extremely large, which enhances the difficulties mentioned previously here.

All of the first four problem characteristics individually make identification of the global optimum infeasible and the reload optimization problem, even if restricted to pure shuffling, has all four of them ! Because of these characteristics, no mathematical optimization method is known which is capable of solving the reload pattern optimization problem globally -that is, find the globally optimal solution at limited computational cost. In mathematical optimization theory, a very essential tool in many optimization methods is a functional expression for both the objective function and its gradient. However, since functional forms exist for neither the objective function nor the gradient, the number of optimization algorithms appropriate for solving this problem is quite limited.

1.2.4 Overview of different optimization techniques

In order to circumvent the mathematical difficulties and infeasibilities associated with reload pattern design, many people have worked on different types of *heuristic* search algorithms that have indeed been successfully applied in generating very good reload designs. Generally, the heuristic search algorithms have a polynomial time behaviour, which means that the worst case computational time of the algorithm is a polynomial function of the problem size N. The heuristic algorithms generally do not require any inherent ordering principle or gradient information and are known to perform reasonably well in large combinatoric optimization problems. In many cases, the heuristic algorithms are based on assessing the effects of a large but limited number of different fuel element permutations in the core in order to travel along a path of successively improved patterns in the solution space towards the final reload design, which is very probably a local optimum. Some variants are somewhat more sophisticated and are not necessarily restricted to successive improvements by allowing (mostly stochastically) transitions to slightly worse patterns as well. In this way, these variants offer the possibility of escaping from local extrema.

Perhaps the simplest example of a heuristic algorithm used for reloading pattern design is the pairwise interchange optimization (PIO) algorithm [Naft 1972, Stout 1973, Lin 1979, Ho 1982, Kim 1987, De Jong 1995, Van Geemert 1997]. In this algorithm, all possible pairwise fuel element interchanges in an initial reloading pattern $\underline{x}^{(0)}$ are considered to see whether such interchanges yield improvements and, if so, the best interchange is applied, yielding a new pattern $\underline{x}^{(1)}$. Subsequently this procedure is successively applied, yielding a series of improved patterns $\underline{x}^{(2)}, \underline{x}^{(3)}, \ldots$, until a pattern is found for which none of the considered pairwise interchanges yields an improvement. Very probably, of course, this pattern will be a local extreme.

Another example of a heuristic algorithm applied to reloading pattern design is successive linear programming [Chitkara 1973, Stillman 1989, Mahlers 1991]. The successive linear

programming method starts with linearizing the objective function $F(\underline{x})$ in the 'neighbour-hood' of an initial reloading pattern $\underline{x}^{(0)}$. This linearisation is used for setting up a local linear assignment problem, for which the optimal solution $\underline{x}^{(1)}$ can be found by linear programming techniques. Then the objective function $F(\underline{x})$ is linearized near $\underline{x}^{(1)}$ to get a following local linear assignment problem with solution $\underline{x}^{(2)}$ and so on. Eventually, after convergence of this process, a local extreme is found.

Two particular heuristic search methods, Simulated Annealing [Parks 1987, Kropaczek 1991, Verhagen 1993, Šmuc 1994, Van Geemert 1999] and Genetic Optimization [Poon 1993, Parks 1996a, DeChaine 1996, Axmann 1996], have been very popular during the last decade and are considered to be quite promising by the reload pattern optimization community. The most important similarity between these two methods is that they are both stochastic methods, offering the possibility to escape from local extrema, and that they are both based on simulating optimization processes that occur *in nature*.

The Simulated Annealing optimization mechanism is numerically analogous to annea-ling processes of many-particle systems (such as a crystal). These systems generally also have a very large and fluctuatory state space, which is even also discrete if the systems are governed by quantum-mechanical laws. The transition processes can be well described by statistical mechanics. In annealing processes, many-particle systems gradually find their way to an energy state corresponding to a very low (if not *the* lowest) potential energy through a very gradual decrease in system temperature and stochastically determined transitions from one (discrete) energy state to another. In reload pattern optimization, this search technique can be applied in the quest for the pattern corresponding to the highest or lowest value of an objective function.

In Genetic optimization techniques it is tried to simulate the Darwinian process of evolution. According to Darwin's evolution theory, the genetic code of a species gradually evolves under external influences (such as, for example, gradual changes in climate) such that, in order to survive, it will automatically eventually adapt to changes in its natural habitat. This can be regarded as a biological (stochastic) optimization algorithm with the "Survival of the Fittest" principle as its driving mechanism.

Another heuristic optimization approach is to apply knowledge-based selection rules [Galperin 1989] for setting up engineering constraints. These selection rules serve to exclude reload patterns with certain specific characteristics *a priori* from evaluation as candidate patterns. In this way, the candidate solution space can be reduced to the extent that all candidate patterns therein can be evaluated individually within limited computatio-nal time. Use of selection rules requires a lot of engineering insight as well as caution since the number of remaining candidate solutions can hardly be reduced to computational-ly feasible proportions without the risk of unintentionally excluding the best candidates from computational evaluation. It might be possible that reload patterns exist outside the subspace defined by the engineering constraints which actually yield good cycle behaviour, in spite of the fact that they violate one or more of the selection laws.

Other authors have tried to handle the core reloading problem by defining a desirable EOC (End-Of-Cycle) core state and then tried to find a reverse depletion strategy to find a BOC (Begin-Of-Cycle) core state where the available fuel bundles are matched [Downar 1986, Alsop 1991, Mahlers 1991]. At EOC, a low critical mass while satisfying the power peaking limit, is usually the target. Though heuristic methods are known to be capable of

finding very good candidate patterns, they can never guarantee that the best solution found is truly the globally optimal solution. However, from the results obtained by different authors [Parks 1996b, De Jong 1995] it may be carefully concluded that, when maximization of fuel utilization is chosen as the objective, the optimum is quite 'flat' in the sense that a lot of 'families' of patterns exist that are quite dissimilar with respect to their age distributions but almost equal with respect to their (nearly globally optimal) quality. This is perhaps the most important reason why the relatively simple search heuristics have been quite successful in generating very satisfactory reloading schemes.

In sophisticated heuristic search procedures such as the ones described here, thousands or even millions of different reload patterns must be evaluated, even in the case when one is considering a very modestly-sized core. This is why, to keep the required computation time within practical proportions, the availability of a computationally efficient method for performing core calculations is absolutely necessary. A calculational scheme in which large storage and execution time requirements are avoided is provided by so-called *nodal methods*, of which different variants have been developed. Examples are the 1½-group diffusion kernel [Chao 1987, De Jong 1995], and the nodal expansion method (NEM) [Bennewitz 1975, Finneman 1977, Smith 1985, Maldonado 1995]. Another way to evaluate the effects of large numbers of different permutations in a refuelling scheme is to treat the permutations as perturbations and apply generalized perturbation theory for assessing their effects on the objective function value [Ho 1982, White 1990, Maldonado 1995, Moore 1996, Van Geemert 1997, Van Geemert 1998].

A number of authors [Kim 1997, De Klerk 1997, Mahlers 1994, Quist 1999a] have worked on the development and implementation of *gradient based methods* for solving the reload pattern optimization problem. Whereas all of the heuristic search procedures discussed sofar are inherently independent of 'inside' gradient information arising from the core model used, these gradient based methods are characterized by a general mathematical approach in which the combination of the reload pattern and all the state variables occuring in the core model is treated as the variational space. The general task description is then to maximize or minimize some objective function subject to constraints consisting of the reload operation equation, the core neutronics equations, the depletion equations and some operational and safety constraints. In this formulation, the problem is non-linear and non-convex as well, and the solution methods can therefore be denoted as *mixed-integer nonlinear optimization methods*. In spite of the need to use only limitedly complicated core models, again no global optimality can be assured. Further, the optimization results may be rather sensitive to the initial configuration of the problem variables, which basically means that these methods do not offer the same absolute robustness as some of the more sophisticated heuristic search algorithms such as simulated annealing or evolutionary algorithms. However, if well implemented and initialized these methods are capable of yielding rather good results within very limited computation time and, in addition, constitute a very promising potential for tackling the combined reload pattern and burnable poison assignment problem [Quist 1999b]. As discussed in chapter 7 of this thesis, *burnable poisons* are materials with very high absorption cross sections that can be added to fresh, unburnt fuel assemblies in order to prevent discrepancies in the spatial power distribution and to serve as instruments for long-term reactivity control. Using them basically enhances the degrees of freedom in configuring the core while still satisfying the power peaking constraint. Obviously, when applying only heuristic search methods, the

reload pattern optimization problem and the burnable poison assignment optimization problem are necessarily decoupled. However, when applying mixed-integer nonlinear optimization methods, it should be possible to tackle both problems simultaneously (and thus in an integral way) [Quist 1999b].

1.2.5 Equilibrium cycle optimization

A large number of reload pattern optimization studies have focussed on optimizing only the forthcoming operation cycle. With the fuel inventory which is available at BOC, it is for example attempted to maximize the length of the forthcoming cycle, given a specific constant core power level during the operation cycle. This objective does not comply with maximum fuel utilization, since a high cycle burnup does not necessarily imply a high burnup of the fuel bundles to be discharged. If one wishes to maximize the cycle length of the forthcoming cycle, one will find that the fresh fuel assemblies will have to be loaded in the central region of the core, whereas the burnt fuel assemblies will be placed closer to the periphery of the core, so as to minimize the neutron leakage from the core. This type of reloading is generally referred to as Centre-to-Outside Loading (COL). For COLs, the fresh fuel assemblies are placed as close to the core centre as is allowed by the power peaking constraint. And for COLs, indeed especially the freshest fuel bundles contribute to the high cycle burnup. Since for COLs however, the older fuel bundles will have a relatively high burnup, successively optimizing reloading design for only the forthcoming cycle can eventually actually lead to shorter cycles.

As nuclear fuel economy is basically a multi-cycle issue, a fair way of evaluating reload patterns is to consider their performance in the case of an *equilibrium cycle* [Chitkara 1973, Lin 1979, De Jong 1995, Van Geemert 1996, Van Geemert 1997, Yamamoto 1997]. The equilibrium cycle (or *cyclic mode*) associated with a reload pattern is defined as the limit fuel cycle which eventually emerges after multiple successive periodic refueling with the same reload pattern. It is interesting to note that for equilibrium cycles, the objectives of a maximum total cycle burnup and the discharge burnup are the same, since for an equilibrium cycle refuelling (replacing discharged fuel bundles by fresh fuel bundles) exactly compensates the total cycle burnup. So for equilibrium cycles, the objectives of a maximum total cycle burnup (or maximum cycle length) and a maximum discharge burnup are equivalent.

1.3 Scope of this thesis

In this thesis, a general description will be given of basic computational methods for calculating the time-dependent power and burnup distributions in a nuclear reactor core, with emphasis on PWR physics and geometry. In particular, a Green's function nodal kernel method for fast core calculations will be presented that is to be applied in the evaluation of large numbers of loading patterns in heuristic search procedures. Theoretical foundations and practical results will be described of optimization based on the 'multiple cyclic interchange' approach, according to which the hunt for the best loading scheme can be decomposed in different stages. In this approach, the transition from the initial stage to the final stage is characterized by an increase in the degree of locality in the search

procedure. The general idea is that, during the first stages, the "elite" cluster containing the group of best patterns must be located, after which the solution space is sampled in a more and more local sense to find the local optimum in this cluster. The transition(s) from global search behaviour to local search behaviour can be either prompt, by defining strictly separate search regimes, or gradual by introducing stochastic acceptance tests.

In order to assess the effects of large numbers of possible changes in refueling schemes within a practical CPU-time frame, a generalized higher-order perturbation-theoretical formalism has been developed and implemented as well. Especially in the case of large PWR cores, for which thousands of fuel element permutations must be evaluated during an optimization search, use of perturbation theory seems very rewarding.

For fast evaluation of a new pattern to be investigated, the pattern can be decomposed into the original, unperturbed reloading scheme and the perturbation in the scheme. A variational technique can be applied to evaluate in first-order approximation the effect of the perturbation on a selected response vector. Explicit consideration of the higher-order terms in the response functional expansion results in a very rapidly converging iterative scheme from which a higher-order estimate of the perturbation in the response vector can be obtained at very low computational cost. In this iterative scheme, the first-order estimate serves as a fixed-source term. The availibility of this higher-order perturbation formalism offers the possibility of fast and (satisfactorily) accurate assessment of the effects with respect to the chosen objective of selecting different reloading schemes, which results in a considerable economy of computation time.

In particular, it has been studied how the first-order gradient information can be applied in fuel management optimization for the *equilibrium cycle*. For application of perturbation theory in equilibrium cycle optimization it is necessary to consider perturbations in the most complex equilibrium cycle parameter, that is, *the reload scheme itself*. An interesting property is that a permutation in a reloading scheme for an equilibrium cycle affects the *entire* time-dependent nuclide density distribution. Using the mathematical invariance equation (a two-point, cyclic boundary condition) for the equilibrium cycle and applying first-order Taylor approximations, very rapidly converging iterative systems were developed with which the perturbed equilibrium cycles can be reconstructed with satisfactory accuracy and very low computational effort.

Finally, it will be described how an existing nodal core simulator was incorporated in a heuristic optimization procedure.

This thesis is stuctured as follows :

In chapter 2, some basic methods for calculating time-dependent power and burnup distributions in a nuclear reactor core will be briefly described.
In chapter 3, the multiple cyclic interchange search approach to the reload pattern optimization problem is introduced.
Chapter 4 contains an introduction to generalized perturbation theory (GPT) and a description of how GPT can be applied to reload pattern optimization.
In chapter 5, it is discussed how GPT can be used in equilibrium cycle optimization.
Chapter 6 contains a description of how an existing nodal core simulator was incorporated in an optimization procedure.
Chapter 7 contains some general conclusions and some recommendations for future work.

References

[Alsop 1991] B.H. Alsop, Y.A. Chao, B.J. Johansen, T. Morita, "Evaluation and Performance of Westinghouse Loading Pattern Search Methodology", *Proceedings Pittsbrough conference*, pp. 22.2 2-1 to 22.2 2-10 (1991).

[Axmann 1997] J.K. Axmann, "Parallel Adaptive Evolutionary Algorithms for Pressurized Water Reactor Reload Pattern Optimizations", *Nuclear Technology* **119**, pp. 276-292 (1997).

[Bennewitz 1975] F. Bennewitz, H. Finneman, H. Moldaschl, "Solution of the Multidimensional Neutron Diffusion Equation by Nodal Expansion", *Proceedings of the Conference on Computational Methods in Nuclear Engineering*, CONF-750413, P.1, Charleston, USA (1975).

[Chao 1987] Y.A. Chao, J.A. Penkrot, "Diffusive Homogeneity - the Priciple of the Superfast Multidimensional Nodal Code SUPERNOVA", *Transactions of the Americal Nuclear Society* **55**, pp. 583-584 (1987).

[Chitkara 1973] K. Chitkara, J. Weisman, "An Equilibrium Approach to Optimal In-Core Fuel Management for Pressurized Water Reactors", *Nuclear Technology* **24**, pp.33-49 (1974).

[DeChaine 1996] M.D. DeChaine, M.A. Feltus, "Fuel Management Optimization Using Genetic Algorithms and Expert Knowledge", *Nuclear Science & Engineering* **124**, 188-196 (1996)

[De Klerk 1997] E. de Klerk, C. Roos, T. Terlaky, T. Illés, A.J. de Jong, J. Valkó, J.E. Hoogenboom, "Optimization of Nuclear Reactor Reload Patterns", *Annals of Operations Research* **69**, 65-94 (1997).

[De Jong 1995] A.J. de Jong, "Reload Pattern Optimization for Batch Refuelled Nuclear Reactors", *report IRI-131-95-010*, Interfaculty Reactor Institute, Delft University of Technology, Delft, The Netherlands, 1995.

[Downar 1986] T.J. Downar, Y. Kim, "A Reverse Depletion Method for Pressurized Water Reactor Core Reload Design", *Nuclear Technology* **73**, pp. 42-54 (1986).

[Duderstadt 1976] J.J. Duderstadt, L.J. Hamilton, "Nuclear Reactor Analysis", John Wiley & Sons, New York (1976).

[Finneman 1977] H. Finneman, F. Bennewitz, M.R. Wagner, "Interface Current Techniques for Multidimensional Reactor Calculations", *Atomkernenergie* **30**, 123 (1977).

[Galperin 1989] A. Galperin, S, Kimhi, M. Segev, "A Knowledge-based System for Optimization of Fuel Reload Configurations", *Nuclear Science & Engineering* **102**, pp. 43-53 (1989).

[Hager 1997] N.R. Hager, "Formosa-P Use In Nuclear Design", *proceedings Advances in Nuclear Fuel Management II conference*, Volume 2, 16.29-16.35, Myrtle Beach, USA (1997).

[Ho 1982] L.W. Ho, A.F. Rohach, "Perturbation Theory in Nuclear Fuel Management Optimization", *Nuclear Science and Engineering* **82**, pp. 151-161 (1982).

[Kim 1987] J. Kim, T.J. Downar, A. Sesonske, "Optimization of Core Reload Design for Low Leakage Fuel Management in Pressurized Water Reactors", *Nuclear Science and Engineering* **113**, pp. 70-76 (1987).

[Kim 1997] T.K. Kim, C.H. Kim, "Mixed Integer Programming for Pressurized Water Reactor Fuel Loading Pattern Optimization", *Nuclear Science and Engineering* **127**, 346-357 (1997).

[Kropaczek 1991] D.J. Kropaczek, P.J. Turinsky, "In-Core Nuclear Fuel Management Optimization for Pressurized Water Reactors utilizing Simulated Annealing", *Nuclear Technology* **95**, pp. 9-32 (1991).

[Lin 1979] B.I. Lin, B. Zolotar, J. Weisman, "An Automated Procedure for Selection of Optimal Refuelling Policies for LWRs", *Nuclear Technology* **44**, pp. 258-275 (1979).

[Mahlers 1991] Y.P. Mahlers, "Algorithms for Solving some Problems of the Nuclear Reactor Optimization", *Annals of Nuclear Energy* **18**(11), pp. 661-664 (1991).

[Mahlers 1994] Y.P. Mahlers, "Core Loading Pattern Optimization for Pressurized Water Reactor Fuel Loading Pattern Optimization", *Nuclear Science and Engineering* **127**, 346-357 (1994).

[Maldonado 1995] G.I. Maldonado, P.J. Turinsky, D.J. Kropaczek, "Employing Nodal Generalized Perturbation Theory for the Minimization of Feed Enrichment during Pressurized Water Reactor In-Core Fuel Management Optimization", *Nuclear Science and Engineering* **121**, 312-325 (1995).

[Moore 1996] B.R. Moore, "Higher Order Generalized Perturbation Theory for BWR In-Core Fuel Management Optimization", *PhD Thesis*, North Carolina State University, USA (1996).

[Naft 1972] B.N. Naft, A. Sesonske, "Pressurized Water Reactor Optimal Fuel Management", Nuclear Technology **14**, pp. 123-132 (1972).

[Quist 1999a] A.J. Quist, R. van Geemert, J.E. Hoogenboom, T. Illés, C. Roos, T. Terlaky, "Application of Nonlinear Optimization to Reactor Core Fuel Reloading", *Annals of Nuclear Energy* **26**, 423-448 (1999).

[Quist 1999b] A.J. Quist et.al., to be published (1999).

[Parks 1987] G.T. Parks, "An Intelligent Stochastic Optimization Routine for In-Core Fuel Cycle Design", *Transactions of the American Nuclear Society* **57**, pp.259-260 (1988)

[Parks 1988] G.T. Parks, J.D. Lewins, "A Point Reactivity Model for In-Core Fuel Cycles", *Nuclear Technology* **82**, pp. 267-274 (1988).

[Parks 1996a] G.T. Parks, "Multi-objective Pressurized Water Reactor Reload Core Design by Nondominated Genetic Algorithm Search", *Nuclear Science & Engineering* **124**, 178-187 (1996)

[Parks 1996b] G.T. Parks, "Loading Pattern Optimization in Hexagonal Geometry using PANTHER", *Proceeding PHYSOR'96 conference* I.66-75 (1996)

[Poon 1993] P.W. Poon and G.T. Parks, "Application of Genetic Algorithms to In-Core Fuel Management Optimization", *Proceedings Joint International Conference on Mathematics and Supercomputing in Nuclear Applications*, Karlsruhe, Volume 1, 777 (1993).

[Reilly 1970] H.J. Reilly, L.E. Peters, "Optimization of fuel loading for high power test reactors", *Nuclear Technology* **9**, pp. 356-363 (1970).

[Silvennoinen 1976] P. Silvennoinen, "Reactor Core Fuel Management", pp. 107-114, *Pergamon Press*, Oxford (1976).

[Smith 1985] K.S. Smith, D.M. Ver Planck, M. Edenius, "QPANDA : An Advanced Nodal Method for LWR Analyses", *Transactions of the American Nuclear Society* **44**, 265 (1983).

[Šmuc 1994] T. Šmuc, D. Pevec, B. Petrović, "Annealing Strategies for Loading Pattern

Optimization", *Annals of Nuclear Energy* **21**, pp. 325-336 (1994)

[Stevens 1995] J.G. Stevens, K.S. Smith, K.R. Rempe, "Optimization of Pressurized Water Reactor Shuffling by Simulated Annealing with Heuristics", *Nuclear Science and Engineering* **121**, 67-88 (1995).

[Stillman 1989] J.A. Stillman, Y.A. Chao, "The Optimum Fuel and Power Distribution for Pressurized Water Reactors", *Nuclear Science and Engineering* **103**, pp. 321-333 (1989).

[Stout 1973] R. Stout, A.H. Robinson, "Determination of Optimal Fuel Loadings in Pressurized Water Reactors using Dynamic Programming", *Nuclear Technology* **20**, pp. 86-102 (1973).

[Strawbridge 1979] L.E. Strawbridge, in H.W. Graves, "Nuclear Fuel Management", pp. 272-278, *J. Wiley and Sons* (1979).

[Van Geemert 1996] R. van Geemert, A.J. Quist, J.E. Hoogenboom, "Reload Pattern Optimization by Application of Multiple Cyclic Interchange Algorithms", *proceedings PHYSOR'96 conference*, Mito, Japan (1996).

[Van Geemert 1997] R. van Geemert, A.J. Quist, J.E. Hoogenboom, "Application of Depletion Perturbation Theory and Sensitivity Analysis for Minimizing the Required Feed Enrichment for an Equilibrium Cycle", *proceedings Advances in Nuclear Fuel Management II conference*, Volume 2, 15.1-15.9, Myrtle Beach, USA (1997).

[Van Geemert 1998] R. van Geemert, J.E. Hoogenboom, A.J. Quist, "In-Core Fuel Management Optimization by Incorporation of a Generalized Perturbation Theoretical Approach in a Heuristic Search Procedure", *proceedings PHYSOR98 conference*, V1.91-101, Long Island, USA (1998).

[Van Geemert 1999] R. van Geemert, P.F.A. De Leege, A.J. Quist, J.E. Hoogenboom, H.P.M. Gibcus, "Research Reactor In-Core Fuel Management Optimization by Application of Multiple Cyclic Interchange Algorithms", *accepted for publication and to be published in Nuclear Engineering and Design* (1999).

[Verhagen 1993] F.C.M. Verhagen, M. van der Schaar, "Simulated Annealing in LWR Fuel Management", *TOPNUX'93 Proceedings* **2**, pp. 37-39 (1993).

[Yamamoto 1997] A. Yamamoto, "Comparison between Equilibrium Cycle and Successive Multi-Cycle Optimization Methods for In-Core Fuel Management of Pressurized Water Reactors", *Proceedings Joint International Conference on Mathematics and Supercomputing in Nuclear Applications* , Volume 1, 769-781, Saratoga, USA (1997).
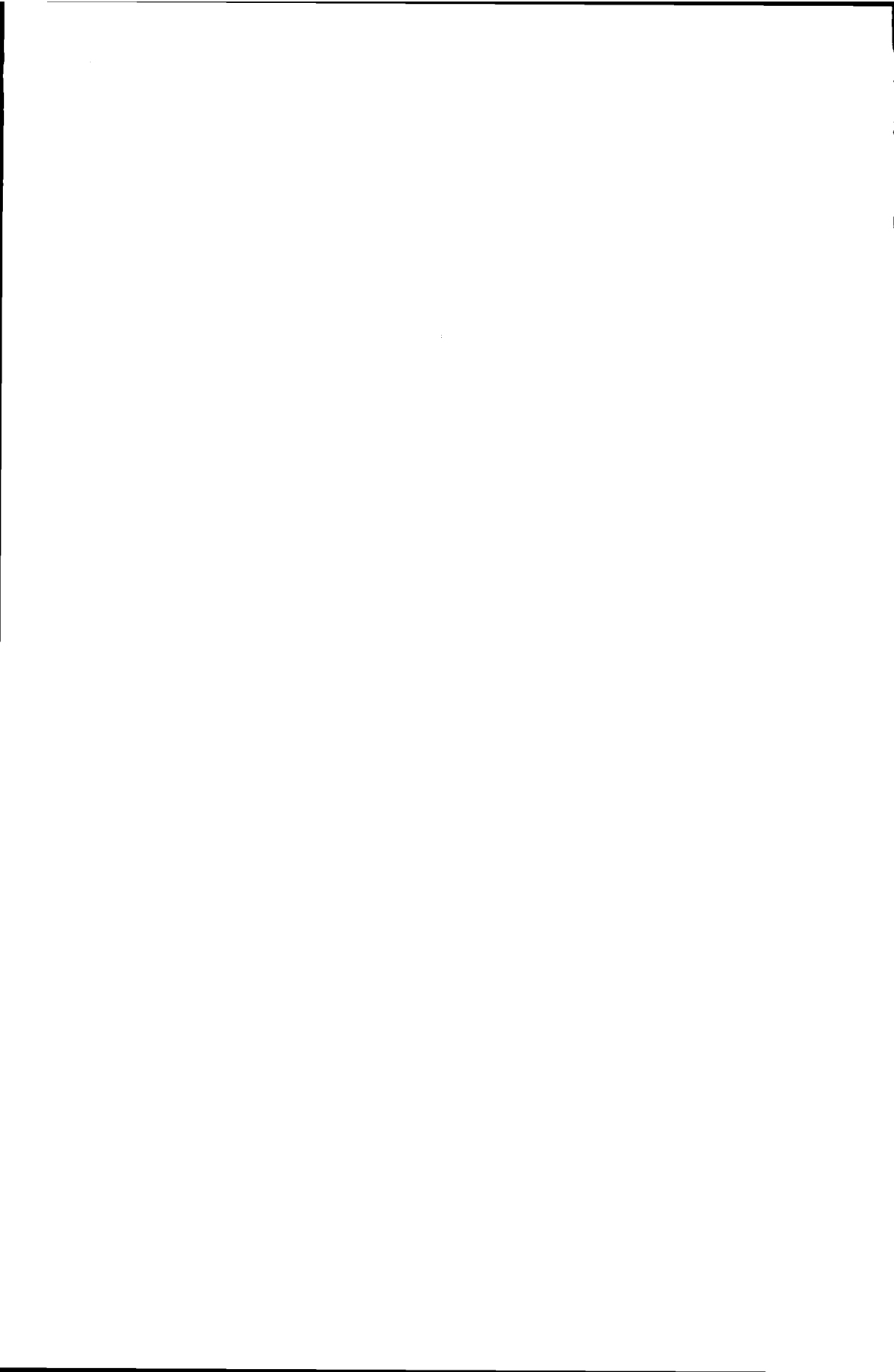
Chapter 2

Basic computational methods for solving the
burnup equations

2.1   The coupled neutron/nuclide field

The way in which a nuclear reactor evolves from BOC to EOC during operation is governed by two fundamental types of equations in nuclear reactor theory [Duderstadt 1976] : the neutronics equation describing the spatial distribution of the neutron density in the reactor, and the burnup equations describing the gradual change in the reactor's material core composition due to depletion of the nuclear fuel. These equations are coupled : the neutron density distribution is determined by the spatial nuclide density distribution and the spatial depletion rate distribution is related to the neutron density distribution. Due to this coupling, time dependence in the nuclide densities induces time dependence in the neutron flux distribution and vice versa. Since the interdependence can only be implicitly formulated, it is impossible to calculate analytically how the combined neutron/nuclide field will evolve from BOC to EOC.

However, since the time derivatives are relatively small, it is justified to apply a *quasi-static* approach [Duderstadt 1976, Williams 1979] in which the cycle time is divided into a certain number of equally long time intervals during which the neutron fluxes are kept constant. These time intervals are chosen sufficiently small with respect to the cycle length (or, more precisely, to the time scale at which significant changes in the neutron flux occur due to burnup). During each time interval, the depletion equations can be solved either analytically or numerically.

The system equations for reactor core analysis are very well documented in the nuclear reactor physics literature and will be only briefly and generally described here. More detailed information can be found in various textbooks and papers [Isbin 1963, Almenas 1992, Duderstadt 1976, Williams 1979]. As this study is focused on optimization of large PWR cores, it is justified to apply the so-called 1½-group approximation in the neutronics calculations. Therefore, the burnup equations discussed here will be presented in terms of the 1½-group PWR core neutronics and depletion model. Nevertheless, extension to a more general or more detailed, multi-group formalism is quite straightforward, and it should be stressed that the presence of more complexity in the core calculations will not significantly influence the applicability of the methodologies presented in the rest of this thesis.

2.1.1. The 1½-group nodal PWR core neutronics and depletion model

The time evolution of a reactor core is basically described by the energy-, space-, and time-dependent neutron flux $\phi(\underline{r},E,t)$ and by the space- and time-dependent nuclide density vector $\underline{N}(\underline{r},t)$. In the 1½-group approximation, two neutron energy groups are used, evidently a fast and a thermal group, and it is assumed that all neutrons released after a

19

nuclear fission belong to the fast group (which is group 1). If we consider the stationary diffusion eigenvalue equation for $\underline{\phi}(\underline{r},t)$ (introducing the *eigenvalue* k_{eff}), in which the material properties are considered quasi-static :

$$\left(\begin{matrix} \left(\underline{\nabla} \cdot D_1 \underline{\nabla} - \Sigma_{a1}(\underline{r}) - \Sigma_{1-2}(\underline{r}) \right) & 0 \\ \Sigma_{1-2}(\underline{r}) & \left(\underline{\nabla} \cdot D_2 \underline{\nabla} - \Sigma_{a2}(\underline{r}) \right) \end{matrix} \right) \cdot \underline{\phi}(\underline{r})$$

$$+ \frac{1}{k_{eff}} \left(\begin{matrix} \nu\Sigma_{f1}(\underline{r}) & \nu\Sigma_{f2}(\underline{r}) \\ 0 & 0 \end{matrix} \right) \cdot \underline{\phi}(\underline{r}) = \underline{0} \qquad (2.1)$$

we can neglect the thermal diffusion term $\nabla D_2 \nabla \phi_2$ with respect to the thermal absorption term $\Sigma_{a2}\phi_2$; in this so-called 1½-group approximation, the thermal flux ϕ_2 can be directly related to the fast flux ϕ_1 :

$$\phi_2 \approx \phi_1 \Sigma_{1-2}/\Sigma_{a2} \qquad (2.2)$$

and thus, in the 1½-group approach, one basically only needs to solve the diffusion equation for the fast flux distribution :

$$\underline{\nabla} \cdot \left(D_1(\underline{r}) \underline{\nabla} \phi_1(\underline{r}) \right) - \left(\Sigma_{a1}(\underline{r}) + \Sigma_{1-2}(\underline{r}) \right) \phi_1(\underline{r})$$

$$+ \frac{1}{k_{eff}} \left(\nu\Sigma_{f1}(\underline{r}) + \nu\Sigma_{f2}(\underline{r}) \frac{\Sigma_{1-2}(\underline{r})}{\Sigma_{a2}(\underline{r})} \right) \phi_1(\underline{r}) = 0 \qquad (2.3)$$

This equation can be written more compactly as

$$\underline{\nabla} \cdot \left(D_1(\underline{r}) \underline{\nabla}\phi_1(\underline{r}) \right) - \Sigma_R(\underline{r}) \phi_1(\underline{r}) + k_{eff}^{-1} \nu\Sigma_F(\underline{r}) \phi_1(\underline{r}) = 0 \qquad (2.4)$$

introducing the fast group loss and production cross sections Σ_R and Σ_F, respectively. Naturally, Eq.(2.4) is accompanied by a set of boundary conditions that require the solution $\underline{\phi}(\underline{r},t)$ to vanish outside the reactor at some boundary. The eigenvalue k_{eff} is called the *effective multiplication factor* [Duderstadt 1976]. If $k_{eff}=1$, the core is critical, if $k_{eff}>1$ it is supercritical and if $k_{eff}<1$ the core is subcritical. Omitting the time parameter for the stationary situation and integrating Eq.(2.4) over the entire core volume V, one obtains

$$k_{eff} = \frac{\int_V \nu\Sigma_F \phi_1(\underline{r}) \, dV}{- \int_V \underline{\nabla} \cdot \left(D_1(\underline{r}) \underline{\nabla}\phi_1(\underline{r}) \right) dV + \int_V \Sigma_R(\underline{r}) \phi_1(\underline{r}) \, dV} \qquad (2.5)$$

By identification of $-D_1(\underline{r})\underline{\nabla}\phi_1(\underline{r})$ as the stationary neutron current density $\underline{J}(\underline{r})$ [Duderstadt

1976] and application of Gauss' theorem it can be found that the first integral in the denominator of Eq.(2.5) represents the (fast) neutron leakage from the core volume :

$$- \int_V \underline{\nabla} \cdot \left(D_1(\underline{r}) \underline{\nabla} \phi_1(\underline{r}) \right) dV = \int_V \underline{\nabla} \cdot \underline{J}(\underline{r}) dV = \oint_{S_{core}} \underline{J}(\underline{r}) \cdot \underline{n} dS \qquad (2.6)$$

This indicates the physical interpretation of k_{eff} as being the ratio of the total neutron production and the total neutron removal rate, the latter being the sum of the total absorption rate and the total rate of leakage of neutrons from the core. In another physical picture [Duderstadt 1976], k_{eff} can be regarded as the ratio of the number of neutrons present in two consecutive neutron generations. After adopting the notation $\lambda = 1/k_{eff}$ which is commonly used in the literature of criticality eigenvalue problems, Eq.(2.5) results in the *lambda eigenvalue equation* :

$$\underline{\nabla} \cdot \left(D_1(\underline{r}) \underline{\nabla} \phi_1(\underline{r}) \right) - \Sigma_R(\underline{r}) \phi_1(\underline{r}) + \lambda \nu \Sigma_F(\underline{r}) \phi_1(\underline{r}) = 0 \qquad (2.7)$$

with the boundary condition $\phi_1(\underline{r}) = 0$, $\underline{r} \in \{\text{boundary}\}$.

It is obvious that the criticality for a nuclear reactor core in operation changes gradually due to burnup, and should be controlled such that it remains stable ($k_{eff} = 1$) throughout the operation cycle. This is realized by externally changing (part of) the core's material composition by gradual adjustment of the control rod depths (typical for BWRs) or gradual adjustment of the homogeneously distributed soluble boron concentration (typical for PWRs). In order to simulate the effect of control rod motion or soluble boron concentration adjustment, a control nuclide N_C can be defined, the value of which is usually found iteratively by adjusting its magnitude until $k_{eff} = 1$. The concentration of the control nuclide is thus determined by the constraint $k_{eff} = 1$ and as such it can be treated as another kind of eigenvalue. Obviously, for eventually determining the spatial flux shape this procedure is somewhat different from directly solving the lambda mode eigenvalue equation (in which, for a given material composition, λ is sought from Eq.(2.7)). It is more difficult to solve numerically but usually slightly closer to reality. However, for most problems the results will not be very sensitive to the approximation used [Williams 1979]. Therefore, in this thesis the lambda mode eigenvalue equation will be considered as the criticality equation to be solved. Since for a PWR core only the radial spatial variations in material properties are important for optimization, it generally suffices to consider a two-dimensional core geometry. Decomposing $\phi_1(x,y,z)$ into $\Phi\psi(x,y) \cdot \cos(\pi z/H)$ for an assumed cosine-shaped axial flux distribution of an cylindrically shaped core with core height H_C gives

$$- D_1(x,y) \left[\frac{\partial^2 \psi_1(x,y)}{\partial x^2} + \frac{\partial^2 \psi_1(x,y)}{\partial y^2} + \left(\frac{\pi}{H_C} \right)^2 \psi_1(x,y) \right]$$

$$+ \Sigma_R(x,y) \psi_1(x,y) = \lambda \nu \Sigma_F(x,y) \psi_1(x,y) \qquad (2.8)$$

in which the term $(\pi/H_C)^2$ is numerically negligible and can therefore be omitted.

In this study, we adopt the convention that the stationary fast flux distribution $\phi_1(\underline{r})$ can be written as $\Phi\psi(\underline{r})$. In this product notation, $\psi(\underline{r})$ is the flux density distribution which is normalized to unity ($\int \psi(\underline{r})dV = 1$) and Φ is a power normalization factor chosen such that $\Phi w_f \int \Sigma_F(\underline{r})\psi(\underline{r})dV = P_{tot}$. We note that w_f denotes the energy released per fission and P_{tot} the total power produced by the core. The stationary diffusion equation must be solved numerically for a core region such as the one depicted in Fig.2.1, in which each square node in the core region represents a fuel element position. Basically, each node has its own node-averaged material properties D_1, Σ_{a1}, Σ_{a2}, $\Sigma_{1\to2}$, $v\Sigma_{f1}$ and $v\Sigma_{f2}$ which are assumed homogeneous in each individual node. In this study, each node was chosen to consist of 10^2 meshpoints. For numerical solution, one can apply a finite-difference approach in conjunction with acceleration techniques for speeding up the iterations [Duderstadt 1976]. For theoretical convenience, to become apparent in chapter 4 of this thesis, the λ-eigenvalue equation can be written compactly as :

$$\mathbf{L}\underline{\phi} = \lambda \mathbf{F}\underline{\phi} \tag{2.9}$$

with $\mathbf{L}$ the loss matrix accounting for diffusion and absorption of fast neutrons, and $\mathbf{F}$ the production matrix. The boundary conditions may consist of actual problem-type boundary conditions, such as the condition that the flux vanishes at the system boundary (like the edges of the system geometry in Fig.2.1), but they may also consist of boundary conditions that enable one to use the *symmetry* properties of the problem under consideration.
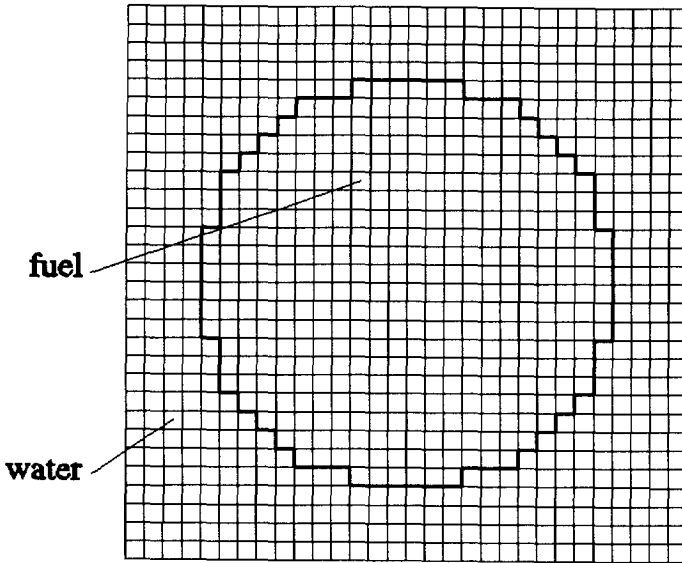

Fig.2.1   Example of a system geometry consisting of a fuel region with
different fuel assemblies, surrounded by a water region

For example, if the material composition of the core depicted in Fig.1.2 features quadrant symmetry, it is possible to model only one quadrant of the core, as shown in the right part

of Fig.2.2, and impose so-called 'reflected' boundary conditions. According to these 'reflected' boundary conditions, the produced flux profiles for the quadrant must be such that, when mirrored in the xz- or yz-plane, they yield perfectly smooth flux distributions for the entire core. Mathematically, the 'reflected' boundary conditions require that the normal vector of the boundary plane and the flux gradient vector are perpendicular to one another, so that their inner product vanishes :

$$\underline{n} \cdot \underline{\nabla} \phi = 0 \qquad\qquad (2.10)$$

In constructing procedures for solving the eigensystem, it is important to realize that the matrices L and F are very *sparse*, that is, most of the matrix elements are zero. In the diffusion matrix L for example, a meshpoint is directly coupled only with itself and (in the two-dimensional case) with its four nearest neighbours, such as indicated graphically in Fig.2.3. Therefore, for each meshpoint (i,j) in a two-dimensional 130x130 mesh corresponding to Fig.2.1, only a limited number of diffusion coupling indicators are necessary.
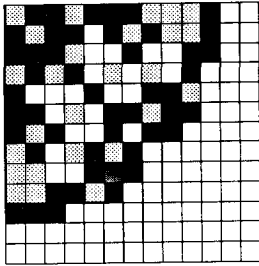


```
                    (1)
                    (i-1,j)

         (4)        (5)        (2)
         (i,j-1)    (i,j)      (i,j+1)

                    (3)
                    (i+1,j)
```

Fig.2.2   Illustration of a quadrant core   Fig.2.3   Neighbour area of the
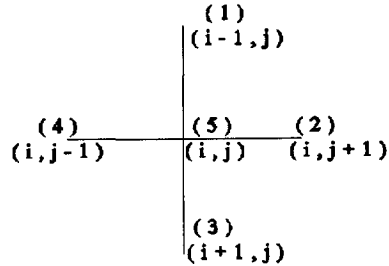   geometry   meshpoint (i,j)

This means that the large sparse matrix L with $\dim\{L\}=130^4$ can be compressed to the compact object L with $\dim\{\tilde{A}\}=130^2 \cdot 5$. How the element $(L \cdot \underline{\phi})_{i,j}$ can be obtained, is explained in appendix A.

Obviously, from a strictly mathematical point of view, the solution of Eq.(2.10) consists of a superposition of the entire spectrum of eigenstates $\underline{\phi}_n$ corresponding to the eigenvalues λ_n. However, only the fundamental solution $\underline{\phi}_0$ is relevant in real life, and the higher modes have meaning only in transition processes or in theoretical applications [Duderstadt 1976].

2.1.2 The quasi-static approach for solving the burnup equations

In this study, we adopted a physical picture in which each node (fuel bundle) I is represented by the vector of its node-averaged nuclide densities $\underline{N}_I(t)$:

$$\underline{N}_I(t) = \left(N_{1,I}(t) \ \ N_{2,I}(t) \ \ . \ \ . \ \ . \ \ N_{(nn),I}(t) \right)^T \qquad (2.11)$$

where (nn) is the number of different nuclide types considered. The coupling of the time-

23

dependent nuclide density field $\underline{N}(t) = \{\underline{N}_I(t), I \in \{1,...,N\}\}$ to the time-dependent neutron flux field $\underline{\phi}(t) = \{\phi_I(t), I \in \{1,...,N\}\}$ is given by :

$$\mathbf{L}\,\underline{\phi} = \lambda\,\mathbf{F}\,\underline{\phi} \tag{2.12}$$

$$\frac{d}{dt}\underline{N}_I(t) = \mathbf{B}_I\left(\underline{N}_I(t), \phi_I(t), \sigma\right)\underline{N}_I(t) , \tag{2.13}$$

$$\text{all } \Sigma_{g,I}(t) = \sum_{q=1}^{(nn)} N_{I,q}(t) \cdot \sigma_{q,g} \tag{2.14}$$

The index g in Eq.(2.18) indicates the neutron process type, and $\mathbf{B}_I$ is given by

$$\mathbf{B}_I(t) = \left[\mathbf{R}_1(\sigma) + \mathbf{R}_2(\sigma)\,\frac{\Sigma_{1\text{-}2,I}(t)}{\Sigma_{a2,I}(t)}\right]\phi_i(t) \tag{2.16}$$

where σ is the microscopic cross sections matrix and $\mathbf{R}_{1,2}(\sigma)$ are the macroscopic cross sections matrices for the energy groups 1 and 2. In order to illustrate this approach, we temporarily assume that the physical behaviour of the reactor is dominated primarily by the nuclide concentrations of ^{235}U, ^{238}U and ^{239}Pu. All three nuclide types feature decay rates which are considered negligible, even at the time scale of fuel cycles. When a ^{238}U nucleus captures a neutron, it will almost instantly be transmuted to ^{239}Pu ; this process is generally denoted as *fuel breeding*. Thus, the nuclide burnup process is given by :

$$\frac{d}{dt}\underline{N}_I(t) = \mathbf{B}_I(t)\,\underline{N}_I(t) \tag{2.16}$$

with the operator $\mathbf{B}_I(t)$ given by :

$$\mathbf{B}_I(t) = \begin{pmatrix} -\sigma_{a5}\,\phi_I(t) & 0 & 0 \\ 0 & -\sigma_{c8}\,\phi_I(t) & 0 \\ 0 & \sigma_{c8}\,\phi_I(t) & -\sigma_{a9}\,\phi_I(t) \end{pmatrix}, \text{ with all } \sigma_q = \left(\sigma_{q,1} + \sigma_{q,2}\,\frac{\Sigma_{1\text{-}2,I}(t)}{\Sigma_{a2,I}(t)}\right) \tag{2.17}$$

and the nuclide densities vector $\underline{N}_i(t)$ given by :

$$\underline{N}_I(t) = \begin{pmatrix} N_{I,5}(t) & N_{I,8}(t) & N_{I,9}(t) \end{pmatrix}^\mathsf{T} \tag{2.18}$$

Due to the coupling between the neutron flux field and the nuclide density field, time dependence in the nuclide densities induces time dependence in the neutron flux distribution. As the time derivatives are relatively small, it is allowed to apply a quasi-static approach in which the cycle time t_T-t_0 is divided into a certain number (n) of equally long time intervals Δt (such that $n\Delta t = t_T$-t_0) during which the neutron fluxes are kept constant.

These time intervals must be chosen sufficiently small with respect to the cycle length (or, more precisely, to the time scale at which significant changes in the neutron flux occur because of burnup). According to this approach, fuel cycle calculations are started with an initial nuclide densities distribution. This collection of nodal nuclide densities is used to calculate initial macroscopic cross sections for each node I. Then the collection of macroscopic cross sections is used to calculate the flux distribution for the first time interval. In the calculation, this flux distribution is kept stationary during the first time interval, so one is able to analytically solve the nuclide burnup equation for this interval. Thus the nuclide densities vector $\underline{N}_I$ at the end of the first interval is given by

$$\underline{N}_I(\Delta t) = \exp\left(\mathbf{B}_I(0)\,\Delta t\right)\underline{N}_I(0) \tag{2.19}$$

where

$$\exp(\mathbf{B}\Delta t) = \begin{pmatrix} e^{-\sigma_{a5}\phi_I(0)\Delta t} & 0 & 0 \\ 0 & e^{-\sigma_{c8}\phi_I(0)\Delta t} & 0 \\ 0 & \dfrac{\sigma_{c8}}{\sigma_{a9}-\sigma_{c8}}\left(e^{-\sigma_{c8}\phi_I(0)\Delta t} - e^{-\sigma_{a9}\phi_I(0)\Delta t}\right) & e^{-\sigma_{a9}\phi_I(0)\Delta t} \end{pmatrix} \tag{2.20}$$

Then the $\underline{N}_I(\Delta t)$ is the initial nuclide densities vector for the second time interval, and the 'new' flux distribution is calculated by solving Eq.(2.12) again with changed cross sections, etc. This procedure is to be successively applied until the end of the fuel cycle (EOC) is encountered. Hence the nuclide densities vector for time step n is :

$$\underline{N}_I(n\Delta t) = \left(\prod_{j=1}^{n} e^{\mathbf{B}_I(j-1)\Delta t}\right)\underline{N}_I(0) \tag{2.21}$$

In practice it is advisable to also explicitly consider the production of higher isotopes along the transmutation chain, of which ^{240}Pu is the most important because of its high neutron capture cross section (see Fig.2.4). For large, complex transmutation schemes, the operator $\mathbf{B}$ consists of much larger matrices, due to which the depletion equations are much more difficult to solve analytically. However, the matrix exponential $\exp(\mathbf{B}\Delta t)$ can be easily calculated by using a Taylor series expansion with prespecified convergence limits :

$$\exp(\mathbf{B}\Delta t) = \mathbf{I} + \mathbf{B}\Delta t + \frac{1}{2!}(\mathbf{B}\Delta t)^2 + \ldots \tag{2.22}$$

Further, it is essential to take into account the generation of *fission products*, the most essential of which are the reactor poison nuclides ^{135}Xe and ^{149}Sm. These nuclides are considered 'poisonous' because of their extremely high thermal absorption cross sections. ^{135}Xe is produced as a direct fission product and as a decay nuclide of the fission product ^{135}Te (via ^{135}I), whereas ^{149}Sm is merely produced as the decay nuclide of the fission
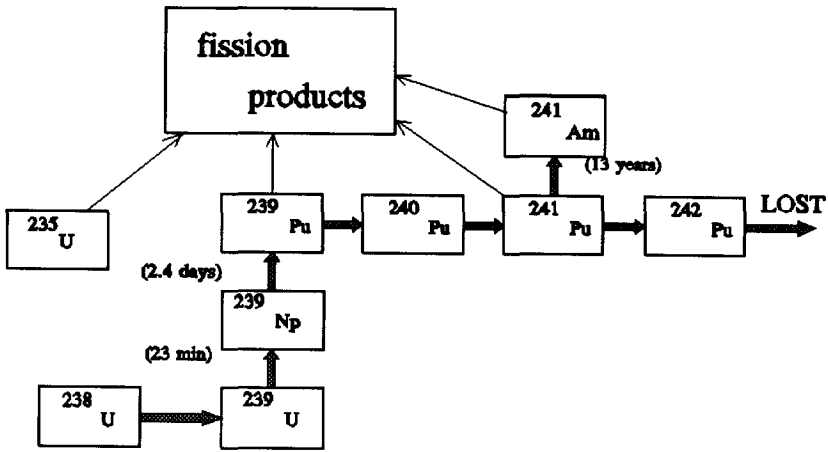
25

Fig.2.4   Example of a transmutation scheme in
which the formation of higher isotopes is
modelled

product ^{149}Nd (via ^{149}Pm). The scheme describing how Xe and Sm are formed from fission is depicted in Fig.2.5. It is convenient to treat the poison nuclide concentrations separately, since they relax to equilibrium values in a relatively short time. Thus, it is justified to treat them as quasi-static quantities [Duderstadt 1976] :

$$\tilde{N}_{Xe,I} = \frac{(\gamma_{Te} + \gamma_I + \gamma_{Xe}) \, \Sigma_{F,I} \, \phi_I}{\lambda_{Xe} + \sigma_{a,Xe} \, \phi_I} \tag{2.23}$$

and

$$\tilde{N}_{Sm,I} = \frac{\gamma_{Nd} \, \Sigma_{F,I}}{\sigma_{a,Sm}} \tag{2.24}$$

In a *realistic* reactor calculation, the generation of much more different fission products should be taken into account. In calculations such as performed in this study, only a limited amount of the most relevant nuclides have been included in the core model. This is why, when using realistic values for the microscopic cross sections for the different nuclides, less fissionable material is required for a critical core. This effect can be compensated by defining a *pseudo fission product* [Hoogenboom 1996] to be added to the modest set of system nuclides. The yield of this pseudo fission product can then be adjusted until a good correspondence to the more elaborate calculation of a 'big' depletion code like ORIGEN [ORNL] is found. In the transmutation scheme implemented in the depletion model
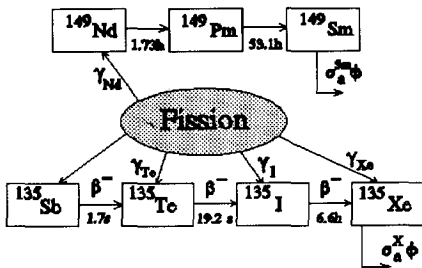
26

Fig. 2.5   Formation of the poisonous nuclides Xe and Sm

applied in this thesis' study, the transmutation chain depicted in Fig.2.4 has been extended with such a pseudo fission product, though for the methodology to be presented in this thesis the *specific* number of nuclides considered is not very relevant.

2.2   Using nodal methods in reload pattern optimization

As argued in chapter 1, there are extremely many possible choices for the way in which to reload the core. Although it is possible to eliminate large parts of the reduced solution space (which are thought to contain only poor-performing patterns) by using knowledge-based selection rules, the number of remaining candidate solutions cannot be reduced to computationally feasible proportions without the risk of excluding the best candidates from computational evaluation. In more intelligent search procedures (such as the ones described in chapter 3), thousands of different reload patterns must be evaluated as well, even in the case in which one is considering a very modestly-sized core. When one has no alternative but to use a code that solves the diffusion equation in a fine mesh, one will have to tolerate the large storage and execution time requirements of the direct finite difference treatment of the diffusion equation, which leads to unacceptably long computation times for evaluating large numbers of different reload schemes. A calculational scheme in which the large storage and execution time requirements are avoided is provided by so-called *nodal methods* [Bennewitz 1975, Finneman 1977, Smith 1985, Chao 1987, De Jong 1995].

The general idea of nodal methods is to decompose the reactor core into relatively large subregions or *node cells* in which the material composition and flux are assumed uniform (or at least treated in an average sense). One then attempts to determine the coupling coefficients characterizing node cell to node cell leakage and then to determine the node cell fluxes themselves. Nodal methods require far less computation time than finite-difference methods, due to which reload pattern optimization procedures in which nodal methods are used in the evaluations of different schemes are capable of evaluating vast amounts of candidate patterns during relatively limited computation times. The mathematics of nodal methods also allows for straightforward development of a generalized perturbation theory formalism, as is described in chapter 4, which offers the possibility of increasing the computational efficiency even further.

2.2.1 Green's function diffusion kernel method

By using the Green's function diffusion kernel method [Chao 1987, De Jong 1995] for 1½-group diffusion theory, particularly fast core calculations can be done. The principal reason for this is that the dimensions of the operators and variables in the kernel eigenvalue equation are significantly reduced due to node cell homogenization. We recall that we chose to abandon the subscript 1 for the fast flux ϕ and note that, according to Green's

function theory, the neutron diffusion eigenvalue equation for the 1½-group approach

$$- \nabla \cdot D(\underline{r}) \nabla \phi(\underline{r}) + \Sigma_R(\underline{r}) \phi(\underline{r}) = \lambda \nu \Sigma_F(\underline{r}) \phi(\underline{r}) \tag{2.25}$$

can be written formally as the kernel relation

$$\phi(\underline{r}) = \lambda \int G(\underline{r},\underline{r}') \nu \Sigma_F(\underline{r}') \phi(\underline{r}') dV' \tag{2.26}$$

with $G(\underline{r},\underline{r}')$ the *diffusion kernel* or *Green's function* for the particular geometry of interest that satisfies

$$\left[- \nabla \cdot D_1(\underline{r}) \nabla + \Sigma_R(\underline{r}) \right] G(\underline{r},\underline{r}') = \delta(\underline{r} - \underline{r}') \tag{2.27}$$

$G(\underline{r},\underline{r}')$ can be interpreted physically as the flux resulting at a position $\underline{r}$ from a unit point source at $\underline{r}'$. If we now adopt the picture in which the reactor core is divided into N node cells, and integrate the kernel equation over the volume V_I of the Ith node cell :

$$\int_{V_I} \phi(\underline{r}) dV = \lambda \int_{V_I} \left[\int_{core} G(\underline{r},\underline{r}') \nu \Sigma_F(\underline{r}') \phi(\underline{r}') dV' \right] dV$$

$$= \lambda \sum_{J=1}^{N} \int_{V_I} \int_{V_J} G(\underline{r},\underline{r}') \nu \Sigma_F(\underline{r}') \phi(\underline{r}') dV' dV \tag{2.28}$$

we see that a balance equation emerges in which the neighbouring nodal fluxes can be interrelated in an algebraic way. In order to obtain a kernel relation relating the different node-averaged fluxes to each other, it is necessary to define a number of spatial averages over the nodal cells, such as the node-averaged fast flux

$$\langle \phi \rangle_I = \frac{1}{V_I} \int_{V_I} \phi(\underline{r}) dV \quad , \tag{2.29}$$

the node-averaged production rate density

$$\langle \nu \Sigma_F \phi \rangle_I = \frac{1}{V_I} \int_{V_I} \nu \Sigma_F(\underline{r}) \phi(\underline{r}) dV \quad , \tag{2.30}$$

and the internodal coupling coefficient

$$T_{IJ} = \frac{V_J}{V_I} \frac{\int_{V_I} \int_{V_J} G(\underline{r},\underline{r}') \nu \Sigma_F(\underline{r}') \phi(\underline{r}') dV' dV}{\int_{V_J} \nu \Sigma_F(\underline{r}') \phi(\underline{r}') dV'} \quad . \tag{2.31}$$

In the model adopted in this study, no spatial variations of the material properties within

one fuel element were considered and all nodal volumes are equal, which reduces the expression for T_{IJ} to

$$T_{IJ} = \frac{\int_{V_I} \int_{V_J} G(\mathbf{r}, \mathbf{r}') \phi(\mathbf{r}') dV' dV}{\int_{V_J} \phi(\mathbf{r}') dV'}$$

(2.32)

Using these expressions for the nodal averages, Eq.(2.28) can be condensed to

$$\langle \phi \rangle_I = \lambda \sum_{J=1}^{N} T_{IJ} \langle \nu \Sigma_F \phi \rangle_J$$

(2.33)

The coupling coefficient T_{IJ} defined here is related to the probability that a fast neutron 'born' in cell J will eventually be captured or downscattered in cell I. However, performing dimension analysis on Eq.(2.33) yields that T_{IJ} cannot be dimensionless, and thus cannot be considered an exact probability. However, if both sides of Eq.(2.33) are multiplied with $<\Sigma_R \phi>_I / <\phi>_I$, we obtain

$$\langle \Sigma_R \phi \rangle_I = \lambda \sum_{J=1}^{N} P_{IJ} \langle \nu \Sigma_F \phi \rangle_J$$

(2.34)

with the elements of the matrix **P** defined by :

$$P_{IJ} = \frac{T_{IJ}}{\langle \phi \rangle_I} \langle \Sigma_R \phi \rangle_I$$

(2.35)

Obviously, Eq.(2.34) can be interpreted as a balance equation, in which the P_{IJ} are dimensionless quantities. In the calculational core models developed in this study, a generally applied approximation is to disregard variations in nuclide densities within the square nodes representing the fuel elements. This means that products like $<\Sigma_R \phi>_I$ can simply be written as $\Sigma_{R,I} <\phi_I>$. Further, for reasons of notational simplicity the brackets indicating that one works with nodal averages will from now on be omitted in this chapter, as well as in the rest of this thesis. In order to argue that the P_{IJ} can be regarded as *diffusion probabilities*, we should consider the sum of both sides of Eq.(2.34) over all node cells I :

$$\sum_{I=1}^{N} \Sigma_{R,I} \phi_I = \lambda \sum_{I=1}^{N} \sum_{J=1}^{N} P_{IJ} \nu \Sigma_{F,J} \phi_J$$

(2.36)

Assuming that, in the dynamic equilibrium effected by the λ-reset, no neutrons leak from the system under consideration (for example, a system containing a core and a sufficient number of water nodes surrounding the core), the total fast neutron removal rate should exactly match the fast neutron production rate multiplied by the λ-eigenvalue :

$$\sum_{I=1}^{N} \Sigma_{R,I} \phi_{1,I} = \lambda \sum_{J=1}^{N} v \Sigma_{F,J} \phi_{1,J} \tag{2.37}$$

Combining Eqs.(2.36) and (2.37) yields that the P_{IJ} must have the property

$$\sum_{I=1}^{N} P_{IJ} = 1 \quad \forall J \tag{2.38}$$

Thus, the P_{IJ} are really dimensionless probabilities, and an individual element P_{IJ} (alternative notation : $P_{I\leftarrow J}$) can be interpreted as the probability that a fast neutron 'born' in node J is eventually captured or downscattered in node I. In a PWR, the removal probabilities are mainly determined by downscattering of fast neutrons to the thermal energy group via collisions with hydrogen nuclei. The downscattering cross section $\Sigma_{1\rightarrow 2}$ is almost perfectly uniform and time-independent, as the concentration of the only material significantly contributing to $\Sigma_{1\rightarrow 2}$ (that is, H_2O) is, naturally, burnup-independent (In reality, this concentration is not strictly uniform as the temperature distribution in the core is not uniform. This effect, which requires thermal-hydraulic analysis for a realistic description, is assumed to be small and is not considered). Further, the variations in the fast absorption cross sections due to burnup are very small compared to the total values of the nodal removal cross sections. Hence, the effect of burnup in the kernel equation can be nearly fully described by the changes in the fission cross sections and, thus, by the changes in the node-averaged infinite multiplication factors.

Using the 1½-group nodal Green's kernel method as described here enables one to nicely reconstruct the diffusion theory core physics in the sense that the ordering of different core configurations in terms of the eigenvalue λ and the power peaking factor f is well-preserved. This is indicated in Fig.2.6 and Fig.2.7. As expected, the numerical results for the power peaking factor reconstruction indicate that for patterns featuring high power peaking, solving the diffusion equation yields a higher power peaking factor than solving the kernel equation. This is caused by the inherent property of the kernel method that it does not account for *tilts* in the intranodal power distributions. The interesting aspect of this property is that for patterns featuring high power peaking, a very accurate reconstruction of the power peaking factor is not that relevant since they will not be feasible anyway. A description of how the diffusion probabilities could be obtained numerically can be found in appendix A. For a calculationally efficient solution of the kernel equation

$$\Sigma_{R,I} \phi_I = \lambda \sum_{J=1}^{N} P_{I\leftarrow J} v \Sigma_{F,J} \phi_J \tag{2.39}$$

it is very convenient to define neighbour regions for each individual node I containing only the neighbouring nodes from which a significant contribution in the summation on the right part of Eq.(2.40) is received. Naturally, the number of neighbour nodes contained in such a region depends on the size of the nodes with respect to the fast diffusion length L_1, and on the criterion determining when a contribution is not considered relevant anymore. In practise, when the set of diffusion probabilities $\{P_{I\leftarrow J}; I,J \in \{1,...,N\}\}$ is known, a

neighbour region for node I can be defined as $\Omega(I)=\{J \in \{1,...,N\} | P_{I \leftarrow J} \geq \varepsilon\}$ with ε the selection criterion (for example, $\varepsilon=0.0001$). For the core geometry considered in this study, the neighbouring regions for central nodes contain 37 nodes (including, of course, the central node itself) for the convergence criterion=0.00005.
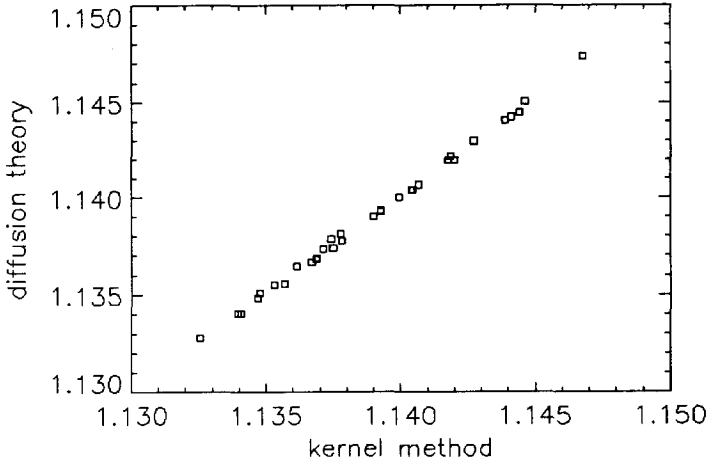

Fig.2.6   Correlation of the values of the uncontrolled multiplication factors found by solving the finite difference diffusion equation and solving the nodal kernel equation, respectively.
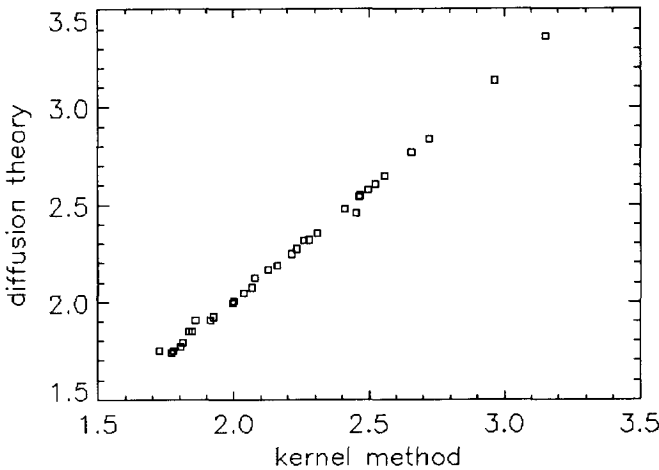

Fig.2.7   Correlation of the values of the power peaking factors found by solving the finite difference diffusion equation and solving the nodal kernel equation, respectively.

31

2.3 Equilibrium Cycle Optimization

Since nuclear reactors are operated for multiple successive fuel cycles, a reasonable way to evaluate reload patterns is, as argued in section 1.2.5, to consider their performance in the case of an *equilibrium cycle* [De Jong 1995, Van Geemert 1996, Van Geemert 1997, Van Geemert 1998]. The equilibrium cycle associated with a reload pattern is defined as the limit fuel cycle that eventually emerges after multiple successive periodic refueling with the same reloading pattern. The reload operation can be specified by a square binary matrix **X**. The elements of **X** are defined by :

$$X_{IJ} = 1 \quad \text{if the fuel bundle that has resided in node J is located in}$$
node I after reloading
$$0 \quad \text{otherwise}$$

If $\Sigma_I X_{IJ}=0$ then obviously the fuel bundle which has resided in node J is to be discharged. If $\Sigma_J X_{IJ}=0$, then apparently none of the older fuel bundles which were already present in the core will be placed in node I. In that case a fresh fuel bundle will be placed in node I. If the fuel bundles are characterized by their nuclide density vectors, the invariance of the equilibrium cycle with respect to the reload operation can be mathematically defined as :

$$N_I^{(equi)}(0) = \sum_{J=1}^{N} X_{IJ} \, N_J^{(equi)}(T) + \left(1 - \sum_{J=1}^{N} X_{IJ}\right) N_{fresh} . \tag{2.40}$$

in which N denotes the number of fuel assembly positions. The equilibrium cycle can be determined iteratively using this invariance condition.

Actually, reload schemes for N-node systems featuring n age groups for the fuel bundles (batches) lead to N/n fuel bundle life history trajectories which represent the sequences of nodes which act as hosts for a particular fuel bundle. The collection of all such history trajectories can be a convenient representation of the associated reload pattern. A handy notation for such a representation is

$$H = \left\{ \begin{matrix} i_1^{(1)} & i_2^{(1)} & i_3^{(1)} & \cdots & i_n^{(1)} \\ \cdot & \cdot & \cdot & \cdot & \cdot \\ \cdot & \cdot & \cdot & \cdot & \cdot \\ i_1^{(N/n)} & \cdots & \cdots & \cdots & i_N^{(N/n)} \end{matrix} \right\} \tag{2.41}$$

The first row of H denotes the first fuel bundle life history trajectory :

$$\text{fresh fuel bundle} \rightarrow \text{node } i_1^{(1)} \rightarrow \text{node } i_2^{(1)} \rightarrow \cdots \text{node } i_n^{(1)} \rightarrow \text{discharge} \tag{2.42}$$

In this denotation, each arrow represents a shuffling operation, as is indicated in Fig.2.8. The unit elements in the binary shuffling matrix **X** associated with H follows from

$$X_{i_m^{(0)}, i_{m+1}^{(0)}} = 1 \text{ for all } m = 1,...,n-1 \text{ , } j = 1,...,\frac{N}{n} \text{ .} \qquad (2.43)$$
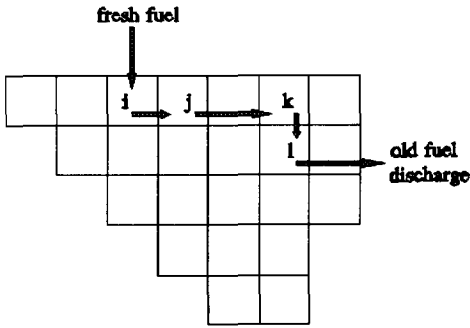

fresh fuel

old fuel
discharge

Fig.2.8   Graphical illustration of how a
fuel element is positioned from
one place to the other during its
lifetime trajectory

A simulation module has been develo-
ped in which the equilibrium fuel cycle
from BOC to EOC is determined iterative-
ly using the nodal 1½-group model des-
cribed in this chapter. All nuclide types
occurring in Fig.2.4 are present in the
calculations. The fuel cycle is divided in a
number of equally long intervals during
which the nodal fluxes are assumed con-
stant (in conformity with the **quasi-static
approximation**). Starting with an initial
nuclide density field, the corresponding
initial fast flux distribution is calculated
by iteration, and normalization with res-
pect to the total core power, and the
effective multiplication factor of the core
is calculated. Then the depletion equations
are solved and the changes in the nuclide densities are calculated. The nuclide density
field at the end of the time interval determines the nodal macroscopic cross sections
required for the fast flux distribution calculation for the next interval. This sequence is
continued until the EOC is encountered, after which a reload operation is applied, yiel-
ding the initial nuclide density field for the *next* fuel cycle. These calculations are conti-
nued until sufficient convergence to an equilibrium cycle has been achieved.

Thus, the simulation module features the following forward algorithm to evaluate the
equilibrium cycle performance of some specific reload operator **X** :

#1   The initial nuclide density field $\{\underline{N}(m=1,h=1\}$ for the first step (m=1) of the
h^{th} cycle is known.
m := 0
#2   m := m + 1
The initial nuclide density field $\{\underline{N}(m,h)\}$ for the mth step of cycle h is known.
Now, the nodal macroscopic cross sections are determined by :

$$\text{all } \Sigma_{I,g,m} = \sum_{q=1}^{(nn)} N_{I,q,m} \, \sigma_{q,g} \qquad (2.44)$$

with the indices q and g indicating different nuclide and process types, respec-
tively. These nodal cross sections are used in the kernel relation to perform an
iterative calculation of the fast flux distribution :

33

with the indices q and g indicating different nuclide and process types, respectively. These nodal cross sections are used in the kernel relation to perform an iterative calculation of the fast flux distribution :

$$\phi_I = \frac{\lambda}{\Sigma_{a1,I} + \Sigma_{1-2,I}} \sum_{J=1}^{N} P_{I-J} \nu \Sigma_{F,J} \phi_J \qquad (2.45)$$

in which the fast fluxes are normalized such that

$$w_f \sum_{I=1}^{N} \Sigma_{F,I} \phi_I = P_c \qquad (2.46)$$

which represents the requirement of a constant power level during operation of the reactor. The prefactor w_f represents the energy released per fission.

#3   Then the analytical solution of the depletion equations with constant $\{\phi\}$ is used to calculate the changes in the nuclide densities, yielding the nuclide densities vectors at the end of the mth time step :

$$\underline{N}_I((m+1)\,\Delta t, h) = \exp\left(B_I^{(m)}\,\Delta t\right) \underline{N}_I(m\,\Delta t, h) \, , \forall I \in \{1, ..., N\} \quad (2.47)$$

with $n\Delta t = T$, the total cycle length.

#4   If m < n go to #2 (n is the total number of time steps in which one fuel cycle is divided).

If m = n perform the reload operation :

$$\underline{N}_I(1, h+1) = \sum_{J=1}^{N} X_{IJ} \, \underline{N}_J(\frac{T}{n}\Delta t, h) + \left(1 - \sum_{J=1}^{N} X_{IJ}\right) \underline{N}_{fresh} \quad \forall I \quad (2.48)$$

and increment h :

h := h + 1

#5   if the hth nuclide density field iterand $\underline{N}(1,h)$ does not sufficiently resemble its predecessor $\underline{N}(1,h-1)$, go to #2

2.4 Representation of the reload pattern solution space by a set of pseudo-randomly generated candidates

In chapter 1, it is argued that in order to evaluate the 'quality' of a reloading scheme, one should not study the associated fuel economy for only the forthcoming cycle. Instead, some method should be available to gain some indication about the scheme's *multi-cycle* performance, knowing that for example a high total core burnup of the forthcoming cycle might prevent the following cycles from being economical. The easiest and most obvious multi-cycle evaluational method is to study the *equilibrium cycle* behaviour. An easy and convenient method for gaining information about the objective and constraint function value ranges is to evaluate

the equilibrium cycle characteristics of a large number of fully randomly generated candidate loading schemes. In this way, some insight can be acquired into what values of the objective and constraint functions are normal, and what can be gained by optimization. Further, good solutions can be extracted from the random sample which may serve as starting points for the more sophisticated heuristic search procedures discussed in chapter 3. The random sample can be viewed as a *representation* of the solution space in terms of performance and constraint parameters. In other words, the collection of performance and constraint parameters can be regarded as a *projection* of the solution space on the performance and constraint parameter space. In Fig.2.9, an example is shown of a random sample of 2000 reload patterns for the large test PWR core shown in Fig.2.1 and Fig.2.2. Obviously, this sample is projected on the two-dimensional performance plane spanned by $k^{(uc)}_{eff}(EOC)$ and the power peaking factor. As indicated, the power peaking constraint $f_{lim} \leq 1.8$ can be represented by a horizontal line, and it turns out that in fact this constraint is violated by the majority of the randomly generated candidate schemes. The operational constraint $k^{(uc)}_{eff}(EOC) \geq 1$ can be represented by the vertical line crossing the horizontal axis at the value 1. Violation of this constraint would mean that the target cycle time would be infeasible since the core would become subcritical before the end of the cycle is reached.

As discussed in section 1.2.3, no ordering principle exists for the reloading schemes or, in other words, it is not possible to map the solution space into regions (of comparable performances) which can be easily defined in terms of the variables of the reload operator. However, it seems that it is possible for equilibrium cycles to establish some rough link between the shape of the power distribution and the equilibrium cycle fuel economy. Utilizing a simplified but elegant analytical model [De Jong 1995], it can be shown that equilibrium cycles are generally more economical when they are characterized by power distribution shapes which are flat with regard to both space and time. Via Haling's theorem (stating that an operation cycle's total maximal power peaking factor during the cycle is minimal in the case of a constant power distribution shape) this general correlation can be translated into the following rough property : loading schemes, which are economical in terms of the equilibrium cycle, generally give rise to rather constant and flat power distributions which thus yield rather low maximal power peaking factors.

Obviously, knowledge of the existence of this general correlation does not reduce the complexity of the *loading pattern* optimization problem in any way since it seems virtually impossible to establish an easy mathematical relationship between the way in which the core is configured and the resulting time-dependent power distributions (interesting attempts in this direction are reported in [De Jong 1992]). Two extreme examples of loading pattern types, depicted in Figs.2.10 and 2.11 are the Centre-to-Outside (COL) loading and the Outside-to-Centre loading (OCL). In the case of COL loading, the fresh fuel assemblies are placed in the centre of the core, whereas the burnt fuel assemblies will be placed closer to the periphery as their burnup increases. In the case of OCL loading, the reverse happens. Generally, in the equilibrium situation they will both give rise to non-optimal operation cycle behaviour with an additional unacceptably high power peaking factor in the COL case. In

35

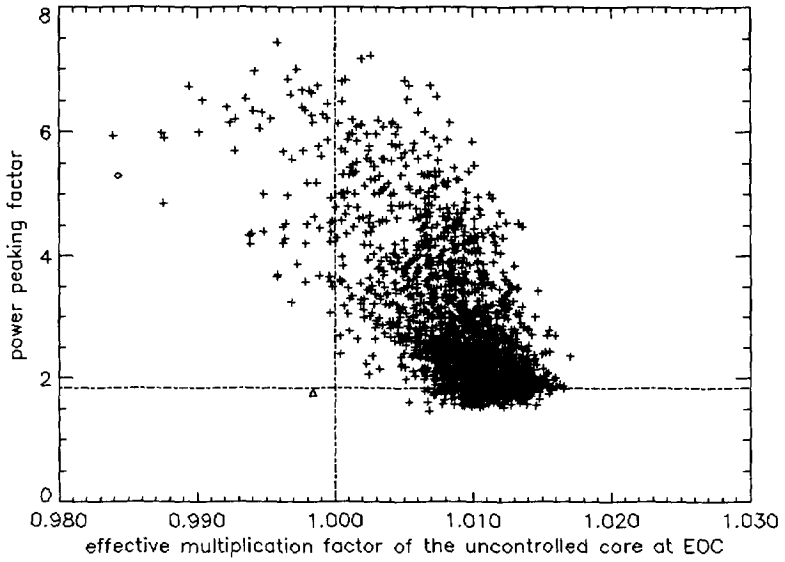applied in this study for handling the loading pattern optimization problem.

Fig.2.9 A random sample of reload patterns for the test core of Fig.2.1.
The diamond and the triangle denote the COL and the OCL
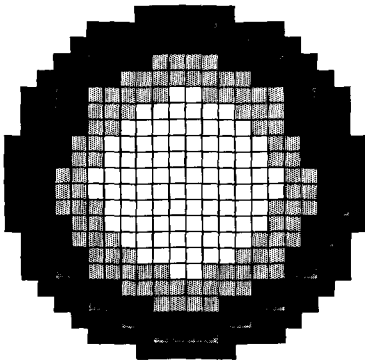patterns illustrated in Fig.2.10 and Fig.2.11, respectively.

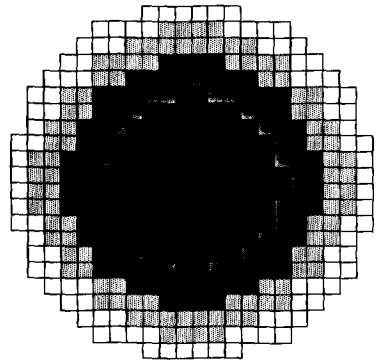Fig.2.10 A Center-to Outside Loading
structure

Fig.2.11 An Outside-to-Center Loading
structure

36

References

[Almenas 1992] K. Almenas, R. Lee, "Nuclear Engineering - An Introduction", Springer-Verlag, New York Berlin Heidelberg, USA (1992).

[Bennewitz 1975] F. Bennewitz, H. Finneman, H. Moldaschl, "Solution of the Multidimensional Neutron Diffusion Equation by Nodal Expansion", *Proceedings of the Conference on Computational Methods in Nuclear Engineering*, CONF-750413, P.1, Charleston, USA (1975).

[Chao 1987] Y.A. Chao, J.A. Penkrot, "Diffusive Homogeneity - the Principle of the Superfast Multidimensional Nodal Code SUPERNOVA", *Transactions of the American Nuclear Society* **55**, pp. 583-584 (1987).

[De Jong 1995] A.J. de Jong, "Reload Pattern Optimization for Batch Refuelled Nuclear Reactors", *report IRI-131-95-010*, Interfaculty Reactor Institute, Delft University of Technology, Delft, The Netherlands (1995).

[Duderstadt 1976] J.J. Duderstadt, L.J. Hamilton, "Nuclear Reactor Analysis", John Wiley & Sons, New York (1976).[De Jong 1992] A.J. de Jong, "In-Core Fuel Management Optimization by Varying the Equilibrium Cycle Average Flux Shape for Batch Refuelled Reactors", *report IRI-131-92-008*, Delft (1992).

[Finneman 1977] H. Finneman, F. Bennewitz, M.R. Wagner, "Interface Current Techniques for Multidimensional Reactor Calculations", *Atomkernenergie* **30**, 123 (1977).

[Hoogenboom 1996] J.E. Hoogenboom, P.F.A. de Leege, J.L. Kloosterman, "Application of Dynamic Pseudo Fission Products and Actinides for Accurate Burnup Calculations", *Proceedings of the International Conference on the Physics of Reactors*, C.31-38, Mito, Japan (1996).

[Isbin 1963] H.S. Isbin, "Introductory Nuclear Reactor Theory", Reinhold Publishing Corporation, New York (1963).

[ORNL] "SCALE-4.2, A Modular Code System for Performing Standardized Computer Analyses for Licensing Evaluation", Oak Ridge National Laboratory.

[Smith 1985] K.S. Smith, D.M. Ver Planck, M. Edenius, "QPANDA : An Advanced Nodal Method for LWR analyses", *Transactions of the American Nuclear Society* **44**, 265 (1983).

[Van Geemert 1996] R. van Geemert, A.J. Quist, J.E. Hoogenboom, "Reload Pattern Optimization by Application of Multiple Cyclic Interchange Algorithms", *Proceedings of the International Conference on the Physics of Reactors*, I.38-47, Mito, Japan (1996).

[Williams 1979] M.L. Williams, "Development of Depletion Perturbation Theory for Coupled Neutron/Nuclide Fields", Nuclear Science & Engineering **70**, 20-36 (1979).

Chapter 3

The Multiple Cyclic Interchange Approach

3.1 Introduction

As argued in chapter 1, the reload pattern optimization problem is characterized by a number of very unpleasant features such as non-linearity, non-convexity, a very implicit and difficult form of the objective function and a total lack of any ordering principle in an almost astronomically large solution space. This is why, during the past two decades, search algorithms have been applied that do not require any gradient information and which are known to perform well in large combinatoric optimization problems. Well-known examples of these are Simulated Annealing (SA) [Parks 1990, Kropaczek 1991, Verhagen 1993, Šmuc 1994, Stevens 1995, Van Geemert 1996] and Genetic Algorithms (GA) [Axmann 1997, DeChaine 1996, Poon 1993, Parks 1996].

In this chapter, a number of alternative reload pattern optimization procedures are proposed that are fundamentally based on the multiple cyclic interchange approach, according to which the search for the reload pattern associated with the highest (or lowest) objective function value can be thought of as divided in multiple stages. The transition from the initial to the final stage is characterized by a decrease in the magnitudes of the considered reload pattern changes. The general idea is that, during the first stages, the "elite" cluster containing the group of best patterns must be located, after which the solution space is sampled in a more and more local sense to find the local optimum in this cluster. The transition(s) from global search behaviour to local search behaviour can be either prompt, by defining strictly separate search regimes, or gradual by introducing stochastic tests for the number of fuel bundles involved in a cyclic interchange. Equilibrium cycle optimization results are reported for test PWR reactor cores of three different sizes.

Further, an optimization method is proposed featuring the implementations of ideas that are characteristic for both SA and GA. In this method, called the Population Mutation Annealing (PMA) method, it is attempted to incorporate the advantageous features of both SA and GA, while removing the disadvantageous features of both methods.

3.1.1 The Multiple Cyclic Interchange Approach

The approaches developed in this chapter consist of the use of multiple cyclic interchange algorithms [Van Geemert 1996, Van Geemert 1998], in which the search for the reload pattern associated with the lowest objective function value can be thought of as divided in multiple stages. The cyclic interchange procedures used can be classified in groups according to the degree of locality or globality of the procedures. This degree is determined by the number of fuel assemblies involved in one cyclic interchange and by the way in which candidate patterns are generated between each acceptance decision. Local search algorithms are based on assessing all possible modest changes (for example,

39

pairwise interchanges of fuel assemblies) in one search step and searching the best pattern by successive local improvements, until no improvement is found. In global search algorithms, larger changes are considered in similar search procedures. It is obvious that an intermediate regime of algorithms exists in which the algorithms are neither local nor global because of their intermediate locality degree. For a special class of global search algorithms, the search consists of the generation of random trajectories in the reload pattern space (by successive application of cyclic shuffling schemes in which the fuel assemblies involved are chosen randomly), starting from successively improved reference patterns. Obviously, this is different from the consideration of, for example, all possible binary permutations to find a new reference pattern. All patterns in such a trajectory are evaluated, yielding a best pattern that becomes the new reference pattern if its associated function value is higher (or lower) than the highest (or lowest) value found in the previous trajectory. This procedure terminates when no improvement is found. When applying only a local search algorithm of this type, the quality of the best pattern found generally depends on the quality of the initial, "trial" reload pattern because of the intrinsic high probability of getting stuck in a local extremum when accepting only improved patterns as new reference patterns.

The concept of *distance* for reload patterns can be defined in terms of differences between the BOC reactivity distributions. The *degree of dissimilarity* D_{XY} [Parks 1996] between two loading patterns **X** and **Y** can be mathematically defined as

$$D_{XY} = \frac{1}{N} \sum_{I=1}^{N} \left(k_I^{(X)} - k_I^{(Y)} \right)^2 \tag{3.1}$$

with the k's indicating the node-averaged multiplication factors. Obviously, the distribution of the k's is determined by the choice of the loading pattern. A *cluster* of reload patterns surrounding a specific pattern can be thought of as the collection of patterns that are close to this specific pattern in terms of this distance concept.

A global search can be regarded as an attempt to *locate* the 'cluster' in reload pattern space that contains the near-optimal patterns, and, hopefully, the optimum pattern. When such a cluster has been located by the termination of a global search in a pattern that is embedded within this cluster, a local search (for example, by applying a pairwise interchange optimization algorithm) can be performed to search for the best pattern within this cluster. A very simple example of this concept is the case where a random sample of reload patterns is evaluated to supply a good trial pattern for initiating a pairwise interchange optimization procedure. Another possibility is the application of a stochastic search concept, leading to a Simulated Annealing approach [Parks 1990, Kropaczek 1991, Van Geemert 1996] in which the transition from global search behaviour to local search behaviour becomes more or less gradual. This gradual transition is effected by the introduction of a stochastic test determining whether a newly examined reloading scheme is accepted as a new reference scheme. Finally, a stochastic search concept is proposed which can be denoted as a "population mutation annealing" approach. The general idea of this method is to combine the advantageous properties of genetic algorithms and the simulated annealing algorithm in one method, and simultaneously filter out the disadvantageous characteristics of these algorithms.
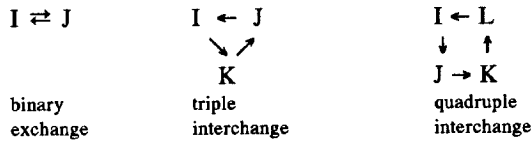
From the results obtained in this study, it can be concluded that all of the search concepts discussed in this chapter, featuring intelligent global to local search behaviour transitions, constitute a robust and reliable reload pattern design procedure.

3.2 Definition of the proposed optimization procedures

3.2.1 Local Cyclic Interchange Search Procedures

In the local cyclic interchange search procedures proposed, all $C(N,n) = N!/(N-n)!n!$ possible n-fold fuel bundle interchanges in the reference pattern are considered to see whether such interchanges yield improvements, and, if so, the best interchange yielding a pattern still satisfying the power peaking constraint is applied, yielding a new reference pattern. Obviously, the changes in terms of Parks's distance concept discussed in section 3.1.2 will be small for modest values of n and for this reason these procedures can, in case of small n, be called local. These search schemes can be successively applied until none of the interchanges yields an improvement. The interchanges applied are *cyclic*. We can, for example, distinguish between binary (pairwise) interchanges, triple or quadruple cyclic interchanges, respectively :

$$I \rightleftarrows J \qquad \begin{array}{c} I \leftarrow J \\ \searrow \nearrow \\ K \end{array} \qquad \begin{array}{c} I \leftarrow L \\ \downarrow \quad \uparrow \\ J \rightarrow K \end{array}$$

| binary | triple | quadruple |
| exchange | interchange | interchange |

In Fig.3.1, a logical flow structure diagram of the procedure is given. In this diagram, the ith reference reload pattern is denoted as H_i, and its corresponding objective function value as $z(H_i)$; the permutation operator associated with the jth considered n-fold cyclic interchange is denoted as $P_j^{(n)}$. Obviously, these procedures have a polynomial time behaviour, since the total calculational time required is directly proportional to $C(N,n)$, which is a polynomial function of N for fixed n. The simplest and most widely used variant is the one for the case $n=2$, and is better known as the *pairwise interchange optimization* algorithm. Needless to say, the total calculational time required also very much depends on the quality of the initial, starting pattern. If, for example, the procedure is started from a local extremum (defined as a local extremum in the sense that none of the $C(N,n)$ interchanges yields an improvement), the procedure will already terminate after one 'sweep'.

3.2.2 Global Random Chain Search Algorithms

It is obvious that a local cyclic interchange algorithm, allowing only changes in the pattern that yield a decrease in the objective function value, might very well cut off search paths that actually lead to the region where the global optimum is to be found. A major obstacle for finding a very good reload pattern from an arbitrary starting pattern is the *power peaking constraint* (PPC). As indicated in Fig.2.9, the majority of randomly chosen reload patterns generally do not satisfy a reasonably chosen PPC. It is to be expected that

41

an initial pattern featuring a rather high power peaking factor cannot possibly result in a loading candidate satisfying the PPC due to only a minor cyclic permutation of fuel elements. In order to overcome this problem, a *global search* should be performed first, enabling the local search procedure to start in a pattern which is already very good in terms of the objective function and which does satisfy the PPC. In a
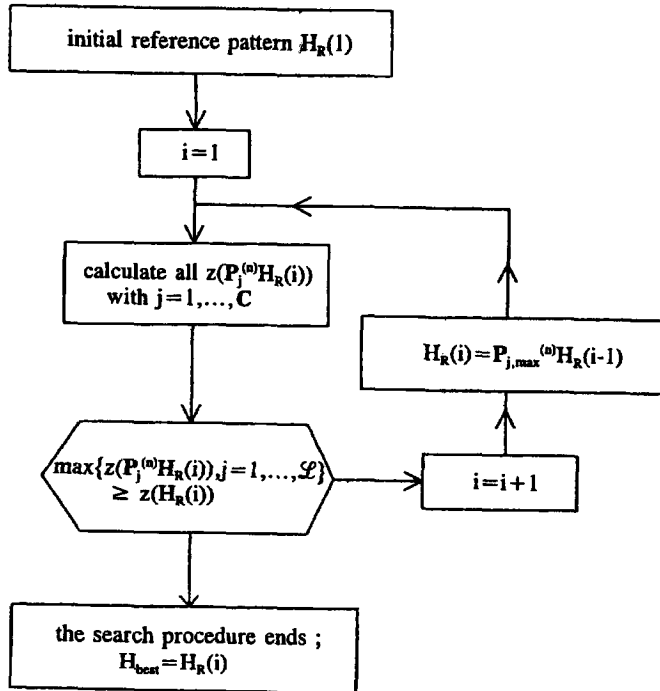

Fig.3.1   Logical flow structure diagram of a local cyclic interchange maximization procedure ; H denotes a reload pattern and $\mathbf{P}^{(n)}$ an n-fold permutation operator.

global search procedure as proposed here, a large number of successive random cyclic interchanges $\mathscr{L}$ are performed in one search step, thus generating a random search chain of $\mathscr{L}$ reload patterns. Of all the patterns generated in the chain, the best pattern is selected as the reference pattern for the next search step. This global search procedure ends when none of the reload patterns generated in the chain gives an improvement with respect to the best pattern found in the previous chain. In this procedure, indicated in Fig 3.2, the initial reference pattern may be chosen arbitrarily. The set of n-fold cyclic permutators $\{\mathbf{P}_j^{(n)}, =1,...,\mathscr{L}-1\}$ generating a random chain $\{H_1,H_2,...,H_{\mathscr{L}-1},H_{\mathscr{L}}\}$ of $\mathscr{L}$ reload patterns by successive random permutations, is chosen fully randomly. Hence, each chain is related to

the reference pattern at the start of the search step by :

$$H_q = \prod_{j=1}^{q} P_j \, H_{initial} \quad , q = 1,\dots,\mathscr{L} \ . \tag{3.2}$$

We note that $P_1^{(a)}=1$, so $H_1=H_R(1)$. In this global search it is recommendable to choose the chain length for the next search steps to be smaller than the chain length used in the first search step, for calculation economy purposes. This is justified since the first search step should yield a good pattern for the following search chains to depart from, whose quality will be less inferior to the quality of the patterns in the elite cluster than the initial trial pattern's quality.
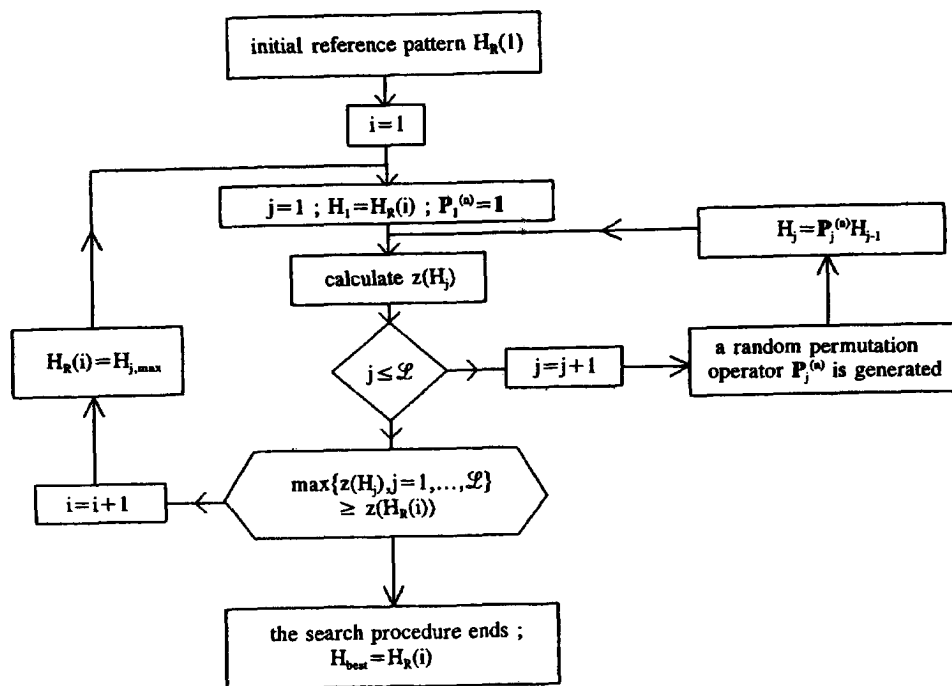

Fig.3.2   Logical flow structure diagram of the global chain search maximization procedure ; H denotes a reload pattern and **P** a permutation operator.

3.2.3 Stochastic Multiple Cyclic Interchange Optimization Procedures

These methods consist of a Simulated Annealing (SA) approach [Parks 1990, Kropac-zek 1991, Verhagen 1993, Šmuc 1994, Stevens 1995, Van Geemert 1996] in which the transition from global to local search behaviour becomes more or less gradual. The gradual nature of this transition is realized by the introduction of a stochastic test determi-

ning whether a newly examined reloading scheme is accepted as a new reference scheme. The SA approach is generally initiated with the definition of an initial reference pattern H_1, after which one randomly permutes a stochastic number N of fuel assemblies and assesses the effect of this permutation on the objective function value. The number N of fuel assemblies involved in the permutation can be chosen to be stochastic in the sense that it obeys a Boltzmann-like probability distribution tending to gradually favour lower values of N as the search procedure proceeds. In SA, an improvement is generally effected by a *decrease* in the objective function value, in analogy with minimization of the potential energy. For each search step i, N_i is determined by :

$$N_i(r_i) = 2 + int [(N_{max} - 1) \cdot min \{ exp (- \frac{z_{best,i-1} - z_i}{T_{i-1}}) , r_i \}]$$ (3.3)

The input variable r_i is obtained from a random number generator producing random numbers that are uniformly distributed on the interval $[0,1)$; $z_{best,i-1}-z_i$ is the best function value improvement found sofar with respect to the function value associated with the initial, "trial" pattern. Thus, Eq.(3.3) represents a *probability distribution*. The annealing temperatures T_i are determined by the initial annealing temperature T_1 and by the recurrence relation $T_i = \alpha T_{i-1}$, with the "cooling parameter" α a number between 0 and 1 (typically, $0.995 < \alpha < 1$). Obviously, in an early stage of the search procedure, when the annealing temperature is still high, N_i will be uniformly distributed between 2 and N_{max} (such as is the case in Fig.3.3 for $N_{max} = 10$) ; as the procedure proceeds, the probability that more than two fuel bundles are involved in the cyclic interchange decreases (Fig.3.4).
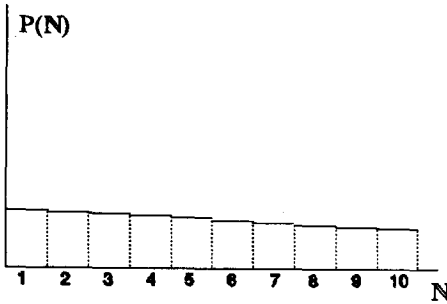

Fig.3.3   Probability distribution for N at a relatively high annealing temperature
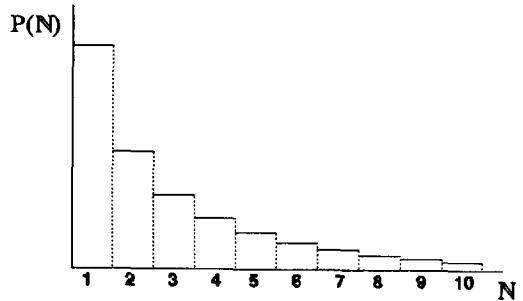
Fig.3.4.   Probability distribution for N at a relatively low annealing temperature

The newly generated pattern is accepted as the next reference pattern with acceptance probability

$$Pr_+ = min \{ exp [- T_i^{-1}(z_i - z_{i-1})] , 1 \}$$ (3.4)

This means that, if the permutation results in an improvement of the objective function value, the newly generated pattern automatically becomes the next reference pattern. In the case of a decrease, a random number a_i is generated, and a stochastic acceptance deci-

sion follows in which the newly generated pattern is rejected if $a_i > \exp[(z_i-z_{i-1})/T_i]$.

Satisfaction of the PPC by the final result can be achieved by the implementation of a technique called *bounds cooling* in the search procedure. According to this approach, the PPC can be made *temperature-dependent* such that the probability that a high PPF reload pattern is rejected increases with falling temperature, until it finally becomes practically unity near the end of the annealing process. This can be very simply achieved by application of the artificial, temperature-dependent PPC

$$p \leq f_{lim} + \alpha\, T_i \qquad\qquad (3.5)$$

instead of the hard PPC : $p \leq f_{lim}$. The constant α should be chosen such that, at $T=T_0$, none of the patterns can be rejected because of the PPC. The physical idea behind this is to gradually push the search process in the "direction" of the regions in the solution space where the PPC is satisfied.

At the heart of the simulated annealing method is an analogy with thermodynamics, as is illustrated in Fig.3.5. At high temperatures, the molecules of a liquid move freely with respect to one another. If the liquid is cooled slowly, thermal mobility is lost. The molecules are often able to line themselves up and form a pure crystal that is completely ordered over a distance up to billions of times the size of an individual molecule in all directions.
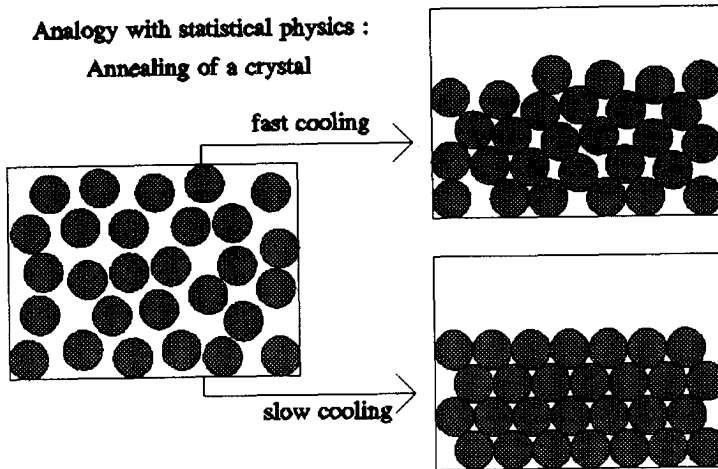
Fig.3.5 An annealing process in nature

This crystal is the state of minimum energy for this system. The amazing fact is that, for slowly cooled systems, nature is able to find this minimum energy state. In fact, if a liquid metal is cooled quickly or "quenched", it does not reach this state but rather ends up in a polycrystalline or amorphous state having a slightly higher energy. Thus, for ensuring that a low energy state is achieved, it is essential to cool *slowly*, allowing ample

45

time for redistribution of the molecules as they loose mobility. This is the technical defintion of *annealing*. The so-called Boltzmann probability distribution

$$P(E_i, T) = \frac{e^{-E_i/k_B T}}{\sum_j e^{-E_j/k_B T}}$$

(3.6)

expresses the idea that a system in thermal equilibrium at temperature T has its energy probabilistically distributed among all different energy states E_i.
Even at low temperatures, there is a chance, though very small, of the system being in a high energy state. Therefore, there is a corresponding chance for the system to get out of a local energy minimum in favour of finding a better, more global one. The quantity k_B (Boltzmann's constant) is a constant of nature relating temperature to 'freedom of change'. In other words, the system sometimes goes *uphill* as well as downhill ; but the lower the temperature, the less likely the occurrence of a significant uphill excursion.

3.2.4 Some results obtained by application of different search procedures

Starting from randomly chosen initial, poor-performing reload patterns that neither yield economical fuel use nor satisfy the power peaking constraint, we have searched for 4-batch reload patterns associated with the best equilibrium cycle behaviours for PWR test cores of three different sizes, containing 96, 224 and 384 fuel assemblies, respectively. The objective was to find the pattern yielding the highest $k_{eff}^{(uc)}(EOC)$ while satisfying the constraint that the power peaking factor remains below 1.8. Octant symmetry was enforced on the fuel distributions, and the following search methods or combinations of search methods were applied :

1   A successive random chain search with $\mathcal{L} = 2000$.

2   A multi-stage, global-to-local search method consisting of the successive application of method 1 with $\mathcal{L} = 2000$ and a binary interchange successive local improvement search.

3   A stochastic multiple cyclic interchange (simulated annealing) search with $N_{max} = 2$, initial annealing temperature $T_1 = 1.0$, cooling parameter $\alpha = 0.998$ and annealing chain length $\mathcal{L} = 5000$.

4   A stochastic multiple cyclic interchange (simulated annealing) search with $N_{max} = M$ ("total number of fuel elements in octant"), initial annealing temperature $T_1 = 1.0$, cooling parameter $\alpha = 0.998$ and annealing chain length $\mathcal{L} = 5000$.

The obtained objective and constraint function values for the three test PWR cores are listed in tables I, II and III, respectively. The fuel age distributions of the obtained final patterns are shown in Figs 3.6-17. In these distributions, the fuel burnup (or age) levels are proportional to the darkness in the different nodal colours. The final results found by all four applied search methods for the largest core, core 3, are plotted in terms of their

performance parameters in Figs. 3.18 along with a random sample cloud of 2000 random-
ly generated patterns for core 3.

TABLE I

List of obtained optimization results for PWR core 1

method	$k_{eff,EOC}^{(uc)}$	maximal power peaking factor
1	1.03382	1.7563
2	1.03497	1.7633
3	1.03613	1.7658
4	1.03502	1.7809

TABLE II

List of obtained optimization results for PWR core 2

method	$k_{eff,EOC}^{(uc)}$	maximal power peaking factor
1	1.0200	1.7764
2	1.0246	1.7785
3	1.0212	1.7424
4	1.0202	1.7658

TABLE III

List of obtained optimization results for PWR core 3

method	$k_{eff,EOC}^{(uc)}$	maximal power peaking factor
1	1.01524	1.6454
2	1.01868	1.5113
3	1.01619	1.6220
4	1.01612	1.7214

Fig.3.6 Fuel age distribution of the
best pattern found by search
method 1 applied to core 1

Fig.3.7 Fuel age distribution of the
best pattern found by search
method 2 applied to core 1

Fig.3.8 Fuel age distribution of the
best pattern found by search
method 3 applied to core 1

Fig.3.9 Fuel age distribution of the
best pattern found by search
method 4 applied to core 1
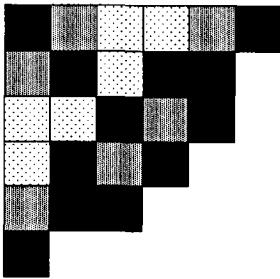

Fig.3.10 Fuel age distribution of the
best pattern found by search
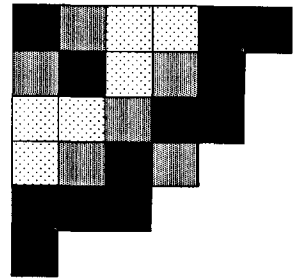method 1 applied to core 2

Fig.3.11 Fuel age distribution of the
best pattern found by search
method 2 applied to core 2

Fig.3.12 Fuel age distribution of the
best pattern found by search
method 3 applied to core 2

Fig.3.13 Fuel age distribution of the
best pattern found by search
method 4 applied to core 2

Fig.3.14 Fuel age distribution of the
best pattern found by search
method 1 applied to core 3

Fig.3.15 Fuel age distribution of the
best pattern found by search
method 2 applied to core 3

Fig.3.16 Fuel age distribution of the
best pattern found by search
method 3 applied to core 3

Fig.3.17 Fuel age distribution of the
best pattern found by search
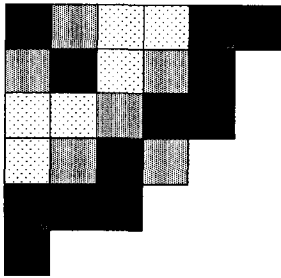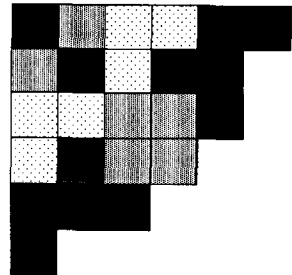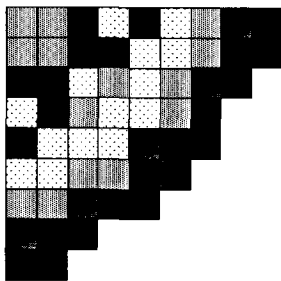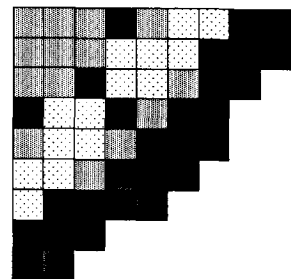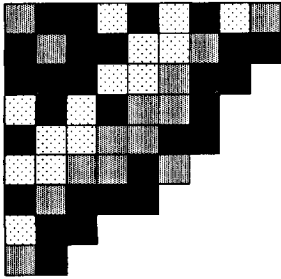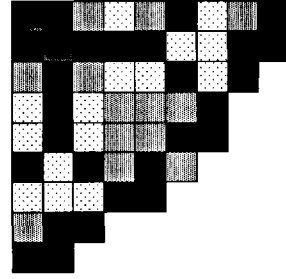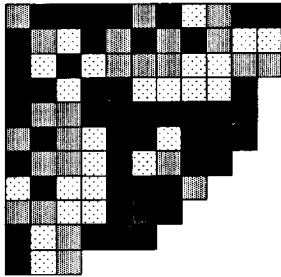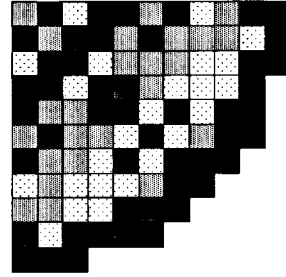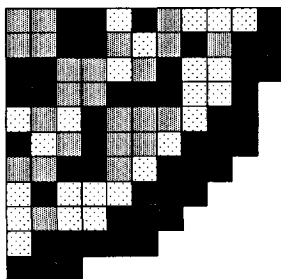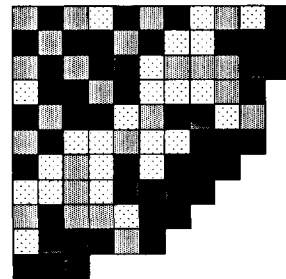method 4 applied to core 3

49
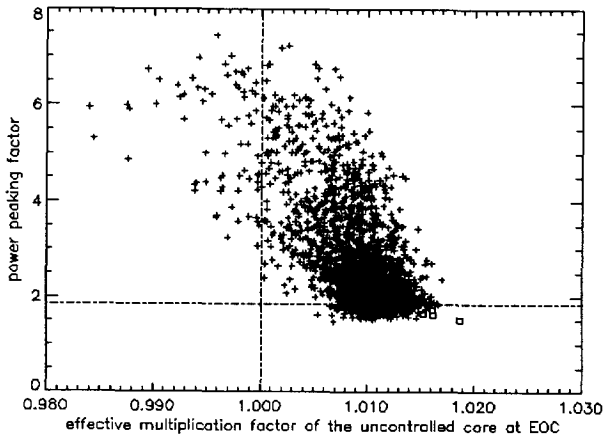
Fig.3.18 Plot of the search results listed in table III, along with a
sample of 2000 randomly generated patterns.

In conformity with what was argued in the introduction, the multi-stage global-to-local search method (method 2) yields the best result for most of the cases (except for the smallest core, core1, for which method 3 gave the best result). The patterns found by the methods 2 and 3 have equal fuel age distributions, but are different in the placement of the individual fuel assemblies within the fuel age groups. This indicates the importance of treating all fuel bundles individually in core loading pattern optimization.

3.3 The population mutation annealing algorithm

3.3.1 Ordering reload patterns in terms of selection probabilities

The results of the different types of heuristic search procedures discussed sofar seem to indicate that the solution space contains elite 'families' of patterns that are all very close to one another in terms of their (top) performances, though they may be very dissimilar in terms of the fuel assignments in the core. In other words, it is suspected that the optimum is quite 'flat', due to which the (theoretically present but untrackable) global optimum is not expected to be more than only marginally superior to the best result of the heuristic search algorithms. The search methods discussed in section 3.2 are generally characterized by the following property : after transition to local search stage, the search trajectory consists of a chain of successive candidate reload patterns that are correlated to one another in terms of their associated fuel age distributions. This almost automatically means that in the final search stage of all of these procedures it will be very likely that one will eventually get stuck in a local extremum *in the specific final search region.*

We would like to have a method available featuring a transition from global to local search behaviour without the necessity of performing this local final search in a specific

50

subregion of the solution space in terms of the fuel age distribution. A very interesting search approach in addition to the groups of search methods discussed in this chapter so far is the following stochastic search concept, which can be denoted as a "population mutation annealing" approach. The general idea of this method is to combine the advantageous properties of the GA and SA algorithms in one method, and simultaneously filter out the disadvantageous characteristics of these algorithms. It is generally known that both the advantage and disadvantage of GAs is that they effect general improvements in large *groups* (denoted as *populations* in terms of their biological analogon) of reload patterns, rather than to gradually search more and more locally along one Markov chain for the best *individual*, as is the case in the SA algorithm. This property can be considered an advantage as it enables one to gain insight into the heterogeneity of the 'elite' families of reload patterns in terms of the spatial fuel assignments. Basically, due to the inherent heterogeneity of the patterns in the population, the solution space sampling occurring during the search is in fact expected to consist of a large number of 'weak' local searches, which is good from a theoretical point of view. However, this property can also be considered a disadvantage since in the end one wants to really search locally within one or more elite clusters for the best pattern within the cluster. As in the SA approach (section 3.2.3), the concept of a decreasing temperature as a process parameter is adopted :

$$T_i = \alpha \, T_{i-1} \tag{3.7}$$

The method is started at a high annealing temperature $T_0=1$ and a randomly chosen initial reload pattern H_0. This pattern is evaluated, yielding the objective function value z_0, and the power peaking factor p_0. Like in the SA method, a "bounds cooling" technique can be applied to the power peaking constraint ; the temperature dependent constraint

$$p \leq f_{lim} + \beta \, T_i \tag{3.8}$$

is used instead of the 'hard' constraint

$$p \leq f_{lim} \tag{3.9}$$

Based on whether the 'hard' power peaking constraint is satisfied for the initial pattern, the value of the penalty parameter ζ_0 is

$$\zeta_0 = \begin{cases} 1 & \text{if } p_0 \geq f_{lim} \\ 0 & \text{otherwise} \end{cases} \tag{3.10}$$

Then, a certain number N_1 of randomly chosen elements in H_0 is permuted, yielding the second pattern H_1 for which z_1, p_1 and ζ_1 are determined as well. For obtaining H_2, a stochastic test determines if H_0 or H_1 is selected as the pattern that, after permutation of a certain number N_2 of randomly chosen elements, results in H_2. For generating the ith pattern H_i, a stochastic test is performed, resulting in one of the patterns H_0, H_1, ..., H_{i-1} to be selected and to serve as the pattern yielding H_i after permutation of N_i randomly chosen elements. In this test, the proposed probability that pattern H_m is chosen from the

51

collection $\{H_0, H_1, ..., H_{i-1}\}$ is defined as

$$P_m = \frac{\exp\left[\dfrac{z_m - z_{max}}{T_i} + \zeta_m\left(\dfrac{T_0}{T_i} - 1\right)\right]}{\displaystyle\sum_{j=1}^{i-1} \exp\left[\dfrac{z_j - z_{max}}{T_i} + \zeta_j\left(\dfrac{T_0}{T_i} - 1\right)\right]} \tag{3.11}$$

with $z_{max} = \max\{z_0, z_1, ..., z_{i-1}\}$ and the penalty parameter ζ_m defined as :

$$\zeta_m = \begin{cases} 1 & \text{if } p_m \geq f_{lim} \\ 0 & \text{otherwise} \end{cases} \tag{3.12}$$

In actually performing this stochastic test, a random number r_i with $0 < r_i < 1$ is generated and use is made of the *cumulative selection probability* function, defined as

$$\theta_m = \sum_{j=0}^{m} P_j \tag{3.13}$$

The stochastic test itself is performed as follows : if $\theta_{m-1} \leq r_i < \theta_m$ then the mth pattern H_m is selected as the 'input' pattern for permutation of the N_i randomly chosen elements. Since $\theta_m - \theta_{m-1} = P_m$, the probability of $\theta_{m-1} \leq r_i < \theta_m$ is directly proportional to P_m. This is exactly what we want with this test. In a time-dependent picture, one can compare this stochastic test with using a 'wheel of fortune' that gets more and more different radially oriented regions (corresponding with patterns) associated with selection outcomes. Of course, the total radial area of the wheel will remain constant. So the number of different regions is incremented with one after each emergence of a new pattern to be evaluated. At a high annealing temperature, the areas of the different regions on the wheel will be more or less the same. However, as the annealing temperature decreases the total area occupied by the 'better' regions (associated with the patterns that have high values of z and satisfy the hard power peaking constraint) will become larger and larger ! The proposed temperature dependence for the number N_i of elements to be permuted, is

$$N(T_i) = N_{min} + \text{int}\left[\left(N_{max} - N_{min} + 1\right) \cdot T_i\right] \tag{3.14}$$

with N_{min} generally chosen as a small number (preferably 2) and N_{max} chosen as a large number (For example : $N_{max} = N-2$, the total number of fuel elements in the system minus 2). If N_{max} is chosen close to N then the generated patterns will, notably in the early stages of the optimization process, be fully random : each pattern will be uncorrelated to its predecessor. We note that the expression (3.14) represents a temperature-dependent *function*, fixing N as a function of the annealing temperature, whereas the expression (3.3) used in the SA approach represents a probability *distribution*. The difference between Eq.(3.14) and Eq.(3.3) basically arises intuitively from the difference in search concept between SA and PMA. In SA, through implementation of the Metropolis acceptance test, a Markov chain is set up leading to a region in the search space that contains good soluti-

ons. Large pattern changes are generally effected by modes subsequent stochastic permutations. So in SA there will generally be relatively large correlations between a pattern and its successor and predecessor. According to this Markov chain search concept of SA, the magnitude of the permutations should not be fixed to large values in order to preserve the occurrence of clear correlations between a pattern and its successor and predecessor, and thus not to disturb the Markov chain concept too much. In the early stage of PMA, the idea is rather *opposite* : we wouldn't like a pattern to be too much correlated to its successor and predecessor to ensure global sampling in the "Wheel of Fortune" picture. So we would like to *guarantee* that, at the early stage, large changes are applied and that at the final stage, small changes are applied. This is why Eq.(3.14) prescribes a fixed N.

Patterns that do not satisfy the power peaking constraint are not allowed to enter the population. However, like in the SA method discussed in section 3.2.3, the *bounds cooling* technique can be applied to this constraint such that

$$p \leq f_{\lim} + \alpha \, T_i \tag{3.15}$$

at the ith evaluation step. Due to this, in the early stages of the process no patterns will be rejected because of their high power peaking factors, ensuring a rather uniform sampling of the search space at the start. The population mutation annealing process proposed here features continuous updating of the probability distribution that stochastically determines the selections of the input patterns for the mutations.

From the definition of the probability distribution (Eq.(3.11)), it can be seen that, at the start of the optimization procedure, featuring the high annealing temperatures $T \approx T_0$, each pattern will have approximately the same selection probability. Also at the high annealing temperatures at the start, the influence of the penalty term in the exponent will be negligible. However, at the extremely low annealing temperatures near the end of the procedure, the selection probability for a pattern which is ranked very low and/or which does not satisfy the power peaking constraint, will have become very small. In accordance with the elite-cluster property, it can be expected that near the end of the procedure, an "elite" collection will have been formed with approximately the same objective function value, but with possibly entirely different core fuel age distributions. In other words, the procedure is expected to boil down to a more or less probabilistic 'parallel' search from different elite locations in the search space.

Due to Eq.(3.14), the final search behaviour of this procedure will be such that only modest changes in the best patterns are evaluated, which is more or less the definition of a local search. The advantage with respect to the simulated annealing method is that, because of the heterogeneity in the ranking of the best performing patterns (in terms of the BOC reactivity distributions), the final (local) search stage will not be confined to a specific region in the solution space. Instead, this final search will be conducted in large numbers of distant elite clusters throughout the search space (with *distance* defined in terms of differences in the fuel assignments). The obvious advantage with respect to the genetic algorithm is that the final search stage really consists of local searches throughout the solution space, whereas standard genetic algorithms are incapable of really searching locally. From the results obtained in this study, this "population mutation annealing" algorithm is found to be rapidly convergent and quite successful, and it is not that difficult to program its stochastic dynamics.

3.3.2 Some results obtained by applying the population mutation annealing algorithm

Starting from the same randomly chosen poor-performing patterns that neither yield economic fuel use nor satisfy the power peaking constraint, we have searched for the reload patterns associated with the best equilibrium cycle behaviours for the same PWR test cores as considered in section 3.2.4, containing 96, 224 and 384 fuel assemblies, respectively. Again, the objective was to find the pattern yielding the highest $k_{eff}^{(uc)}(EOC)$ while satisfying the constraint that the power peaking factor remains below 1.8. The PMA process parameters were chosen as : $N_{min}=2, N_{max}=46$ en for the annealing parameter we again chose the value $\alpha=0.998$. The results are listed in table IV. From the results obtained here, it can be concluded that this method promises to be a better and more appropriate optimization tool for reload pattern optimization than any of the other methods which were discussed in section 3.2. The PMA method performs according to expectation and, for all three PWR cores considered, the best optimization results were obtained. In Figs. 3.25-27, the best PMA search results are illustrated for cores 1,2 and 3.
It is very interesting to observe how the cumulative selection probability distribution evolves as a function of the annealing temperature. Since each annealing temperature value is uniquely determined by $T_i = \alpha^i \cdot T_0$, one could also say that the cumulative selection probability distribution is plotted as a function of the number of patterns selected sofar.

TABLE IV

List of obtained optimization results for the three PWR cores

core	$k_{eff.EOC}^{(uc)}$	maximal power peaking factor
1	1.0365	1.7705
2	1.0247	1.7834
3	1.0201	1.7906

In Fig.3.19 and Fig.3.20 this distribution is plotted for two different annealing temperatures characterizing the different search stages, from the initial search stage (almost linear curve) via intermediate search stages to the final search stage. Clearly, the patterns become better as the search proceeds, since the cumulative selection probability distributions become steeper and steeper. This is, of course, in contrast to the evolution of the best function value found, which stagnates as the improvements become smaller and smaller, as indicated in Fig.3.21. The actual selection probability distributions are plotted in Figs.3.22 and 3.23 at annealing temperatures $T=0.00045 \cdot T_0$ and $T=0.000052 \cdot T_0$, respectively. Finally, in Fig.3.24 the improvement path of the PMA search for core 3 is plotted along with the random sample cloud of 2000 randomly generated patterns. Visual comparison with Fig.3.18 reconfirms the numerical comparison between table III and table IV indicating that the PMA result is significantly better for this case than the results of any of the other search procedures discussed in section 3.2.4.
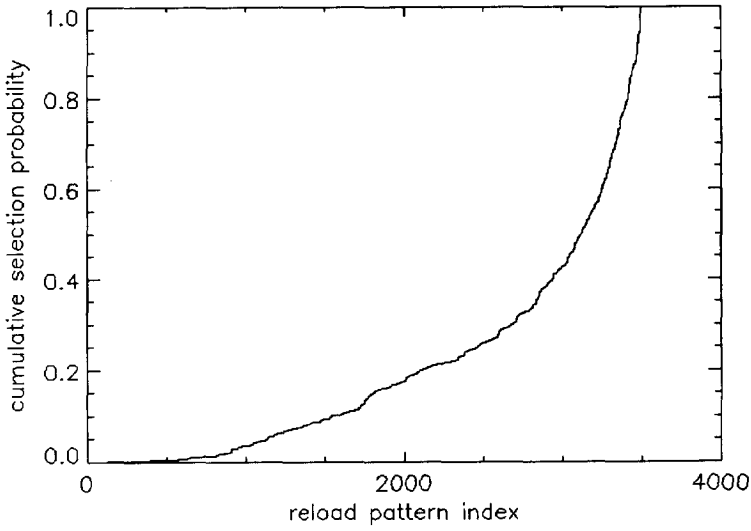
Fig.3.19 Cumulative selection probability distribution at $T = 0.0091 \cdot T_0$
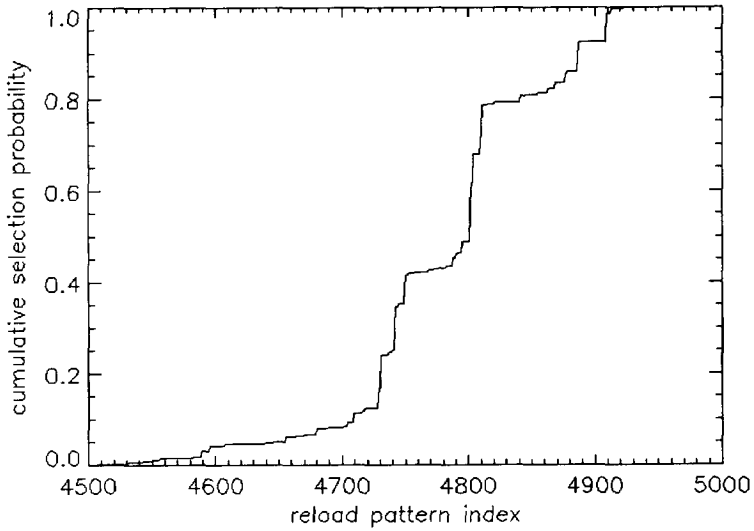
Fig.3.20 Cumulative selection probability distribution at $T = 0.000052 \cdot T_0$
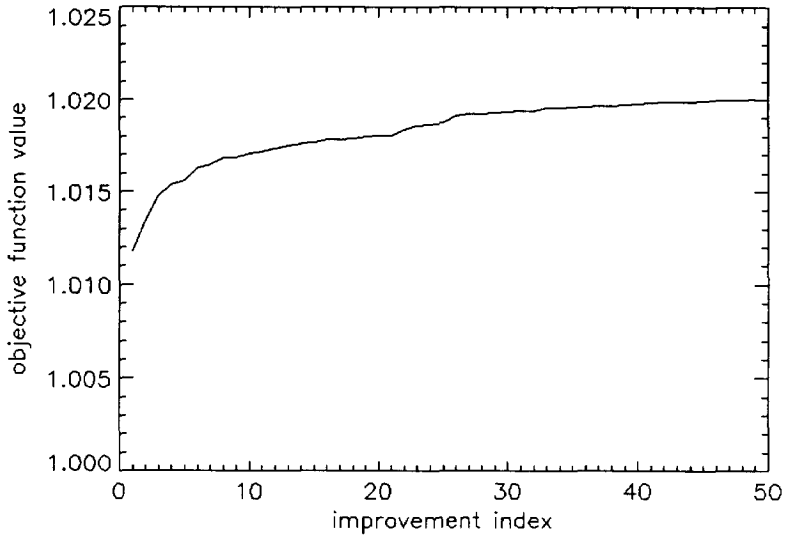
Fig.3.21 Convergence towards the best search result
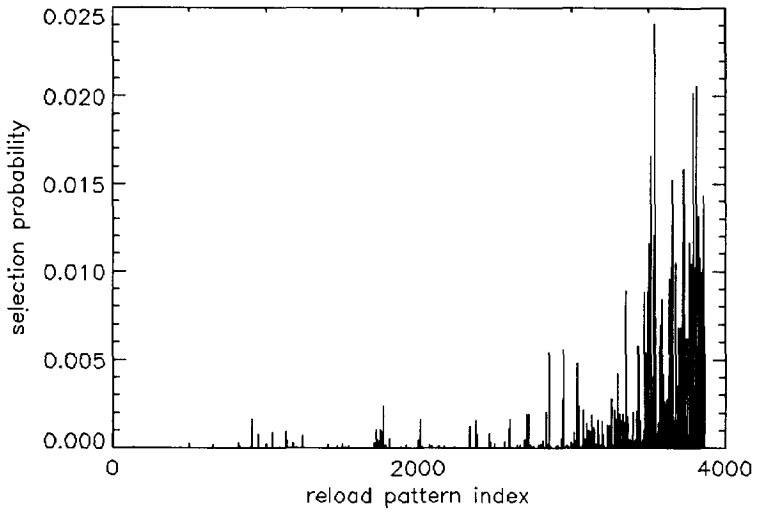
Fig.3.22 Selection probability distribution at $T=0.00045 \cdot T_0$

56
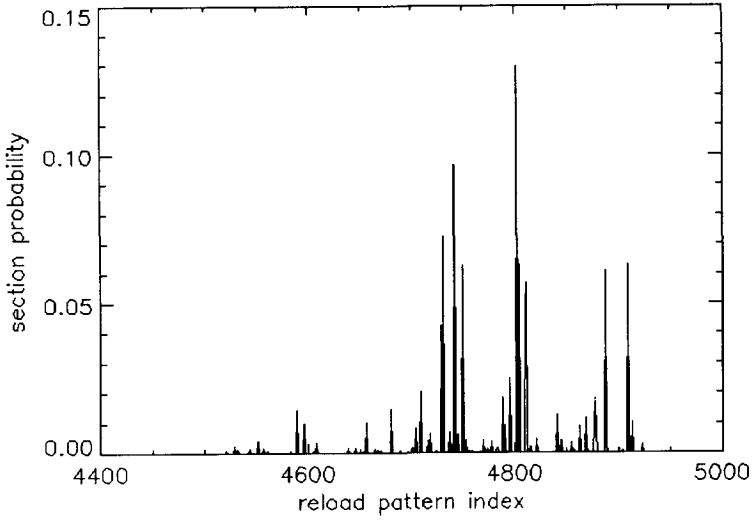
Fig.3.23 Selection probability distribution at $T = 0.000052 \cdot T_0$
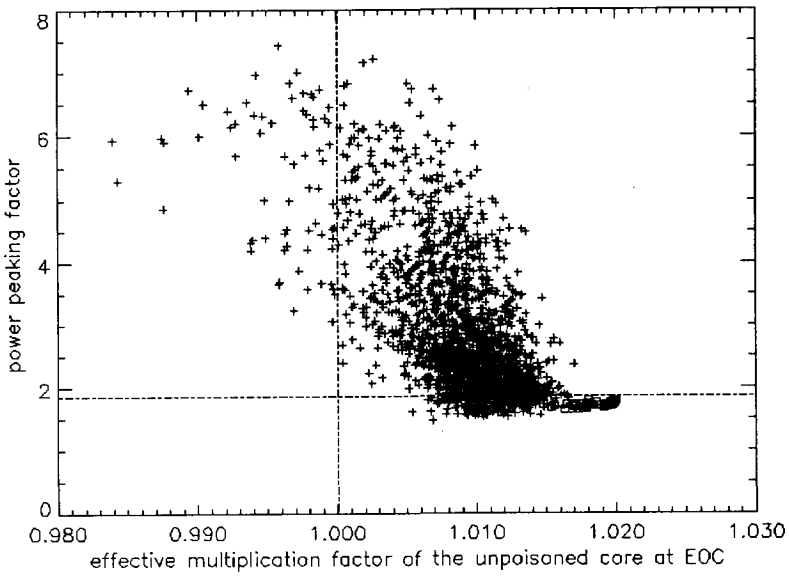
Fig.3.24 PMA Optimization trajectory for core 3, plotted
along with a cloud of randomly generated patterns

57
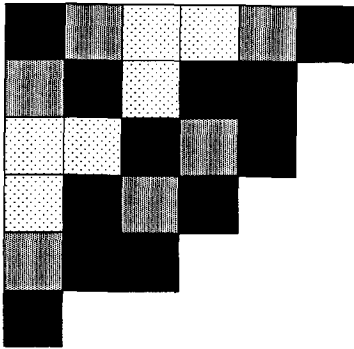
Fig.3.25 Fuel age distribution of the
best pattern found by the PMA
method applied to core 1
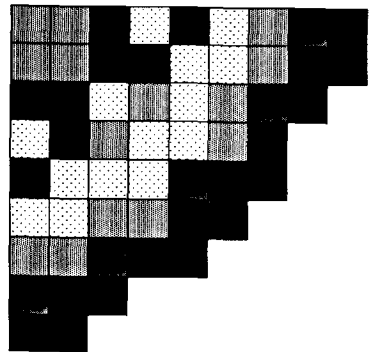
Fig.3.26 Fuel age distribution of the
best pattern found by the PMA
method applied to core 2
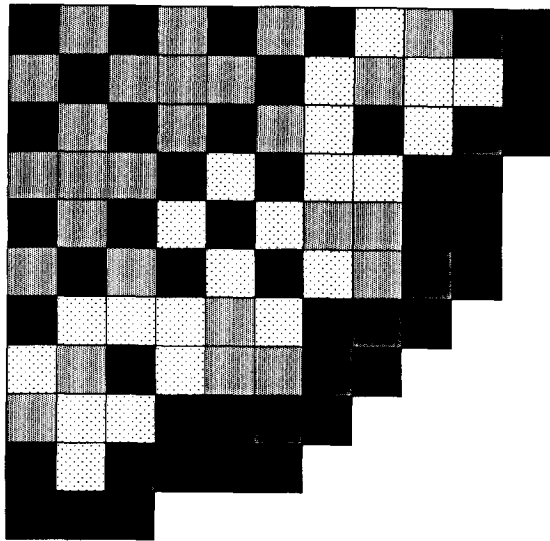
Fig.3.27 Fuel age distribution of the best pattern found
by the PMA method applied to core 3.

58

3.4 Conclusions

We conclude that all of the search methods that were applied here lead to relatively good solutions of the reload pattern optimization problem for the modestly-sized core that was considered, even when using a very bad initial trial pattern. It should be noted that the PMA search algorithm presented in section 3.3 is clearly the best optimization method in terms of the objective function values. It is important to note here that the procedures were deliberately started from a bad initial trial pattern to test their reliability. All of the search procedures have proved capable of finding their way from any starting point in the disordered search space towards the 'region' of nearly optimal patterns. In this sense all of the search concepts evaluated have proved their robustness.

We would like to stress here that, especially with regard to the stochastic optimization procedures treated in sections 3.2.3 (SA) and 3.3 (PMA), a lot of separate work can be done on optimization of the search process parameters to further improve the performance of the searches. And of course other variants can be developed as well, incorporating additional ideas originating from statistical physics or biology to further enhance their optimization ability.

As is generally known, genuine global optimality of the pattern found can hardly be guaranteed, but the quality of the results can be visualized by plotting the obtained patterns along with a plot of a large sample of randomly generated reload patterns in a performance plane.

Application of heuristic search methods as described here allows for a *black box* approach in which gradient information is not required, and in which the system equations governing the behaviour of the reactor core system do not have to be implemented in the optimization procedure. In the optimization procedure, the system equations are isolated in an external simulator module that generally simply returns the objective function value and informs the optimization shell about whether or not any reactor physics constraints are violated. In particular the PMA search approach presented in section 3.3 has proved to be insensitive to the lack of a well-defined ordering principle for reload matrices, and therefore constitutes a robust and reliable method for finding a good fuel distribution in a nuclear reactor core.

References

[Axmann 1997] J.K. Axmann, "Parallel Adaptive Evolutionary Algorithms for Pressurized Water Reactor Reload Pattern Optimizations", *Nuclear Technology* 119, pp. 276-292 (1997).

[DeChaine 1996] M.D. DeChaine, M.A. Feltus, "Fuel Management Optimization Using Genetic Algorithms and Expert Knowledge", *Nuclear Science & Engineering* 124, 188-196 (1996).

[Kropaczek 1991] D.J. Kropaczek, P.J. Turinsky, "In-Core Nuclear Fuel Management Optimization for Pressurized Water Reactors utilizing Simulated Annealing", *Nuclear Technology* 95, pp. 9-32 (1991).

[Parks 1987] G.T. Parks, "An Intelligent Stochastic Optimization Routine for In-Core Fuel Cycle Design", *Transactions of the American Nuclear Society* 57, pp.259-260 (1988)

[Parks 1996a] G.T. Parks, "Multi-objective Pressurized Water Reactor Reload Core

Design by Nondominated Genetic Algorithm Search", *Nuclear Science & Engineering* **124**, 178-187 (1996).

[Poon 1993] P.W. Poon and G.T. Parks, "Application of Genetic Algorithms to In-Core Fuel Management Optimization", *Proceedings Joint International Conference on Mathematics and Supercomputing in Nuclear Applications*, Karlsruhe, Volume 1, 777 (1993).

[Šmuc 1994] T. Šmuc, D. Pevec, B. Petrović, "Annealing Strategies for Loading Pattern Optimization", *Annals of Nuclear Energy* **21**, pp. 325-336 (1994)

[Stevens 1995] J.G. Stevens, K.S. Smith, K.R. Rempe, "Optimization of Pressurized Water Reactor Shuffling by Simulated Annealing with Heuristics", *Nuclear Science and Engineering* **121**, 67-88 (1995).

[Van Geemert 1996] R. van Geemert, A.J. Quist, J.E. Hoogenboom, "Reload Pattern Optimization by Application of Multiple Cyclic Interchange Algorithms", *proceedings PHYSOR'96 conference*, Mito, Japan (1996).

[Van Geemert 1999] R. van Geemert, A.J. Quist, J.E. Hoogenboom, "Research Reactor In-Core Fuel Management Optimization by Application of Multiple Cyclic Interchange Algorithms", *to be published in Nuclear Engineering and Design's topical issue on Research Reactor Fuel Management* (1999).

[Verhagen 1993] F.C.M. Verhagen, M. van der Schaar, "Simulated Annealing in LWR Fuel Management", *TOPNUX'93 Proceedings* **2**, pp. 37-39 (1993).

Chapter 4

Application of Generalized Perturbation Theory to In-Core Fuel Management

4.1 Introduction to Generalized Perturbation Theory

4.1.1 Efficient evaluation of permutation effects

In reload pattern optimization, search algorithms are very often based on assessing the effects of permutations in the reloading scheme, followed by acceptance decisions in which the permutation yielding the largest increase in the objective function to be maximized (while satisfying the reactorphysical constraints) is chosen to determine the next reference scheme in the search procedure. Generally, the exact value of the objective function for an operation cycle can only be determined after the completion of an iterative procedure to obtain the cycle solution from BOC (Begin-of-Cycle) to EOC (End-of-Cycle). This implies that reload pattern optimization methods in which large numbers of different refueling schemes must be evaluated in this way are quite expensive from a computational point of view. However, for fast evaluation of a new reloading scheme to be examined, it is possible to decompose this scheme into the original, unperturbed reloading scheme and the perturbation in the scheme. A spatial extension of a variational technique that was introduced by Pomraning [Pomraning 1967] and defined for depletion perturbation theory by Gandini [Gandini 1975] and Williams [Williams 1979] can be applied to evaluate in first-order approximation the effect of the perturbation on a selected response vector. The theory on which the variational technique is based is generally referred to as *generalized perturbation theory* (GPT) [White 1990, Maldonado 1995, Moore 1997, Van Geemert 1998]. Explicit consideration of the higher-order terms in the response functional expansion results in a very rapidly converging iterative scheme from which the *exact* perturbation in the response vector can be obtained at very low computational cost. In this iterative scheme, the first-order prediction of the response vector perturbation serves as a fixed-source term. The availility of this perturbation formalism offers the possibility of fast assessment of many different reloading schemes. This results in a considerable economy of computation time for *any* heuristic reload pattern optimization procedure based on assessing the effects of permutations in the candidate loading schemes.

4.1.2 The generalized variational approach

The time evolution of a PWR core is basically described by the energy-, space-, and time-dependent neutron flux $\phi(t)$ and by the space- and time-dependent nuclide density matrix $\underline{N}(t)$. Generally, since the neutronic and depletion equations are coupled, a quasi-static approach, featuring a number of time steps i, must be adopted for numerical simulation of how the core evolves from BOC to EOC. In this approach, it is assumed that the neutronics eigenvalue equation, determining the spatial flux shape $\psi(t)$ can, after omitting

the time dependence for notational convenience, be written compactly as

$$(L - \lambda F) \underline{\psi} = \underline{0} \tag{4.1}$$

where the eigenvalue λ is the reciprocal of the effective multiplication factor of the uncontrolled (i.e. without external reactivity control) core k_{eff} and L and F are the loss and production operator, respectively. A possible choice for the normalisation requirement for the spatial flux shape vector is

$$\| \underline{\psi} \| = \sum_I \psi_I = 1 \tag{4.2}$$

with the index I denoting the different core nodes in the system geometry. In the 1½-energy group approximation adopted in this study, there is effectively only one energy group, but this formulation can be easily extended for incorporation of multiple energy groups. An extension of the perturbation theoretical method proposed by Williams [Williams 1979] has been developed and applied which eventually provides the possibility to assess the *exact* influence of a variation in the nuclide density field on the *flux distribution* in the core for a certain time step. In conformity with the variational approach, this can be realized by treating the quasi-static equations as constraints on the response, and appending them to the response function using Lagrange multipliers. In the formalism to be presented here, many inner product definitions occur, which can be most conveniently written using the Dirac bracket notations :

$$\langle \underline{a} | \underline{b} \rangle = \sum_I a_I b_I \tag{4.3a}$$

and

$$\langle \underline{a} | C | \underline{b} \rangle = \sum_I a_I \sum_J C_{IJ} b_J \tag{4.3b}$$

with $\underline{a}$ and $\underline{b}$ denoting vectors and C denoting a matrix. In appendix B, more examples will be given on how to interpret the notations in this chapter. For each response quantity A, the following functional $\Re$ can be defined, in which the quasi-static equations are appended to the response function using the Lagrange multipliers $\underline{\Gamma}_A^*$ and a_A :

$$\Re = A - \langle \underline{\Gamma}_A^* | L - \lambda F | \underline{\psi} \rangle - a_A (\langle \underline{1} | \underline{\psi} \rangle - 1) \tag{4.4}$$

with $\underline{1}$ a vector with all components equal to 1. If λ and $\underline{\psi}$ satisfy Eq.(4.1) and Eq.(4.2), the value of the functional equals the value of the response quantity A. We note that the second term in Eq.(4.4) can be written as :

$$\langle (L^* - \lambda F^*) \underline{\Gamma}_A^* | \underline{\psi} \rangle \tag{4.5}$$

with L^* and F^* the adjoint operators of L and F, respectively. We note that these adjoint loss and production operators are directly dependent on the nuclide density distribution : $L=L(\underline{N})$ and $F=F(\underline{N})$. If the nuclide density distribution $\underline{N}$ is perturbed ($\underline{N} \to \underline{N}' = \underline{N} + \delta \underline{N}$, resulting in $L(\underline{N}) \to L'(\underline{N}') = L(\underline{N}) + \delta L$ and $F(\underline{N}) \to F'(\underline{N}') = F(\underline{N}) + \delta F$), this influences $\Re$:

$$\mathfrak{R} \rightarrow \mathfrak{R}'(\underline{N}',\psi',\lambda'), \tag{4.6}$$

where the prime variables refer to their perturbed values. Again, if λ' and ψ' are exact solutions to the *perturbed* equations, then $\mathfrak{R}' = A'$. Substracting the expressions for the perturbed and the unperturbed response functional and ordering the terms gives

$$\delta\mathfrak{R} = \delta A - \left\langle \Gamma_A^* \mid \delta L - \lambda\,\delta F \mid \psi \right\rangle + \delta\lambda \left\langle \Gamma_A^* \mid F \mid \psi \right\rangle$$

$$- \left\langle (L^* - \lambda\,F^*)\Gamma_A^* + a_A 1 \mid \delta\psi \right\rangle \quad (1^{st} \text{ order})$$

$$- \left\langle \Gamma_A^* \mid \delta L - \lambda\,\delta F - \delta\lambda F \mid \delta\psi \right\rangle + \delta\lambda \left\langle \Gamma_A^* \mid \delta F \mid \psi \right\rangle \quad (2^{nd} \text{ order})$$

$$+ \delta\lambda \left\langle \Gamma_A^* \mid \delta F \mid \delta\psi \right\rangle \quad (3^{rd} \text{ order}) \tag{4.7}$$

Of interest is the choice of the nodal flux ψ_J in node J as the response quantity A. Noting that $\delta A = \delta\psi_J = \psi_J' - \psi_J$ can be written as $<\delta_J \mid \delta\psi>$, with the Kronecker delta vector defined as the vector of which the Jth element equals unity and all other elements are zero, Eq.(4.7) can be written for this case as :

$$\delta\mathfrak{R} = \delta\psi_J = - \left\langle \Gamma_J^* \mid \delta L - \lambda\,\delta F \mid \psi \right\rangle + \delta\lambda \left\langle \Gamma_J^* \mid F \mid \psi \right\rangle$$

$$- \left\langle (L^* - \lambda\,F^*)\Gamma_J^* + a_J 1 - \underline{\delta}_J \mid \delta\psi \right\rangle$$

$$- \left\langle \Gamma_J^* \mid \delta L - \lambda\,\delta F - \delta\lambda F \mid \delta\psi \right\rangle + \delta\lambda \left\langle \Gamma_J^* \mid \delta F \mid \psi \right\rangle$$

$$+ \delta\lambda \left\langle \Gamma_J^* \mid \delta F \mid \delta\psi \right\rangle \tag{4.8}$$

with $\delta\mathfrak{R}$ simply replaced by $\delta\psi_J$, assuming that $\delta\lambda$ and $\delta\psi$ are such that the perturbed equations are satisfied. The second and the third term on the right of Eq.(4.8) will vanish if Γ_J^* satisfies the adjoint flux shape equation

$$\left(L^* - \lambda\,F^* \right) \cdot \Gamma_J^* = - a_J 1 + \underline{\delta}_J \equiv Q_J^* \tag{4.9}$$

and the orthogonality condition

$$\left\langle \Gamma_J^* \mid F \mid \psi \right\rangle = 0 \tag{4.10}$$

with a_J still to be determined. For argueing how this combined objective can be realized, it is worthwhile to consider the eigenset $\{\lambda_n^*, \psi_n^*; n=0,1,2,...\}$ of the *adjoint* equation :

63

$$\left(L^* - \lambda_n^* F^* \right) \cdot \psi_n^* = \underline{0} \tag{4.11}$$

Generally, $\lambda_n^* = \lambda_n$. The fundamental adjoint flux shape ψ_0^* (conventionally written simply as ψ^*) is a very important quantity. The basic reason for this is the validity of a mathematical orthogonality property that can be proved in the following way : after premultiplication of Eq.(4.1) with the mth eigenvector ψ_m^*, recalling the commutativity property $<\psi_m^* | L | \psi_n> = <L^*\psi_m^* | \psi_n>$ and employing Eq.(4.11), we obtain

$$\lambda_m \left\langle \psi_m^* | F | \psi_n \right\rangle = \lambda_n \left\langle \psi_m^* | F | \psi_n \right\rangle \tag{4.12}$$

Hence, since $\lambda_n \neq \lambda_m$ in the case $m \neq n$, the inner product $<\psi_m^* | F | \psi_n>$ should vanish for the case $m \neq n$. Thus, the validity of the well-known property

$$\left\langle \psi_m^* | F | \psi_n \right\rangle = c_n \delta_{nm} \tag{4.13}$$

has been established. The implication of this property is that, if some adjoint flux shape Γ^* is to be orthogonal to the fission rate distribution $F\psi_0$, it should not contain any component of ψ_0^*, i.e., it should be orthogonal to ψ_0^*. So, Eq.(4.10) basically requires that the Lagrange multiplier Γ_j^* is not allowed to contain any component of the fundamental solution of the homogeneous adjoint equation $(L^* - \lambda F^*)\psi^* = \underline{0}$. This fundamental mode is the only eigenstate which does *not* yield zero when multiplied with $F\psi$, since the eigensets $\{\psi_n^*, n=0,1,...\}$ and $\{\psi_n, n=0,1,...\}$ obey the general orthogonality property (4.13). Thus, $<\psi_n^* | F | \psi>$ unequals zero only in the case $n=0$. More specifically, if Γ_p^* is the particular solution to Eq.(4.9) satisfying Eq.(4.10) such that $<\Gamma_p^* | F | \psi>$ vanishes, where ψ^* is the fundamental solution to the homogeneous equation, then $\Gamma_p^* + b\psi^*$ is also a solution of Eq.(4.9) *for all b*. However, due to Eq.(4.10) the value of b is fixed to be zero, so that Γ^* will not be 'contaminated' with the fundamental solution ψ^*. Hence, there is only one unique solution satisfying both Eq.(4.9) and (4.10). In each step in the iterative process of solving Eq.(4.9), this can be effected by application of a filtering operation, written in program language style as

$$\Gamma_j^* := \Gamma_j^* - \frac{\left\langle \Gamma_j^* | F | \psi \right\rangle}{\left\langle \psi^* | F | \psi \right\rangle} \psi^* \tag{4.14}$$

The choice for the multiplier a_j is determined by the fact that Eqs.(4.1) and (4.9) specify that $\langle \psi | Q_j^* \rangle = 0$. This becomes obvious when analysing the inner product $\langle \psi | Q_j^* \rangle$:

$$\left\langle \psi | Q_j^* \right\rangle = \left\langle \psi | L^* - \lambda F^* | \Gamma_j^* \right\rangle = \left\langle (L - \lambda F)\psi | \Gamma_j^* \right\rangle = \left\langle \underline{0} | \Gamma_j^* \right\rangle = 0 \tag{4.15}$$

Using this result and using $<\underline{1} | \psi> = 1$, a_j is obtained :

$$a_j = \left\langle \underline{\delta}_j | \psi \right\rangle = \psi_j \tag{4.16}$$

If Eqs.(4.9),(4.10),(4.16) are satisfied by Γ_j^* and a_j, the expression for the *first-order*

prediction of the change in the response flux $\delta\psi_J$, denoted by $\delta^{(1)}\psi_J$, is

$$\delta^{(1)}\mathfrak{R} = \delta^{(1)}\psi_J = -\left\langle \Gamma_J^* \mid \delta L - \lambda\,\delta F \mid \underline{\psi} \right\rangle \tag{4.17}$$

Obviously, it is possible to treat *all* nodal fluxes in the system as response quantities. The collection of all associated Lagrange multipliers $\underline{\Gamma}^* = \{\Gamma_1^*, \Gamma_2^*, \ldots, \Gamma_N^*\}$, with N the number of nodes in the system geometry, can then be used to obtain a *first-order* estimate of the perturbation in the *entire* nodal flux distribution :

$$\delta^{(1)}\mathfrak{R} = \delta^{(1)}\underline{\psi} = -\left\langle \underline{\Gamma}^* \mid \delta L - \lambda\,\delta F \mid \underline{\psi} \right\rangle \tag{4.18}$$

If Eqs.(4.9),(4.10) and (4.16) are satisfied, the *exact* expression for $\delta\underline{\psi}$ can be written as :

$$\delta\underline{\psi} = \delta^{(1)}\underline{\psi} - \left\langle \underline{\Gamma}^* \mid \delta L - \delta(\lambda F) \mid \delta\underline{\psi} \right\rangle + \delta\lambda\left\langle \underline{\Gamma}^* \mid \delta F \mid \underline{\psi} \right\rangle \tag{4.19}$$

with $\delta(\lambda F) = \delta\lambda F + \lambda\delta F + \delta\lambda\delta F$. As the unknown spatial perturbation $\delta\underline{\psi}$ appears on both sides of the equation, Eq.(4.19) represents an iterative solution scheme for obtaining $\delta\underline{\psi}$. This iterative scheme features the first-order estimate $\delta^{(1)}\underline{\psi}$ as a *fixed-source* term, and has the pleasant property that it can converge very rapidly. It is apparent that, in order to implement this scheme, a formula should be available to estimate the change in the eigenvalue $\delta\lambda$. After each calculation of an improved estimate of the perturbed spatial flux distribution $\underline{\psi}'^{(n)}$, the eigenvalue perturbation estimate $\delta\lambda^{(n+1)}$ can be obtained after premultiplication of the perturbed flux eigenvalue equation with the fundamental adjoint flux distribution $\underline{\psi}^*$ and using the property $(L^* - \lambda F^*)\underline{\psi}^* = \underline{0}$:

$$\delta\lambda^{(n+1)} = \frac{\left\langle \underline{\psi}^* \mid \delta L \mid \underline{\psi}'^{(n)} \right\rangle - \lambda\left\langle \underline{\psi}^* \mid \delta F \mid \underline{\psi}'^{(n)} \right\rangle}{\left\langle \underline{\psi}^* \mid F' \mid \underline{\psi}'^{(n)} \right\rangle} \tag{4.20}$$

with λ the unperturbed eigenvalue. Thus, with the node-averaged flux distribution as the response vector, Eqs.(4.19) and (4.20) eventually yield a higher-order, rapidly converging iterative scheme containing the source term $\delta^{(1)}\underline{\psi}$, from which the *exact* perturbed node-averaged flux distribution can be obtained at low computational cost :

$$\left\{ \begin{array}{l} \delta\underline{\psi}^{(n+1)} = \delta^{(1)}\underline{\psi} - \left\langle \underline{\Gamma}^* \mid \delta L - \delta(\lambda^{(n)}F) \mid \delta\underline{\psi}^{(n)} \right\rangle + \delta\lambda^{(n)}\left\langle \underline{\Gamma}^* \mid \delta F \mid \underline{\psi}^{(n)} \right\rangle \\[3mm] \delta\lambda^{(n+1)} = \dfrac{\left\langle \underline{\psi}^* \mid \delta L - \lambda\,\delta F \mid \underline{\psi}'^{(n)} \right\rangle}{\left\langle \underline{\psi}^* \mid F' \mid \underline{\psi}'^{(n)} \right\rangle} \end{array} \right. \tag{4.21}$$

The convergence properties of this iterative scheme depend on the magnitude of the considered perturbation in the nuclide density distribution and thus basically on the magnitude of the perturbation in the operator λF. For example, for modest octant-symmetric permutations in the core depicted in Fig.1.2, involving 4 fuel elements per octant, not more than 4 iterative steps were needed to achieve an accuracy consistent with the accuracy of 10^{-4} in the calculated flux distributions. In the forward calculations, no

less than about 50 iterative steps are required to reconstruct the perturbed flux distribution and eigenvalue. The execution of one step in the iterative scheme (4.21) takes about 25% more CPU-time than the execution of one iterative step in the 'forward' scheme (without use of Lagrange multipliers). Hence, for permutations of this modest magnitude, a calculational speed-up of a factor of about 10 can be realized.

Using scheme (4.21), rather large perturbations can be treated as well, but the convergence rate will then be somewhat lower, with which the speed-up factor is reduced. For very large perturbations involving the more or less random permutations of *all* fuel elements, the iterative scheme (4.21) may even not converge at all, but diverge in an oscillating way !

It is not very trivial to predict mathematically when (4.21) will converge and when it will diverge, since $\delta(\lambda F)$ will generally contain both positive and negative elements and thus is not a positive-definite operator. Therefore in this study we obeyed the conservative rule of not using GPT for evaluating perturbations consisting of simultaneous (octant-symmetric) shufflings of more than a quarter of the total number of fuel elements.

In Figs.4.1a and 4.1b respectively, examples are given of a small and a large spatial nuclide density perturbation in terms of the ^{235}U concentrations in the big PWR core containing 384 elements. In Fig.4.1a, four randomly chosen unity elements in the reload operator X, corresponding to different fuel ages were cyclically permuted in each octant, whereas in Fig.4.1b twelve randomly chosen unity elements, three of each different fuel age, were randomly permuted. Of course, for the equilibrium cycle this means that basically all nuclide densities in all positions are affected. The resulting spatial flux perturbations are shown in Figs.4.2a and 4.2b.
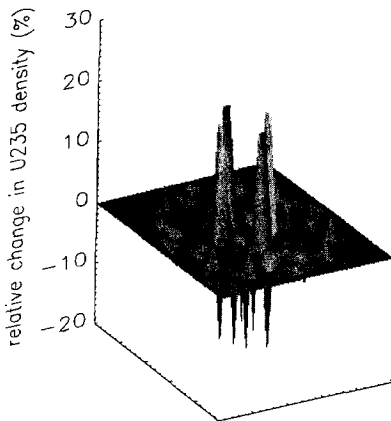
Fig.4.1a
Modest spatial ^{235}U density perturbation
due to octant-symmetric permutation of 4
unity elements in the reload operator X,
plotted in percentage changes with respect
to the ^{235}U concentration in fresh fuel.
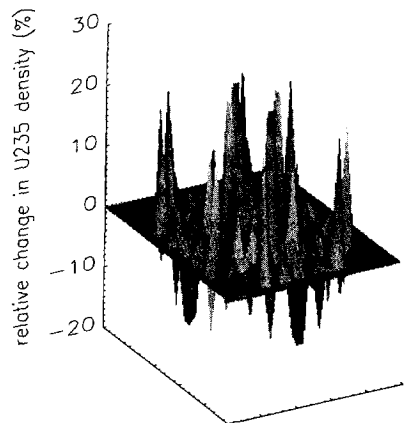
Fig.4.1b
Large spatial ^{235}U density perturbation
due to octant-symmetric permutation of 12
unity elements in the reload operator X,
plotted in percentage changes with respect
to the ^{235}U concentration in fresh fuel.
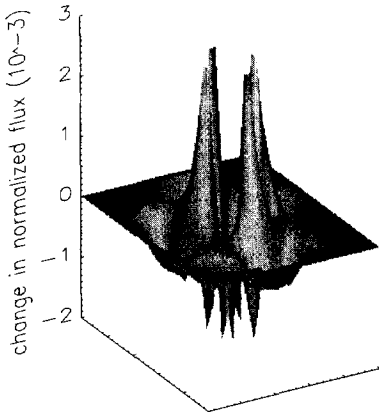
Fig.4.2a

Spatial flux perturbation due to the modest octant-symmetric permutation of 4 unity elements in the reload operator **X**. We note that the core-averaged normalized flux density for this case is 0.0104.
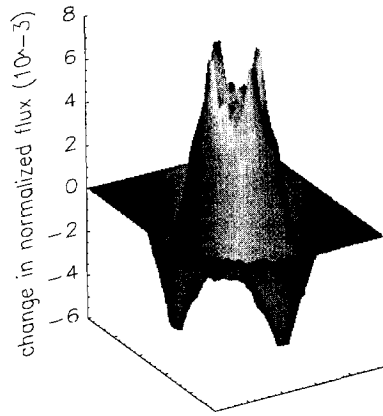
Fig.4.2b

Spatial flux density perturbation due to the large octant-symmetric permutation of 12 unity elements in the reload operator **X**, We note that the core-averaged normalized flux density for this case is 0.0104.

Obviously, the perturbation in Fig.4.2b is more oscillatory since the alternations between positive and negative elements in the operator $\delta(\lambda F)$ will be more frequent. In tables I and II the qualities and computational requirements of the GPT reconstructions for $\delta\lambda$ and $\delta\psi$ are compared to the results and computational burden of using the plain forward iterative calculation scheme. The convergence criterion for both methods was set to the value 10^{-4}.

TABLE I

A comparison of the CPU-requirements and results (λ-eigenvalue and power peaking factor change Δp) of the GPT iterative method and the standard forward iterative method for the perturbation shown in Fig.4.1a. The listed required CPU-times were obtained for a DEC-α600 5/266.

iterative method	$\delta\lambda$	Δp	number of iterative steps required for $\varepsilon = 10^{-4}$	required CPU-time(s)
GPT	$1.9 \cdot 10^{-5}$	-0.0931	4	0.0072
forward	$1.9 \cdot 10^{-5}$	-0.0922	50	0.0700

67

TABLE II

A comparison of the CPU-requirements and results (λ-eigenvalue and power peaking factor change Δp) of the GPT iterative method and the standard forward iterative method for the perturbation shown in Fig.4.1b. The listed required CPU-times were obtained for a DEC-α600 5/266.

iterative method	$\delta\lambda$	Δp	number of iterative steps required for $\varepsilon = 10^{-4}$	required CPU-time(s)
GPT	0.00656	0.5417	8	0.00144
forward	0.00657	0.5435	50	0.0700

In this study, the use of this higher-order formalism has been combined with an *equilibrium cycle* iterative perturbation theoretical method (to be discussed in chapter 5). In this way, the limit cycle iterations involved in a heuristic equilibrium cycle optimizati-on procedure can be fastened significantly ([Van Geemert 1997]), as will be descibed in chapter 5. Of essential importance in the equilibrium cycle iterative perturbation theoreti-cal method is the use of so-called burnup sensitivity operator **S** which can relate, in first-order approximation, the perturbation in the equilibrium cycle BOC nuclide density distribution to the perturbation in the equilibrium cycle EOC nuclide density distribution, with the perturbation occurring due to a change in the reload operator : $\mathbf{X} \rightarrow \mathbf{X'}$. This specific iterative method has the major advantage that it will *always* converge due to the fact that the sensitivity operator **S** is positive-definite and fixed, and furthermore has a norm $\|\mathbf{S}\|$ which is by definition smaller than unity. The disadvantage of the method is that it does not feature higher-order accuracy, so it basically serves to provide an initial estimate for the perturbed equilibrium cycle. However, since burnup is a rather linear process in a nuclear reactor, these initial estimates are generally remarkably good. And the method can be used for fast prediction of the perturbed power peaking factor which, if indicating an inadmissibly high power peaking, may serve to exclude a lot of uninteres-ting candidate patterns from evaluation. In this way, considerable amounts of calculation time can be saved.

In the next section, it will be described how the different burnup sensitivity coefficients can be determined by applying a spatial extension of the variational technique introduced by Williams [Williams 1979].

4.2. Depletion Perturbation Theory

4.2.1 Sensitivity theory for coupled neutron/nuclide fields

Generalized perturbation theory as described in section 4.1.2 provides a powerful, rapidly converging iterative scheme with which the effects on the flux distribution of perturbations in the nuclide density distribution can be predicted with higher order accuracy and low computational cost. For purposes which will become apparent in

68

chapter 5, it is also very convenient to have a sensitivity matrix indicating, in first-order approximation, how the EOC nuclide density distribution is affected by a change in the BOC nuclide density distribution. Since the time dependent neutronics field and the nuclide density field implicitly depend on one another, a spatial perturbation in the BOC nuclide density field at BOC (so at $t=t_0$) will perturb the *entire* neutron/nuclide field for the forthcoming cycle. In depletion perturbation theory (DPT) [Gandini 1975, Williams 1979], it is always assumed that the BOC nuclide density distribution is known exactly. The major problem to overcome is that, due to the fact that the neutronics field and the nuclide density field are governed by a set of coupled (differential) equations, it is impossible to calculate directly how a perturbation in the combined neutron/nuclide field will propagate from BOC to EOC. Nevertheless, in conformity with what has been described in section 4.1.2, a variational approach can be applied to a more general response functional as proposed by Williams [Williams 1979] consisting of *all* system equations for *all* time steps, including the nuclide transmutation equations. Again, these equations can be treated as constraints on the response, and appended to the response function using Lagrange multipliers. This eventually provides the possibility to assess directly, in first-order approximation, the influence of a small variation in the *initial* (BOC) core state on the *final* (EOC) state of the core. The interesting case will be treated of the response being the concentration of nuclide type q in node J at the end of the operation cycle, so defined at $t=t_T$. In order to stress that the response is defined at $t=t_T$, the response quantity is denoted as $N_{J,q}(t_T)$. In analogy with what has been described in section 4.1.2, a general response functional can be defined, in which the quasi-static equations are appended to the response function using Lagrange multipliers. Naturally, in this more general picture a number of additional system equations must be included in the functional, i.e. the nuclide transmutation equation and the constant power level equation. The transmutation equation dictating the time evolution of the nuclide density field can be written as

$$\frac{\partial}{\partial t} \underline{N}(t) = \left(\hat{\sigma} \, \Phi(t) \, \underline{\psi}(t) + \hat{D} \right) \underline{N}(t) \tag{4.22}$$

with $\hat{\sigma}$ denoting the absorption cross sections matrix and $\hat{D}$ the decay operator. We note that the operators active in the *nuclide type space* are marked with a hat, and that an *implicit product in the nuclide type space* occurs when the operators $\hat{\sigma}$ and $\hat{D}$ appear in combination with the nuclide density field $\underline{N}(t)$ (see appendix B). The fast flux can be written as a product of the time dependent shape function $\psi(\underline{r},t)$ (which is normalized such that $\int \psi(\underline{r},t)dV = 1 \; \forall \; t$) and a time dependent power normalisation factor $\Phi(t)$. This allows for convenient implementation of the condition that the reactor power is restricted to remain at a constant level. Using the inner product notation this condition can be written as :

$$w_f \, \Phi(t) \left\langle \, \Sigma_F(t) \mid \underline{\psi}(t) \, \right\rangle = P_{total} \quad \text{for all } t \tag{4.23}$$

Applying the Lagrange multipliers $\underline{\Gamma}^*_i$, P^*_i and $\underline{N}^*(t)$, the general response functional can be written as :

$$\Re = N_{J,q}(t_T^-) + \sum_{i=0}^{T-1} \int_{t_i}^{t_{i+1}} \left\langle \underline{N}^*(t) \left| \hat{\sigma} \, \Phi_i \, \underline{\psi}_i + \hat{D} - \frac{\partial}{\partial t} \right| \underline{N}(t) \right\rangle dt$$

$$- \sum_{i=0}^{T-1} \left\langle \Gamma_i^* \mid L_i - \lambda_i F_i \mid \underline{\psi}_i \right\rangle - \sum_{i=0}^{T-1} P_i^* \left(w_f \, \Phi_i \left\langle \Sigma_{F,i} \mid \underline{\psi}_i \right\rangle - P_c \right) \qquad (4.24)$$

If $\underline{N}(t)$, $\underline{\psi}_i$, λ_i and Φ_i are exact solutions to the quasi-static burnup equations, then $\Re = N_{J,q}(t_T^-)$. If the BOC nuclide density distribution $\underline{N}(t_0^+)$ is perturbed ($\underline{N}(t_0^+) \rightarrow \underline{N}'(t_0^+)$), this influences $\Re$:

$$\Re \rightarrow \Re'(\underline{N}'(t), \underline{\psi}_i', \Phi_i', \lambda_i'), \qquad (4.25)$$

where the prime variables refer to their perturbed values. Again, if $\underline{N}'(t)$, $\underline{\psi}_i'$, Φ_i', λ_i' are exact solutions to the perturbed quasi-static equations, then $\Re' = N_{J,q}'(t_T^-)$. Expanding $\Re$ about the unperturbed state and *neglecting second-order terms*, we have :

$$\Re' = \Re + \int_{t_0}^{t_T} \left\langle \frac{\partial \Re}{\partial \underline{N}(t)} \middle| \delta \underline{N}(t) \right\rangle dt + \sum_{i=0}^{T-1} \left(\frac{\partial \Re}{\partial \lambda_i} \delta \lambda_i + \frac{\partial \Re}{\partial \Phi_i} \delta \Phi_i + \left\langle \frac{\partial \Re}{\partial \underline{\psi}_i} \middle| \delta \underline{\psi}_i \right\rangle \right) \qquad (4.26)$$

Like in section 4.1.2, most of the contributions can be forced to vanish by defining the Euler-Lagrange equations for the adjoint fields Γ_i^*, P_i^* and $\underline{N}^*(t)$. When these equations (which will be plainly called the adjoint equations) are satisfied, a relatively simple first-order perturbation expression remains that *directly* relates the perturbation in the final time response response $\delta N_{J,q}(t_T^-)$ to the perturbation in the initial nuclide density distributi-on $\delta \underline{N}(t_0^+)$. For example, the functional derivative with respect to Φ_i is :

$$\frac{\partial \Re}{\partial \Phi_i} = \int_{t_i}^{t_{i+1}} \left\langle \underline{N}^*(t) \middle| \hat{\sigma} \, \underline{\psi}_i \, \underline{N}(t) \right\rangle dt - P_i^* \, w_f \left\langle \Sigma_{F,i} \middle| \underline{\psi}_i \right\rangle \qquad (4.27)$$

For this expression to vanish, the multiplier P_i^* should be chosen such that :

$$P_i^* = \frac{1}{w_f \left\langle \Sigma_{f,i} \middle| \underline{\psi}_i \right\rangle} \int_{t_i}^{t_{i+1}} \left\langle \underline{N}^*(t) \middle| \hat{\sigma} \, \underline{\psi}_i \, \underline{N}(t) \right\rangle dt \qquad (4.28)$$

Employing the commutativity property of adjoint operators, the functional derivative with respect to $\underline{\psi}_i$ can be written as

$$\frac{\partial \Re}{\partial \underline{\psi}_i} = \int_{t_i}^{t_{i+1}} \left\langle \underline{N}^*(t) \mid \hat{\sigma} \, \Phi_i \underline{N}(t) \right\rangle dt - \left(L_i^* - \lambda_i F_i^* \right) \Gamma_i^* - w_f P_i^* \, \Phi_i \Sigma_{F,i} \qquad (4.29)$$

In analogy with Eq.(4.9), this partial derivative will vanish if Γ_i^* satisfies the inhomoge-neous adjoint flux shape equation

$$\left(\mathbf{L}_i^* - \lambda_i \mathbf{F}_i^* \right) \cdot \mathbf{\Gamma}_i^* = \mathbf{Q}_i^* \tag{4.30}$$

with the adjoint source

$$\mathbf{Q}_i^* = \int_{t_i}^{t_{i+1}} \left\langle \underline{\mathbf{N}}^*(t) \mid \hat{\sigma} \, \Phi_i \, \underline{\mathbf{N}}(t) \right\rangle dt \, . - w_f \, P_i^* \, \Phi_i \Sigma_{F,i} \tag{4.31}$$

and $\mathbf{L}^*$ and $\mathbf{F}^*$ the adjoint operators of $\mathbf{L}$ and $\mathbf{F}$, respectively. The requirement that $\partial \Re / \partial \lambda_i$ vanishes results in the same orthogonality condition as Eq.(4.10) :

$$\left\langle \mathbf{\Gamma}_i^* \mid \mathbf{F}_i \mid \psi_i \right\rangle = 0 \tag{4.32}$$

and forces $\underline{\mathbf{\Gamma}}_i^*$ to be orthogonal to the fission source at $t=t_i$. The Euler condition corresponding to a variation in $\underline{\mathbf{N}}(t)$ is more complex than for the other variables. This is basically because $\underline{\mathbf{N}}(t)$ is the only 'forward' quantity that is allowed to vary continuously. Due to this, a significant part of its contribution in the variation functional is embedded in an integral, while the other part consists of terms defined at discrete equidistant moments t_i containing the 'snapshots' $\underline{\mathbf{N}}(t_i)$ of the nuclide density fields. To derive the Euler condition for $\underline{\mathbf{N}}^*(t)$, the variation of $\Re$ with respect to $\delta \underline{\mathbf{N}}(t)$ must be considered :

$$\delta \Re[\delta \underline{\mathbf{N}}(t)] = \int_{t_0}^{T_T} \left\langle \frac{\partial}{\partial \underline{\mathbf{N}}(t)} N_{J,q}(t_T^-) \,\middle|\, \delta \underline{\mathbf{N}}(t) \right\rangle dt +$$

$$+ \sum_{i=0}^{T-1} \left\{ \int_{t_i}^{t_{i+1}} \left\langle \underline{\mathbf{N}}^*(t) \,\middle|\, \hat{\sigma} \, \Phi_i \psi_i + \hat{\mathbf{D}} - \frac{\partial}{\partial t} \,\middle|\, \delta \underline{\mathbf{N}}(t) \right\rangle dt - \left\langle \mathbf{\Gamma}_i^* \,\middle|\, \frac{\partial \mathbf{L}_i}{\partial \underline{\mathbf{N}}_i} - \lambda_i \frac{\partial \mathbf{F}_i}{\partial \underline{\mathbf{N}}_i} \,\middle|\, \psi_i \right\rangle \cdot \delta \underline{\mathbf{N}}_i \right.$$

$$\left. - w_f P_i^* \, \Phi_i \left\langle \psi_i \,\middle|\, \frac{\partial \Sigma_{F,i}}{\partial \underline{\mathbf{N}}_i} \right\rangle \cdot \delta \underline{\mathbf{N}}_i \right\} \tag{4.34}$$

Using the adjoint matrices σ^T and $\mathbf{D}^T$ and partial integration with respect to t yields

$$\int_{t_i}^{t_{i+1}} \left\langle \underline{\mathbf{N}}^*(t) \,\middle|\, \hat{\sigma} \, \Phi_i \psi_i + \hat{\mathbf{D}} - \frac{\partial}{\partial t} \,\middle|\, \delta \underline{\mathbf{N}}(t) \right\rangle dt = \left\langle \underline{\mathbf{N}}^*(t_{i+1}^-) \mid \delta \underline{\mathbf{N}}(t_{i+1}^-) \right\rangle - \left\langle \underline{\mathbf{N}}^*(t_i^+) \mid \delta \underline{\mathbf{N}}(t_i^+) \right\rangle$$

$$+ \int_{t_i}^{t_{i+1}} \left\langle \delta \underline{\mathbf{N}}(t) \,\middle|\, \hat{\sigma}^T \, \Phi_i \psi_i + \hat{\mathbf{D}}^T + \frac{\partial}{\partial t} \,\middle|\, \underline{\mathbf{N}}^*(t) \right\rangle dt \tag{4.35}$$

Hence, all *integral* terms in the summation for $\delta \Re[\delta \underline{\mathbf{N}}(t)]$ will vanish if the following

71

adjoint transmutation equation is satisfied during the time intervals $[t_i,t_{i+1}]$, $i=0,...,T-1$:

$$\left(\hat{\sigma}^T \Phi_i \underline{\Psi}_i + \hat{D}^T + \frac{\partial}{\partial t} \right) \underline{N}^*(t) + \frac{\partial}{\partial \underline{N}(t)} \left\{ N_{J,q}(t_T^-) \right\} = \underline{0} \tag{4.36}$$

which reduces the expression for the differential of $\Re$ to :

$$\delta \Re[\delta \underline{N}(t)] = \sum_{i=0}^{T-1} \left\{ - \left\langle \underline{N}^*(t_{i+1}^-) \mid \delta \underline{N}^*(t_{i+1}^-) \right\rangle + \left\langle \underline{N}^*(t_i^+) \mid \delta \underline{N}(t_i^+) \right\rangle \right.$$

$$\left. - \left\langle \Gamma_i^* \left| \frac{\partial L_i}{\partial \underline{N}_i} - \lambda_i \frac{\partial F_i}{\partial \underline{N}_i} \right| \Psi_i \right\rangle \cdot \delta \underline{N}(t_i^+) - w_f P_i^* \Phi_i \left\langle \Psi_i \left| \frac{\partial \Sigma_{F,i}}{\partial \underline{N}_i} \right\rangle \cdot \delta \underline{N}(t_i^+) \right\} \tag{4.37}$$

We point out that

$$\frac{\partial}{\partial \underline{N}(t)} \left\{ N_J(t_T^-) \right\} = \underline{\delta}_{Jq} \delta^-(t-t_T) \tag{4.38}$$

with the delta function $\delta^-(t)$ defined as

$$\delta^-(t) = \lim_{\Delta \downarrow 0} \left\{ \begin{array}{ll} \Delta^{-1} \; , & -\Delta < t < 0 \\ 0 \; , & \text{otherwise} \end{array} \right. \tag{4.39}$$

and the elements of the Kronecker delta-object $\underline{\delta}_{Jq}$ defined by :

$$\left[\underline{\delta}_{Jq} \right]_{ij} = \left\{ \begin{array}{ll} 1 & \text{if } i=J \text{ and } j=q \\ 0 & \text{otherwise} \end{array} \right. \tag{4.40}$$

Development of the summation gives :

$$\delta \Re[\delta \underline{N}(t)] = \underline{N}^*(t_0^+) - \left\langle \Gamma_0^* \left| \frac{\partial L_0}{\partial \underline{N}_0} - \lambda_0 \frac{\partial F_0}{\partial \underline{N}_0} \right| \Psi_0 \right\rangle \cdot \delta \underline{N}(t_0^+)$$

$$- P_0^* w_f \Phi_0 \left\langle \Psi_0 \left| \frac{\partial \Sigma_{F,0}}{\partial \underline{N}_0} \right\rangle \cdot \delta \underline{N}(t_0^+) + \left\{ \underline{N}^*(t_1^-) - \underline{N}^*(t_1^+) - \left\langle \Gamma_1^* \left| \frac{\partial L_1}{\partial \underline{N}_1} - \lambda_1 \frac{\partial F_1}{\partial \underline{N}_1} \right| \Psi_1 \right\rangle + \right.$$

$$\left. - P_1^* w_f \Phi_1 \left\langle \Psi_1 \left| \frac{\partial \Sigma_{F,1}}{\partial \underline{N}_1} \right\rangle \right\} \delta \underline{N}(t_1^+) + ... - \left\langle \underline{N}^*(t_T^-) \mid \delta \underline{N}(t_T^+) \right\rangle \tag{4.41}$$

For further reduction of the expression for the differential of $\Re$, most of the terms

containing the $\delta\underline{N}(t_i)$, except the ones at the boundary points $t=t_0{}^+$ and $t=t_T{}^-$, can be forced to vanish if the adjoint nuclide densities are allowed to be *discontinuous* at the time boundaries t_i :

$$\underline{N}^*(t_i^-) = \underline{N}^*(t_i^+) - \left\langle \underline{\Gamma}_i^* \left| \frac{\partial L_i}{\partial \underline{N}_i} - \lambda_i \frac{\partial F_i}{\partial \underline{N}_i} \right| \Psi_i \right\rangle - P_i^* w_f \Phi_i \left\langle \Psi_i \left| \frac{\partial \Sigma_{F,i}}{\partial \underline{N}_i} \right. \right\rangle \qquad (4.42)$$

The last term can be forced to vanish by simply demanding that :

$$\underline{N}_I^*(t_T) = \underline{0} \quad \text{for all I} \qquad (4.43)$$

The presence of the delta time function in the source term of Eq.(4.38) basically sets the final time boundary condition for $\underline{N}^*(t)$:

$$\underline{N}^*(t_T^-) = \underline{N}^*(t_T^+) + \lim_{\Delta \downarrow 0} \int_{t_T^+}^{t_T - \Delta} \left[\frac{\partial}{\partial t} \underline{N}(t) \right] dt$$

$$= \underline{0} + \lim_{\Delta \downarrow 0} \int_{t_T^+}^{t_T - \Delta} \left[-\underline{\delta}_{Jq} \delta^-(t - t_T) + \hat{\sigma} \Phi_i \Psi_i + \hat{D} \right] dt = \underline{\delta}_{Jq} \qquad (4.44)$$

Thus, all integral terms in the summation vanish if the adjoint transmutation equation is satisfied,

$$\left(\hat{\sigma}^T \Phi_i \Psi_i + \hat{D}^T + \frac{\partial}{\partial t} \right) \underline{N}^*(t) = 0 \ , \ t_i \le t \le t_{i+1} \ \forall \ i \in \{0,...,T-1\} \qquad (4.45)$$

with the final time condition

$$\begin{cases} \underline{N}^*(t_T) = \underline{0} \\ \lim_{t \uparrow t_T} \underline{N}^*(t) = \underline{\delta}_{J,q} \end{cases} \qquad (4.46)$$

If the adjoint nuclide transmutation equation is satisfied, the only term remaining in the development of $\delta\Re/\delta\underline{N}_i(t)$ is the zeroth one, from which it follows that the sensitivity for variations in the initial state is given by

$$\underline{S}_I = \underline{N}_{I,0}^{*(+)} - \left\langle \underline{\Gamma}_0^* \left| \frac{\partial L_0}{\partial \underline{N}_{I,0}} - \lambda_0 \frac{\partial F_0}{\partial \underline{N}_{I,0}} \right| \Psi_0 \right\rangle - P_0^* w_f \Phi_0 \Psi_{I,0} \frac{\partial \Sigma_{F,I,0}}{\partial \underline{N}_{I,0}} \qquad (4.47)$$

$\underline{S}_I$ is the sensitivity vector that relates variations in $\underline{N}_I(t=t_0)$ to the resulting variation δA,

chosen here as δN_{Jq}. Hence, for variations in the entire system, the object S can be defined :

$$S = \left\{ \underline{S}^{(Jq)} \middle| J=1,\ldots,N \ ; \ q=1,\ldots(nn) \right\} \tag{4.48}$$

The columns of the sensitivity matrix S are the sensitivity vectors $\underline{S}_I$; the rows of S correspond to the different nuclide types considered. Thus, the prediction by first order depletion perturbation theory of the change in the functional resulting from a perturbation in $\underline{N}_I(t=t_0)$ is :

$$\delta N_{Jq} [\, \delta \underline{N}(t)\,] = \left\langle S \,\middle|\, \delta \underline{N}_0 \right\rangle = \sum_{I=1}^{N} \underline{S}_I \cdot \delta \underline{N}_{I,0} \tag{4.49}$$

This rather complex formalism provides the adjoint field equations for the quasi-static approximation. A set of adjoint equations exists that corresponds to the entire set of system equations, consisting of the nuclide transmutation equation, the flux shape equation and the power constraint equation. Additionally, it is convenient to impose further restrictions on the adjoint fields -namely, that $\underline{\Gamma}^*_i$ be orthogonal to the fission rate distribution and that $\underline{N}^*(t)$ be discontinuous at each time boundary. The adjoint field equations, listed in Eqs.(4.28), (4.30) and (4.36) are mathematically coupled, linear equations containing the unperturbed forward values for $\underline{N}(t)$, ψ_i, λ_i and Φ_i.

4.2.2. Solution of the adjoint quasi-static equations.

The practical utility of the adjoint equations, like that of the forward quasi-static equations, depends on how easily they can be solved numerically. It turns out that the calculational flow for solving the adjoint equations is quite similar to that for the forward solution, except that it proceeds *backward* in time. As is shown in Eq.(4.31), the flux adjoint source Q_i^* at t_i depends on an integral of $\underline{N}^*(t)$ over the *future* time interval $[t_i,t_{i+1}]$. Further, the final value of $\underline{N}$ at the end of each time interval is fixed by the "jump" condition (Eq.(4.42)). Its magnitude depends not only on the future behaviour of $\underline{N}$ but also on $\underline{\Gamma}^*$ and P^* at the final time of the interval. Thus, the adjoint equations have to be solved backward in time. For solving the adjoint equations, the flow chart as proposed by Williams [Williams 1979], shown in Fig.4.3, can be implemented.

In Fig.4.4a, a very simple example is given of a local BOC nuclide density perturbation, consisting of a local increase of the ^{235}U density in the central nodes of the large PWR core. Naturally, the direct result of this is that these central nodes and their surrounding (neighbouring) nodes will have a larger power density. As the total core-integrated power is constant, this means that the power densities in the other nodes will (have to) decrease. Thus, as the burnup proceeds the ^{235}U in the central nodes will be more rapidly depleted, so that their surplus of ^{235}U will be smaller at EOC than at BOC. In the directly neighbouring nodes, in which the power density was raised as well, the more rapid depletion due to the increased power density eventually results in a lower ^{235}U density (negative peaks). In the more peripherically positioned nodes, the fuel will be less rapidly depleted with respect to the unperturbed case, with the result that the ^{235}U density in those nodes will be somewhat higher with respect to the unperturbed case. In Fig.4.4b,

the resulting EOC nuclide density perturbation is plotted. This effect can be calculated by either the computationally expensive way of repeating the neutronics- and burnup-calculations from BOC to EOC, or by the computationally cheap way of calculating the inner product $<S|\delta \underline{N}_{BOC}>$. When one considers the CPU-time required for performing many neutronics and depletion calculations, the advantage of using DPT is evident.

And, due to the more or less linear nature of the (slow) depletion processes, the quality of the first-order DPT prediction is quite good for modest perturbations. The EOC nuclide density perturbation illustrated in Fig.4.4b could be predicted with DPT featuring an accuracy of 6 % in the predicted change.
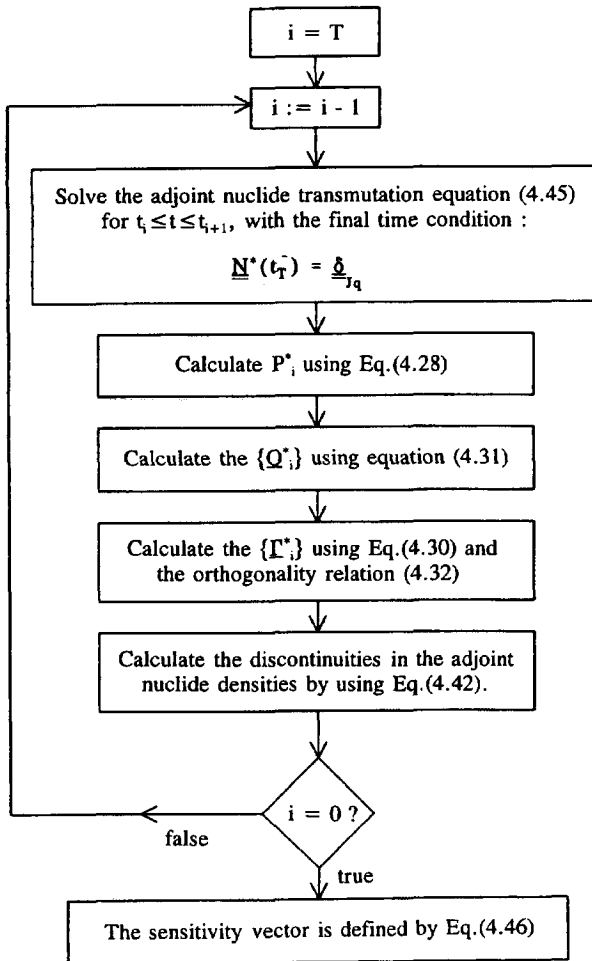

Fig.4.4
William's backward algorithm for solving the adjoint equations
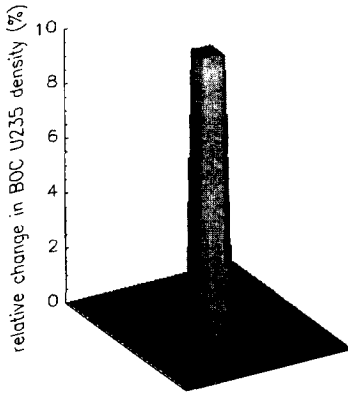
Fig.4.4a

A local BOC nuclide density perturbation consisting of a local increase of the ^{235}U concentration in the central nodes, plotted in percentage change with respect to the ^{235}U concentration in fresh fuel.
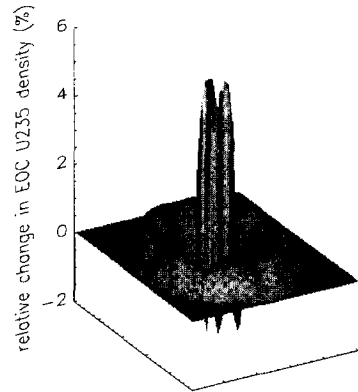
Fig.4.4b

Spatial EOC ^{235}U density perturbation due to the BOC nuclide density perturbation illustrated in Fig.4.3a, plotted in percentage change with respect to the ^{235}U concentration in fresh fuel.

References

[Gandini 1975] A. Gandini, "Time-Dependent Generalized Perturbation Theory for Burn-up Analysis", CNEN RT/FI(75) 4, Comit. Nazionale per l'Energia Nucl., Rome (1975).

[Maldonado 1995] G.I. Maldonado, P.J. Turinsky, D.J. Kropaczek, "Employing Nodal Generalized Perturbation Theory for the Minimization of Feed Enrichment during Pressurized Water Reactor In-Core Nuclear Fuel Management Optimization", Nuclear Science and Engineering 121, 312-325 (1995).

[Moore 1997] B.R. Moore, P.J. Turinsky, "Analysis of Higher Order Generalized Perturbation Theory for BWR Fuel Management Optimization", proceedings Advances in Nuclear Fuel Management-II conference 15.33-41, Myrtle Beach, USA (1997).

[Pomraning 1967] G. Pomraning, Journal of Mathematical Physics, 8, 149 (1967).

[Van Geemert 1997] R. van Geemert, A.J. Quist, J.E. Hoogenboom, "Application of Depletion Perturbation Theory and Sensitivity Analysis for Minimizing the Required Feed Enrichment for an Equilibrium Cycle", proceedings Advances in Nuclear Fuel Management-II conference 15.1-10, Myrtle Beach, USA (1997).

[Van Geemert 1998] R. van Geemert, J.E. Hoogenboom, A.J. Quist, "In-Core Fuel Management Optimization by incorporation of a Generalized Perturbation Theoretical Approach in a Heuristic Search Procedure", proceedings PHYSOR98 conferentie, V1.91-101, Long Island, USA (1998).

[Williams 1979] M.L. Williams, "Development of Depletion Perturbation Theory for Coupled Neutron/Nuclide Fields", Nuclear Science and Engineering 70, 20-36 (1979).

[White 1990] J.R. White, K.M. Avila, "Developing Feasible Loading Patterns Using Perturbation Theory Methods", proc. PHYSOR90 conference, Marseille, France (1990).

Chapter 5

Perturbation Theory for the Equilibrium Cycle

5.1 Development of sensitivity analysis for the cyclic mode

We recall that, as argued in section 2.3, since nuclear reactors are operated for multiple successive cycles, a reasonable way to evaluate reload patterns is to consider their performance in the case of an *equilibrium cycle*. The equilibrium cycle associated with a reload pattern is defined as the limit fuel cycle that eventually emerges after multiple successive periodic refueling with the same reload pattern. In reload pattern optimization, solution algorithms are often based on the assessment of the effects of permutations in the fuel bundle shuffling scheme, followed by acceptance decisions in which the permutation yielding the largest improvement in the objective function value (while satisfying the reactor physics constraints) is chosen to determine the next reference pattern in the search procedure. Generally, the exact value of the objective function for an equilibrium cycle can only be determined after the completion of a forward iterative procedure to obtain the equilibrium cycle solution from BOC to EOC. This implies that reload pattern optimization methods in which large numbers of different refueling schemes must be evaluated in this way are quite expensive from a computational point of view. However, it is possible to obtain sensitivity information, linking variations in the EOC nuclide density distribution to variations in the BOC nuclide density distribution, by using the variational techniques discussed in section 4.2. The availibility of this sensitivity information, in combination with the neutronics generalized perturbation theoretical iterative method discussed in section 4.2, offers the possibility of fast assessment of the effects with respect to the chosen objective of choosing modestly different reloading schemes, which results in a considerable economy of computation time.

A lot of work (see references chapter 4) has already been done in the field of applying perturbation theory to fuel management, but most of it is dedicated to non-equilibrium cycle fuel management. Yang and Downar [Yang 1989] did develop perturbation theoretical methods for the equilibrium cycle, in order to assess the effects of changes in reactor-physical parameters on the required feed enrichment or on the cycle length for a *constrained* equilibrium cycle. Constrained here means that either the feed enrichment or the cycle length are dictated by the condition that the effective multiplication factor $k_{eff}^{(uc)}$(EOC) of the uncontrolled core (without external reactivity control, such as control rods or soluble boron) at EOC is fixed at a certain value (usually unity). In their paper, either the feed enrichment is fixed, whereas the length of the equilibrium cycle is subject to this EOC condition, or vice versa.

However, for application in loading pattern optimization, it is necessary to consider changes in a more abstract equilibrium cycle parameter, which is *the reload pattern itself*. It is important to realize that, since one is studying equilibrium cycle behaviour, a change in the shuffling scheme affects the *entire* BOC fuel density distribution [Van Geemert 1997, Van Geemert 1998]. This is different from the situation in non-equilibrium cycle

optimization, in which the reload operator can be simply interpreted as a fuel assembly assigment matrix rather than as a node-to-node shuffle-and-discharge matrix ; in non-equilibrium cycle optimization, a change in the reload operator only affects the BOC fuel density field in a limited number of nodes.

In this chapter, iterative schemes are developed that offer the capability to calculate the perturbed fuel density distribution with first-order accurracy and very limited computational effort. This is basically done by using the sensitivity information obtained by application of the depletion perturbation theoretical method discussed in section 4.2 for linking the variations in the EOC nuclide density distribution to the variations in the BOC nuclide density distribution. In section 5.1.3 it will be illustrated how the combined technique mentioned above can be used in a procedure to minimize the feed enrichment subject to the EOC criticality condition $k_{eff}^{(uc)}(EOC) = 1$ while the equilibrium cycle length is kept fixed.

5.1.1 The two-point boundary condition for the forward nuclide density fields

We recall from section 2.3 that the *equilibrium cycle* is the limit fuel cycle that emerges when a specific refueling pattern is applied many times in succession, with a constant cycle length between each pair of successive reload operations. The refueling, which is applied after termination of the reactor operation cycle, consists of a discharge of the oldest fuel bundles, followed by a permutation of the remaining fuel bundles in the core, after which the remaining vacancies are filled with fresh fuel bundles that are all identical. Like in section 2.3, we define :

$$X_{IJ} = 1 \qquad \text{if the fuel bundle which has resided in node J is located in node I after reloading}$$
$$\quad 0 \qquad \text{otherwise}$$

If the fuel bundles are characterized by their nuclide density vectors $\underline{N}$, the invariance of the equilibrium cycle with respect to the reload operation can be written as :

$$\underline{N}_I(t_0^+) = \sum_{J=1}^{N} X_{IJ} \, \underline{N}_J(t_T^-) + \left(1 - \sum_{J=1}^{N} X_{IJ}\right) \underline{N}_F . \qquad (5.1)$$

with N denoting the number of fuel assembly positions, $\underline{N}_F$ the fresh fuel nuclide density vector and t_0^+ and t_T^- the times just after and before the refueling, respectively. As discussed in chapter 2, the equilibrium cycle can be determined iteratively using this invariance condition, which can be mathematically classified as a *two-point boundary condition*.

A very interesting fundamental property of the equilibrium cycle is that *any* perturbation in the reload operator X ($X \rightarrow X' = X + \delta X$), irrespective of its magnitude, will propagate itself such that basically the *entire* equilibrium operation cycle is affected. The only way to find the *exact* difference between the perturbed and the unperturbed equilibrium cycle is to repeat the equilibrium cycle iteration for the perturbed reload operator X'.

However, in the next few sections it is investigated in what way a variational approach and the use of the DPT formalism discussed in section 4.2 can help in developing a

method enabling one to rapidly predict how a reload operator perturbation will affect the equilibrium cycle.

5.1.2 An equilibrium cycle two-point boundary condition for the adjoint fields

The two-point boundary condition (5.1) is the key formula in the iterative process of obtaining the forward equilibrium cycle for a given cycle length. In equilibrium cycle sensitivity analysis, a two-point boundary condition can be defined for the time-dependent adjoint fields as well. For this, it is necessary to add the reload operation term to the nuclide transmutation equation, such that the nuclide transmutation equation for n different successive reload operations becomes :

$$\frac{\partial}{\partial t}\underline{N}_I(t) = \left(\hat{\sigma}\,\Phi(t)\,\psi_I(t) + \hat{D}\,\right)\underline{N}_I(t) +$$

$$\sum_{m=1}^{n}\left\{\sum_{J=1}^{N} X_{IJ}^{(m)}N_J(t) + \left[1 - \sum_{J=1}^{N} X_{IJ}^{(m)}\right]\underline{N}_F - \underline{N}_I(t)\right\}\delta^-(t - t_T^{(m)}) \quad (5.2)$$

with $\delta^-(t)$ defined as in Eq.(4.39). As discussed earlier, the equilibrium cycle is the limit operation cycle that emerges when a specific refueling pattern is applied many times in succession (so $X_{IJ}^{(m)} = X_{IJ}$ for all m), with a constant cycle length between each pair of successive reload operations. In order to derive the cyclic mode condition, we will for simplicity assume that the time-dependent λ-eigenvalues and the time-dependent flux- and power distributions will not be significantly different from the unperturbed ones. Thus, for the sake of temporary convenience we will omit the associated constraint equations and Lagrange multipliers $\underline{\Gamma}^*_i$, P^*_i and a_i and regard the infinitesimal change in the value of the reduced functional $\Re_{red}$ due to an infinitesimal change in the time-dependent nuclide density field of the equilibrium cycle :

$$\delta\,\Re_{red}[\delta\underline{N}(t)] = \sum_{i=0}^{T-1}\int_{t_i}^{t_{i+1}}\frac{\partial A}{\partial\underline{N}_I(t)}\cdot\delta\underline{N}_I(t)dt +$$

$$\sum_{i=0}^{T-1}\int_{t_i}^{t_{i+1}}\sum_{I=1}^{N}N^*_I(t)\cdot\left\{\left(\hat{\sigma}\,\Phi_i\,\psi_{I,i} + \hat{D} - \frac{\partial}{\partial t}\right)\delta N_I(t) + \left[\sum_{J=1}^{N}(X_{IJ} - \delta_{IJ})\delta N_J(t)\right]\delta^-(t - t_T)\right\}dt \quad (5.3)$$

We note that the second term of Eq.(5.3) can be written as

$$\sum_{i=0}^{T-1}\int_{t_i}^{t_{i+1}}\sum_{I=1}^{N}\sum_{J=1}^{N}N^*_I(t)\cdot\left\{\delta_{IJ}\left(\hat{\sigma}\,\Phi_i\,\psi_{I,i} + \hat{D} - \frac{\partial}{\partial t}\right) + (X_{IJ} - \delta_{IJ})\delta^-(t - t_T)\right\}\delta N_J(t)dt \quad (5.4)$$

Using the property

$$\left\{ \delta_{IJ} \left(\hat{\sigma} \, \Phi_i \, \Psi_{I,i} + \hat{D} - \frac{\partial}{\partial t} \right) + \left(X_{IJ} - \delta_{IJ} \right) \delta^-(t - t_T) \right\}^* =$$

$$\delta_{IJ} \left(\hat{\sigma}^T \Phi_i \, \Psi_{I,i} + \hat{D}^T + \frac{\partial}{\partial t} \right) + \left(X_{JI} - \delta_{IJ} \right) \delta^-(t_T - t) \qquad (5.5)$$

all integral terms can be shown to vanish if :

$$\frac{\partial A}{\partial N_I(t)} + \sum_{J=1}^{N} \left\{ \delta_{IJ} \left(\hat{\sigma}^T \Phi_i \, \Psi_{I,i} + \hat{D}^T + \frac{\partial}{\partial t} \right) + \left(X_{JI} - \delta_{IJ} \right) \delta^-(t - t_T) \right\} N^*_J(t) = 0 \qquad (5.6)$$

For the delta type EOC response functions, defined at $t = t_T^-$, we have :

$$\frac{\partial A}{\partial N_I(t)} = \frac{\partial A}{\partial N_I(t_T^-)} \, \delta^-(t - t_T) \qquad (5.7)$$

Hence, the adjoint nuclide transmutation equation is

$$\frac{\partial}{\partial t} N^*_I(t) = -\left(\hat{\sigma}^T \Phi_i \, \Psi_{I,i} + \hat{D}^T \right) N^*_I(t) + \left[N^*_I(t) - \sum_{J=1}^{N} X_{JI} N^*_J(t) - \frac{\partial A}{\partial N_I(t_T^-)} \right] \delta^-(t_T - t) \qquad (5.8)$$

One can see that actually this equation is the same as the forward depletion equation, but with the time running backward instead of forward. Obviously, during the subsequent 'in-cycle' intervals the adjoint equation

$$\left(\hat{\sigma}^T \Phi_i \, \Psi_{I,i} + \hat{D}^T + \frac{\partial}{\partial t} \right) N^*_I(t) = 0 \quad \text{for all } i = T-1, \ldots 0 \qquad (5.9)$$

must be satisfied. Further, one can simply derive the two-point boundary condition for the adjoint fields by straightforward integration from t_T^+ to t_T^- :

$$N^*_I(t_T^+) - N^*_I(t_T^-) \equiv \int_{t_T^+}^{t_T^-} \frac{\partial}{\partial t} N^*_I(t) \, dt = N^*_I(t_T^+) - \sum_{J=1}^{N} X_{JI} N^*_J(t_T^+) - \frac{\partial A}{\partial N_I(t_T^-)} \qquad (5.10)$$

from which the two-point boundary condition for the adjoint fields follows :

$$N^*_I(t_T^-) = \sum_{J=1}^{N} X_{JI} N^*_J(t_T^+) + \frac{\partial A}{\partial N_I(t_T^-)} \qquad (5.11)$$

If, like in section 4.2, we again focus on the choice of $N_{I',q'}(t_T^-)$ as the response quantity,

we will (again) have

$$\frac{\partial A}{\partial N_I(t)} = \underline{\delta}_{I',q'}\, \delta^-(t-t_T) \tag{5.12}$$

with the elements of the object $\underline{\delta}_{I',q'}$ defined as in Eq.(4.42), and Eq.(5.11) becomes :

$$N_I^*(t_T^-) = \sum_{J=1}^{N} X_{JI} N_J^*(t_T^+) + \delta_{II'}\underline{\delta}_{q'} \tag{5.13}$$

When the adjoint fields $\underline{N}^*(t)$ satisfy Eq.(5.13) for this case, they will indicate precisely how small perturbations in the BOC nuclide density distribution will propagate throughout the burnup process and the successive identical reload operations. The solution $\underline{N}^*(t)$ of Eq.(5.13) can be used to calculate directly how, for example, a small variation in the feed enrichment will propagate in the equilibrium cycle EOC fuel density distribution :

$$\delta\underline{N}(t_T^-) \approx \left\langle \underline{N}^*(t_T^-) \mid 1 - X \mid \delta N_F \right\rangle \tag{5.14}$$

5.1.3 Evaluating the effects of the reload operator perturbation $X \to X'$

Substracting the forward invariance condition Eq.(5.1) for the perturbed and the unperturbed case yields the difference equation

$$\delta N_I(t_0^+) = \sum_{J=1}^{N} X_{IJ}\,\delta N_J(t_T^-) + \sum_{J=1}^{N} \delta X_{IJ}\Big(N_J(t_T^-) - N_F\Big) + \sum_{J=1}^{N} \delta X_{IJ}\delta N_J(t_T^-) \tag{5.15}$$

As it turns out, major problems are encountered when trying to treat changes in the *reload operator*, $X \to X' = X + \delta X$ with cyclically solved adjoint functions. The change in the reduced response functional can be written as :

$$\delta \Re_{red} = \left\langle \underline{N}^*(t_T^-) \mid X \mid \delta\underline{N}(t_T^-) \right\rangle + \left\langle \underline{N}^*(t_T^-) \mid \delta X \mid \underline{N}(t_T^-) - \hat{1}\delta N_F \right\rangle$$

$$+ \left\langle \underline{N}^*(t_T^-) \mid \delta X \mid \delta\underline{N}(t_T^-) \right\rangle \tag{5.16}$$

The basic property that spoils the application of these adjoint fields is that, on the essentially perturbed nodal positions, the contribution to the response functional difference $\Re'-\Re$ due to the first term in Eq.(5.16), which is forced to vanish by having the $\underline{N}^*(t)$ satisfy Eq.(5.13), is *never* the most important term in the development of $\Re'-\Re$! In the flux Generalized Perturbation Theory treated in section 4.1, we had the fortunate property that, for modest perturbations, the expression $<\underline{\Gamma}^* \mid L-(\lambda F) \mid \delta\psi \mid >$ (the term that is nicely forced to vanish) is larger in magnitude than the residual term $<\underline{\Gamma}^* \mid \delta L-\delta(\lambda F) \mid \psi+\delta\psi \mid >$. Due to the discrete nature of X, this is not the case for the term $<\underline{N}^*(t_T^-) \mid X \mid \underline{N}(t_T^-)>$ with respect to $<\underline{N}^*(t_T^-) \mid \delta X \mid \underline{N}(t_T^-) - 1 N_F > + <\underline{N}^*(t_T^-) \mid \delta X \mid \underline{N}(t_T^-)>$, and therefore this 'first-order prediction' term will not reliably indicate what the real perturbation will be

like. And of course, this unfortunately also means that no setup of any converging higher-order iterative system like described in section 4.1 will be possible.

In the next section, a new approach will be presented with which one will yet be able to iteratively predict with reasonable accurracy how the equilibrium nuclide density distributions at BOC and EOC are effected by a change $X \rightarrow X' = X + \delta X$.

5.1.4 Iterative determination of the perturbed nuclide density distributions

We propose the following method for predicting the effect on the equilibrium BOC nuclide density distribution $\underline{N}(t_0^+)$ of the simultaneous change $X^{(ref)} \rightarrow X'$, $\underline{N}_F \rightarrow \underline{N}_F'$ in the reload operator and the fresh fuel composition : in order to obtain the perturbation equation we define $\underline{N}_I'(t_0^+) = \underline{N}_I(t_0^+) + \delta\underline{N}_I(t_0^+)$ as the perturbed equilibrium BOC nuclide density distribution associated with the perturbed reload operator X' and fresh fuel composition $\underline{N}_F'$. The equilibrium cycle two-point boundary condition for the perturbed situation is

$$\underline{N}_I'(t_0^+) = \sum_{J=1}^{N} X_{IJ}' \underline{N}_J'(t_T^-) + (1 - \sum_{J=1}^{N} X_{IJ}') \underline{N}_F' \quad , \tag{5.17}$$

which can also be written as :

$$\underline{N}_I(t_0^+) + \delta\underline{N}_I(t_0^+) = \sum_{J=1}^{N} X_{IJ}' [\underline{N}_J(t_T^-) + \delta\underline{N}_J(t_T^-)] + (1 - \sum_{J=1}^{N} X_{IJ}') [\underline{N}_F + \delta\underline{N}_F] \tag{5.18}$$

After substracting Eq.(5.1) from Eq.(5.18) and application of the first-order DPT approximation

$$\delta\underline{N}_J(t_T^-) = \sum_{J'=1}^{N} \left[\frac{\delta\underline{N}_J(t_T^-)}{\delta\underline{N}_{J'}(t_0^+)} \right] \delta\underline{N}_{J'}(t_0^+) \tag{5.19}$$

the following perturbation equation is obtained :

$$\delta\underline{N}_I(t_0^+) = \sum_{J=1}^{N} X_{IJ}' \left\{ \sum_{J'=1}^{N} \left[\frac{\delta\underline{N}_J(t_T^-)}{\delta\underline{N}_{J'}(t_0)} \right] \delta\underline{N}_{J'}(t_0^+) \right\}$$

$$+ \sum_{J=1}^{N} \delta X_{IJ} (\underline{N}_J(t_T^-) - \underline{N}_F) + (1 - \sum_{J=1}^{N} X_{IJ}') \delta\underline{N}_F \tag{5.20}$$

The second and third term on the right act as *source terms* for the perturbation effect. For determining the sensitivities $[\delta\underline{N}_J(t_T^-)/\delta\underline{N}_{J'}(t_0^+)]$, one can apply the DPT method described in section 4.2. Figs.5.1a,b and 5.2a,b illustrate two examples of spatial perturbations in the equilibrium cycle ^{235}U density field due to the application of an N-fold octant-symmetric permutation in the trajectory representation (Eq.(2.46)) for the large

PWR core illustrated in Fig.2.1, predicted directly by solving Eq.(5.20) and calculated exactly by repetition of the full equilibrium cycle iteration (with the changed reload pattern implemented), respectively. Figs.5.1a,b and 5.2a,b are characterized by the values N=4 and N=12, respectively.

The resemblance between the calculated spatial perturbation shapes for each N indicates that the result obtained by the computationally efficient application of sensitivity analysis complies very satisfactorily with the result obtained by the computationally expensive re-execution of the equilibrium cycle iteration. The lack of any clear visual dissimilarity between Figs.5.1a, 5.1b and Figs.5.2a, 5.2b indicates this convincingly. For the specific case shown in Figs.5.1a,b, the highest peaks were reconstructed with a 4 % relative deviation in the calculated density change, whereas the lower peaks featured deviations of not more than 8 %. For the case shown in Figs.5.2a,b, these relative deviations were 5 % and 10 %, respectively. In Figures 5.3a and 5.3b, the absolute relative change distribution divided by the maximum nodal density change is plotted for the cases shown in Figs.5.1a,b and 5.2a,b, respectively. We note here that the magnitudes of the BOC ^{235}U changes plotted in Figs.5.1a,b and 5.2a,b correspond to percentage changes of up to 30 % of the fresh fuel ^{235}U-density.

Fig.5.1a Spatial perturbation effect predicted by 'quick' solution of Eq.(5.17) for N=4.

Fig.5.1b Spatial perturbation effect predicted by re-execution of the equilibrium cycle iteration for N=4.
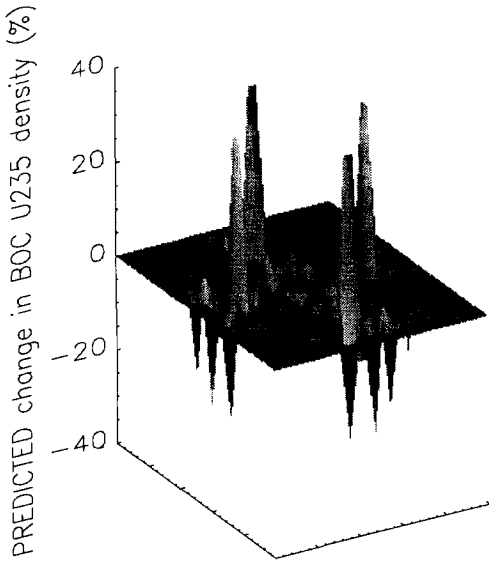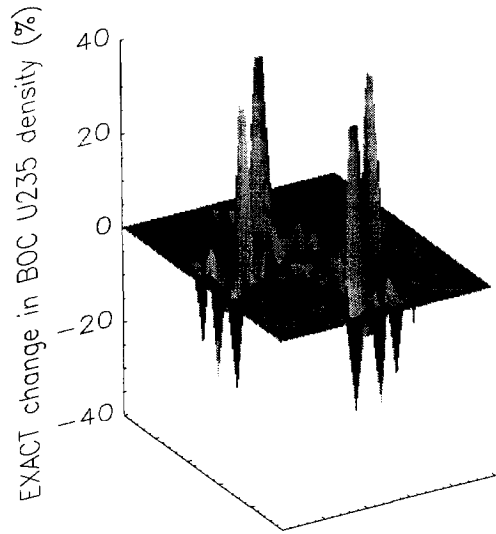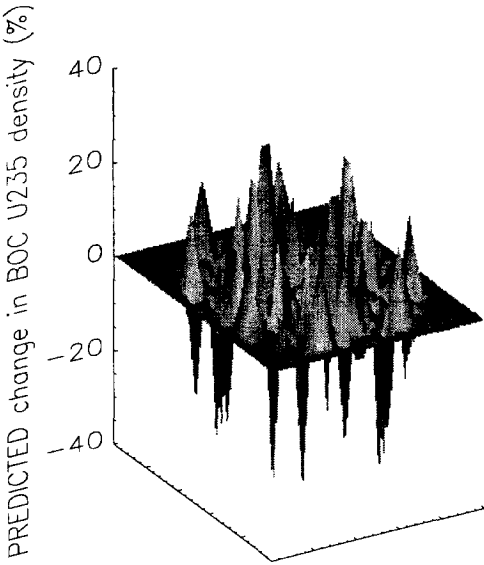
Fig.5.2a Spatial perturbation effect predicted by 'quick' solution of Eq.(5.17) for N=9.
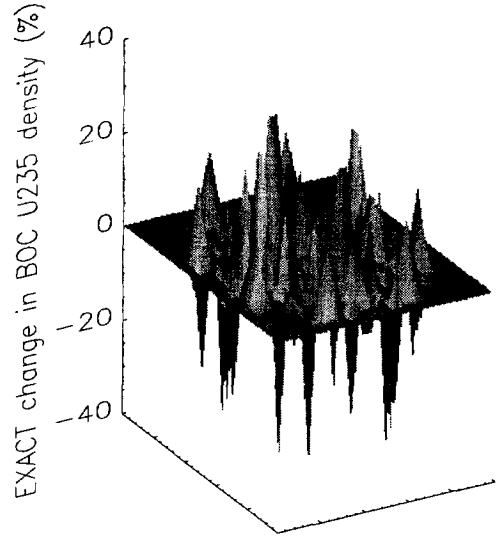
Fig.5.2b Spatial perturbation effect predicted by re-execution of the equilibrium cycle iteration for N=9.
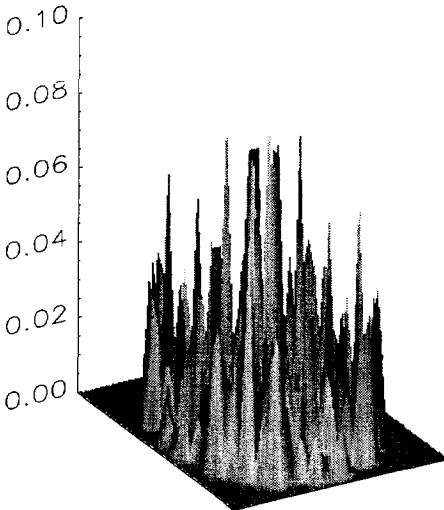

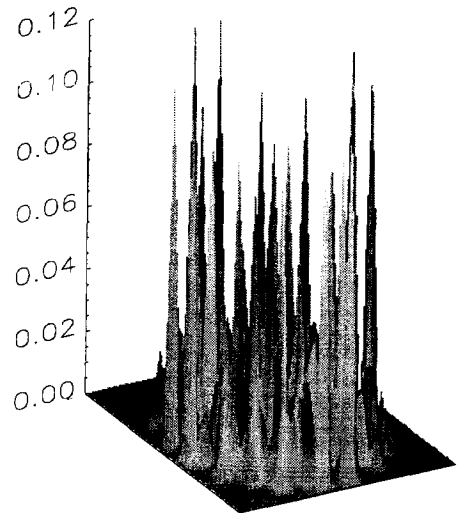Fig.5.3a Absolute relative change distribution for N=4

Fig.5.3b Absolute relative change distribution for N=9

5.1.5 Fastening the equilibrium cycle iterations

The combined system of Eq.(5.20) and Eq.(4.21) has been applied in this study for fastening the equilibrium cycle iterations. Firstly, of course, a full reference forward equilibrium cycle iteration must be done, involving solving Eq.(4.1) for several successive time steps with computationally cheap depletion calculations in between and application of reload operations at each EOC, until sufficient convergence has been achieved. After this, all the adjoint equations must be solved systematically, using the forward equilibrium cycle solution. In this way, the depletion sensitivity coefficients $[\delta \underline{N}_J(t_T^-)/\delta \underline{N}_{J'}(t_0^+)]$ to be used in Eq.(5.20) and the adjoint fields $\underline{\Gamma}^*$ to be used in Eq.(4.21) are determined. When all the sensitivity information is available, the solution of Eq.(5.20) yields a good estimate of the change in the equilibrium cycle BOC nuclide density distribution as a result of some perturbation to be assessed. Using the system (4.21), the neutronics equations for the different consecutive time steps in the perturbed situation can be solved very rapidly, with computationally cheap depletion equations in between. Basically, Eq.(5.20) simply supplies a good initial estimate for the perturbed BOC nuclide density distribution, after which *all* neutronics calculations are performed by solving the iterative system (4.21).

However, the convenient advantage of the availability of the first-order estimate $\delta^{(1)}\underline{N}_{BOC}$ for $\delta\underline{N}_{BOC}$ resulting from solving (5.20) is that one can almost directly estimate the perturbed maximal power peaking factor (PPF) of the perturbed equilibrium cycle, *without even having to perform an equilibrium cycle iteration using the fast GPT system (4.21)*. 'Almost directly' means that, based on $\delta^{(1)}\underline{N}_{BOC}$, one neutronics calculation (either with or without using Generalized Perturbation Theory) can be performed to estimate the perturbed PPF. If this perturbed PPF exceeds a certain threshold value, conservatively chosen somewhat higher than the PPF limit, further evaluation of the candidate pattern involved can be terminated, thus further saving valuable calculation time (almost 90% of the time needed for a GPT equilibrium cycle iteration). The best quality indication for the fast predictive power of applying the solution of Eq.(5.20) can be found in the good correlation between the quickly predicted perturbed PPFs and perturbed PPFs obtained by repetition of the Equilibrium Cycle iterations. This correlation is plotted in Fig.5.4. Application of the combined formalism represented by Eqs.(5.20) and (4.21) yields a considerable *reduction of the computational costs for the limit cycle iterations.* The price to be paid, of course, is that an extensive set of adjoint equations must be solved a few times during the search procedure. However, the time needed for this is in the order of only a limited number of forward reference limit cycle iterations. In the implementation described in the next section, for example, obtaining all the required adjoint field solutions takes about five minutes CPU-time on a DEC-α600 5/266. A high accuracy equilibrium cycle iteration requires about 9 seconds on the same processor, and hence a full feed enrichment iteration like described in the next section takes 9 seconds times the number of feed enrichment iterations required. In the end, in terms of the overall reduction in CPU-time requirements, the investment of solving the adjoint equations pays off easily in the case of heuristic search procedures featuring evaluations of several thousands of different candidate loading schemes. In the next sections, an example will be given of how the formalism can be implemented in a heuristic search approach as discussed in section 3.3. Further, the CPU-time savings due to the application of the perturbation theory methods discussed here will be quantified for this specific example.
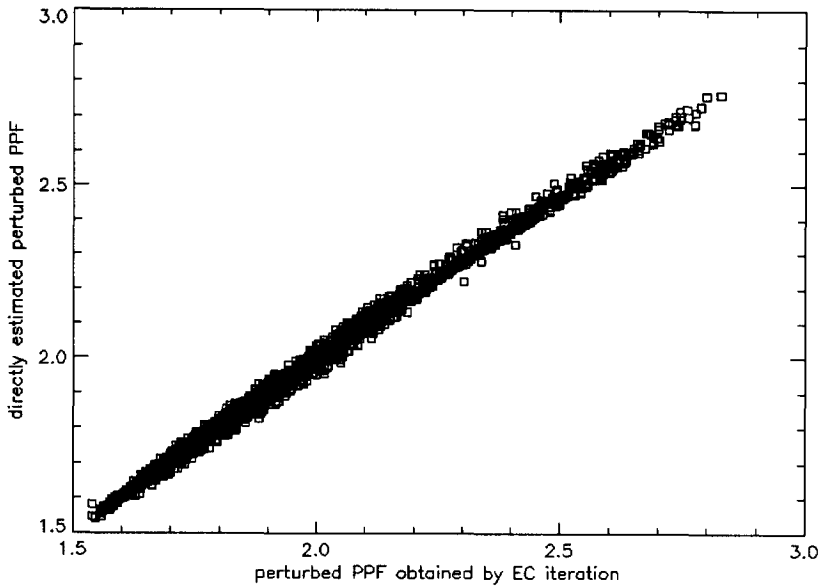
Fig.5.4 Correlation between the quickly predicted perturbed PPFs and perturbed PPFs
obtained by repetition of the Equilibrium Cycle iterations

5.2 An adjusted PMA approach

Encouraged by the fact that, in principle, successive modest reload operator perturbati-
ons may set up a trajectory in the search space leading to the best regions, it was decided
to adjust the PMA approach discussed in section 3.3 such that it will be suitable for
incorporation of the GPT method treated in section 4.1. Because of the apparent necessity
of not considering too large changes in the reload operator for the iterative system (4.21)
to converge, we adjusted this search approach somewhat. In this adjusted PMA approach,
successive populations of reload patterns are generated in search processes similar to the
one described in section 3.3.1. However, the number of random permutations involved in
generating a new candidate member of the population is constrained to an upper limit,
ensuring convergence of the iterative system (4.21), and faster cooling is applied. In this
way, GPT can be applied for fast evaluation of the new population members, in the
subspace defined by the $N \leq N_{max}$ constraint. For the case that, under this constraint, yet a
candidate be encountered yielding oscillatory divergent behaviour, an 'escape' procedure
has been added that terminates the evaluation of this specific candidate, and initiates the
generation of a new candidate in the procedure. In this particular case, one may safely
assume that the non-convergent candidate involved inherently features high power peaking
and thus would not be fully evaluated anyway. When the annealing temperature has fallen
below a certain threshold value, the best pattern obtained sofar becomes the next referen-
ce pattern for which the new adjoint fields will be calculated, the annealing temperature is

re-set to its initial value, and another constrained PMA search starts. This algorithm is successively applied until no improvement is obtained in the last constrained PMA search, which marks the end of the entire procedure.

For the large 4-batch refueled PWR core illustrated in Fig.2.1 and starting from a fixed initial, mediocre-performing reload pattern that satisfies the power peaking constraint $PPF \leq 1.8$, we have searched for the loading scheme associated with the lowest required feed enrichment (FE) subject to the power peaking constraint $PPF \leq 1.8$ and the EOC constraint $k_{eff,EOC}^{(uc)} = 1$. The adjusted PMA approach was applied, and the search results are illustrated graphically in Fig.5.5, along with a projection of a randomly generated sample on the performance plane. If the direct solution of Eq.(5.20) indicated that $PPF \geq 1.82$ for a pattern under consideration, the full evaluation of this pattern was terminated (which happened in more than half of the cases, thus further reducing the total time required for the search).

We should point out here that, since for each (fully evaluated) candidate pattern the minimal required equilibrium cycle feed enrichment (MRFE) was calculated, several limit cycle iterations had to be performed *within* a loop of iteratively determining MRFE (generally from 5 up to 9). The final search result (that is, the reload pattern corresponding to the lowest encountered MRFE subject to $PPF \leq 1.8$) is plotted in Fig.5.6. The MRFE iterations were done using the scheme :

$$FE_i := FE_{i-1} + \frac{1 - k_{eff,EOC}^{(i-1)}}{k_{eff,EOC}^{(i-1)} - k_{eff,EOC}^{(i-2)}} \left(FE_{i-1} - FE_{i-2} \right) \tag{5.21}$$

In table I, some search information is listed. The CPU-times listed are valid for the DEC-α600 5/266 processors available in our institute. We note that a significant contribution to the cumulative CPU times in the third column arise from the computational efforts invested in solving the adjoint field equations (about 400 s for each reference pattern and thus about 400 s at the start of each cooling process).

TABLE I

Listing of search information ; the CPU-times are valid for a DEC-α600 5/266.

cumulative number of cooling processes	best improved MRFE	cumulative CPU time (sec) with PT	cumul. CPU time (sec) without PT
0	2.0677 %	0	0
1	2.0572 %	859	60000
2	2.0502 %	2392	120000
3	2.0404 %	4617	180000
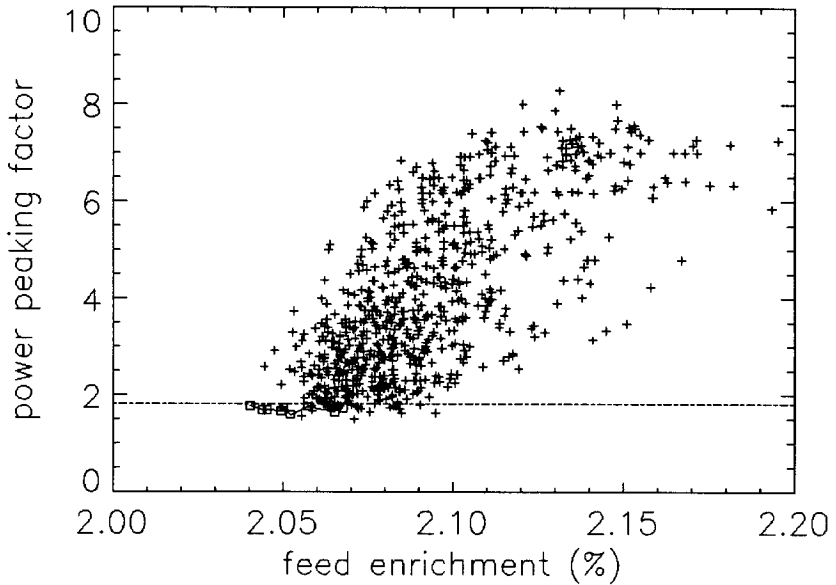
Fig.5.5 PMA search trajectory for feed enrichment for the constrained equilibrium cycle with PPF ≤ 1.8, plotted along with the projection of a collection of randomly generated patterns. The squares indicate the consequtive improvements.
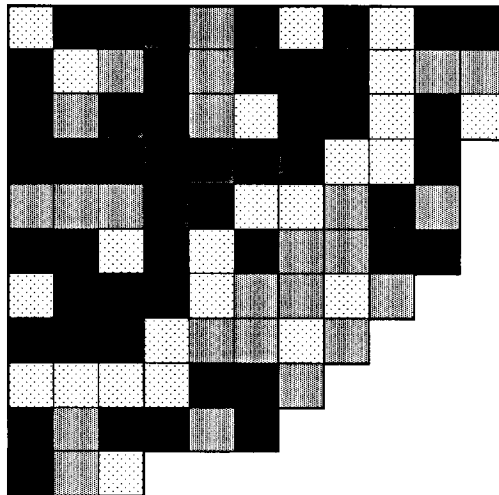
Fig.5.6 The reload pattern corresponding to the lowest encountered MRFE (subject to PPF ≤ 1.8)

5.3 Conclusions

We conclude that the perturbation methods described in chapters 3 and 4 are well applicable to heuristic equilibrium cycle optimization procedures that are based on assessing the effects of many different permutations in the loading scheme. Application of the combined formalism represented by Eqs.(5.20) and(4.21) yields a considerable reduction of the computational costs for the limit cycle iterations. The price to be paid, the necessity of solving an extensive set of adjoint equations a few times during the search procedure, is very modest if the evaluations of several thousands of candidate schemes can be significantly accelerated using the adjoint fields. The solution of Eq.(5.20), to be obtained at low computational cost, generally agrees satisfactorily with the actual perturbation in the equilibrium cycle BOC nuclide density field. Furthermore, this solution can be directly applied in a quick, one time-step GPT neutronics calculation to check if a newly considered reload scheme will satisfy the power peaking constraint, and thus to save valuable CPU-time when this is not the case.

References

[Van Geemert 1997] R. van Geemert, A.J. Quist, J.E. Hoogenboom, "Application of Depletion Perturbation Theory and Sensitivity Analysis for Minimizing the Required Feed Enrichment for an Equilibrium Cycle", proceedings "Advances in Nuclear Fuel Management-II" conference, 15.1-10, Myrtle Beach, USA (1997).

[Van Geemert 1998] R. van Geemert, J.E. Hoogenboom, A.J. Quist, "In-Core Fuel Management Optimization by Incorporation of a Generalized Perturbation Theoretical Approach in a Heuristic Search Procedure", proceedings PHYSOR98 conference, 95-105, Long Island, USA (1998).

[Yang 1989] W.S. Yang, T.J. Downar, "Depletion Perturbation Theory for the Constrained Equilibrium Cycle", Nuclear Science and Engineering 102, 365-380 (1989).
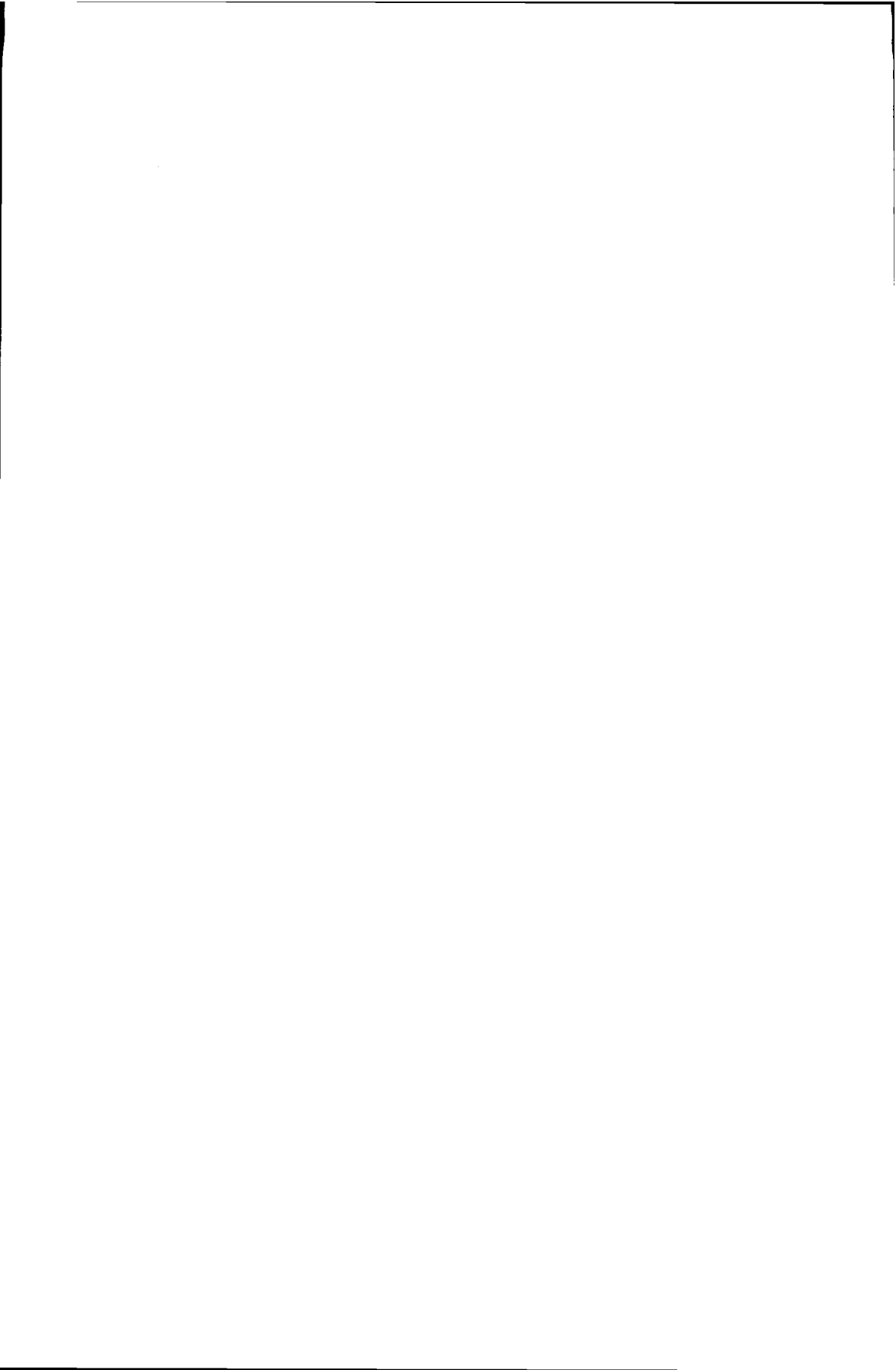
Chapter 6

Core Design Optimization by Integration of a Fast 3-D Nodal Code in a Heuristic Search Procedure

6.1. The Hoger Onderwijs Reactor

The Hoger Onderwijs Reactor (HOR) is a 2MWth pool-type research reactor situated at the Interfaculty Reactor Institute in Delft, the Netherlands. Its main purpose is to serve as a scientific facility for reactor physical experiments and to supply neutron beams for use in neutron scattering experiments and neutron activation analysis. It contains highly enriched MTR-type fuel elements, and features a core dimension of approximately 47 cm x 57 cm x 60 cm. The core grid plate has 42 positions, normally loaded with fuel elements including control elements and several reflector elements, containing Be-metal, as is indicated in Fig.6.1. The reactor is operated continuously 5 days a week. The maximum licensed excess reactivity is 6%, which requires replacement of a few elements and reshuffling at a three-month interval. We will assume here that the reshuffling operation consists of discharging one fuel element (sometimes, two fuel elements are discharged) with the highest assembly-averaged burnup, followed by a permutation of a limited number of fuel elements such that the vacancy in the core created by discharging the highly-burnt fuel element travels to a position somewhat nearer to the central region in the core, where it is filled with a fresh fuel element. An automated design tool is being developed optimizing the core loading patterns for the HOR. As a black box evaluator, the 3-D nodal code SILWER, which up to now has been used only for evaluation of pre-determined core designs, is integrated in the core optimization procedure. SILWER [Paratte 1996] is a part of PSI's ELCOS computer code package and features optional additional thermal-hydraulic, control rods and xenon poisoning calculations. This allows for fast and accurate evaluation of different core designs during the optimization search. Special attention is paid to handling the input- and outputfiles for SILWER such that no adjustment of the code itself is required for its integration in the optimization programme. In this chapter, the optimization objective, the safety and operation constraints, as well as the optimization procedure, are discussed.

6.1.1 Optimization objective and constraints for the HOR

In this study, we are interested in optimizing the trajectory along which the fuel element vacancy travels to a position near or in the central region, and find the loading scheme associated with the highest allowable value of the effective multiplication factor of the uncontrolled core $k_{eff}^{(uc)}(BOC)$ (that is, the core with all control rods fully withdrawn) at Begin-Of-Cycle. Successive maximization of $k_{eff}^{(uc)}(BOC)$ for each forthcoming cycle may lead to longer cycle lengths, or to a smaller multi-cycle-averaged number of fresh fuel assemblies to be fed into the core. The *safety constraints* are the maximum core reactivity constraint, the shutdown margin constraint and the power peaking constraint. The maxi-
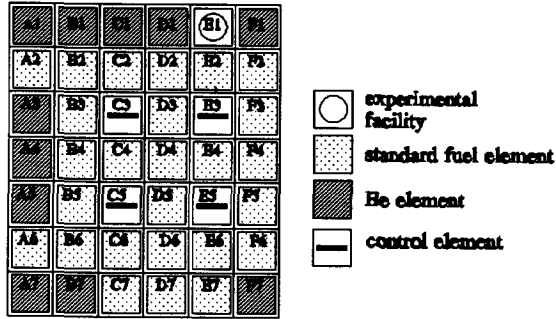
Fig.6.1 Schematic view of the HOR core

mum core reactivity constraint dictates that $k_{eff}^{(uc)}$(BOC) at Begin-Of-Cycle should remain below 1.06. The shutdown margin constraint requires that it should at all times be possible to shut the reactor down by inserting the two control rods with the least reactivity worth, with the other two rods fully withdrawn. This last mentioned constraint usually requires that a fresh fuel element be placed in the vicinity of a control rod. The power peaking constraint (defined in section 2.4) can be derived from thermal-hydraulic analysis. The *operation constraints* are first of all related to a target cycle length of about three months, which requires a minimum core reactivity at BOC. There is also a constraint on $k_{eff}^{(uc)}$(EOC), which should be larger than 1.03 for compensating the equilibrium xenon poisoning effect, the temperature effect, and the short-lived fission product buildup effect.

6.2. SILWER : A Fast 3-D Nodal Diffusion Code

The heart of the automated design procedure consists of the fast 3-D nodal code SILWER, which is a part of the LWR core analysis code system ELCOS [Paratte 1996] of PSI (Paul Scherrer Institute, Villigen, Switzerland). As is generally known, nodal codes are powerful tools for full core (three-dimensional) reactor calculations such as criticality, burnup, etc. In ELCOS the modules CORCOD and SILWER are used for nodal calculations. CORCOD computes interpolation coefficients based on few-group homogenised macroscopic cross sections prepared by the cell code SCALE. A set of subroutines called SSLINK (SCALE_SILWER_LINK) [Leege 1997] has been developed to extend the capabilities of the SCALE code system with the nodal method used in SILWER. These macroscopic cross sections are generated for several independent state variables, which can be : power density, burnup, water density, water temperature, fuel temperature, etc. The data stored for each group comprise homogenized macroscopic cross sections (total scattering, absorption, production and fission) as well as the fission spectrum, flux, neutron mean velocities and the microscopic absorption cross section of ^{135}Xe. The fit coefficients, the degrees of approximation and the interpolation coefficients are stored as

92

well. The output file of CORCOD is produced once, and can be read by the SILWER code. SILWER simulates the reactor core in steady state operation by three-dimensional neutronic and thermal hydraulic calculations. Two different nodal diffusion modules are available : one with polynomial expansion (multi-group, more than two) and the other with analytical solutions (two-group) of the diffusion equation in each node. The multi-group method is important for small reactor cores with high leakage where a two-group treatment is not sufficient. The HOR research reactor in Delft is a typical example of such a small high leakage core for which the module based on polynomial expansion should be used. In the multi-group picture, a five-group approach was adopted.

6.2.1 The Automated Design Procedure

The optimization control structure is shown in Fig.6.2. The heuristic optimization shell consists of a number of separate modules which can be used to set up a multiple cyclic interchange [Van Geemert 1997] search procedure. Core configurations to be evaluated are stored compactly and can be read by the module SINFIG (Silwer Input File Generator) which then produces an input file to be read by SILWER. The files containing the core configurations also contain data indicating what type of core calculation is to be performed by SILWER.
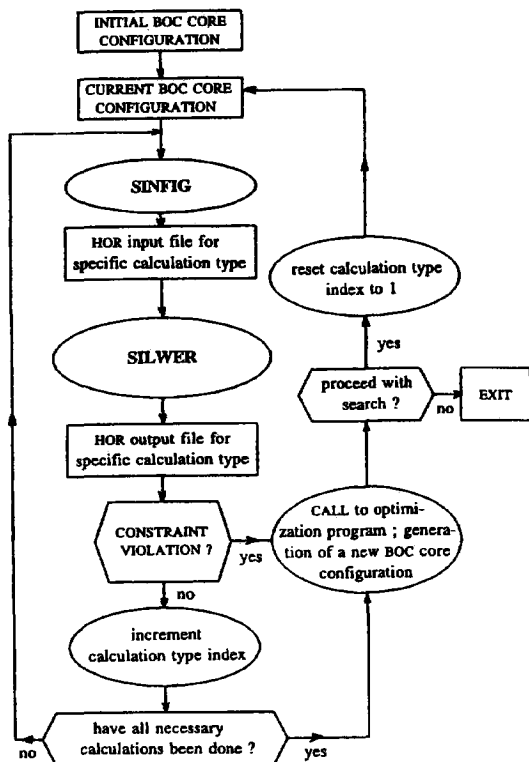
Fig.6.2 The optimization control structure.

93

Basically, 5 different types of calculations can be distinguished which are relevant for the optimization process :

1   The BOC 'clean core' calculation in which the effective multiplication factor of the clean core is calculated, in order to check whether the BOC reactivity constraint is satisfied. 'Clean core' means : zero power level, no xenon or short-lived fission products present, and all control rods withdrawn.

2   Six different rod drop calculations in which all six different combinations of two out of four control rods are fully inserted in the core with the other two rods fully withdrawn, in order to check if for each of the six cases the shutdown margin constraint is satisfied.

3   The criticality search calculation in which the uniform critical depth of the control rods is determined (in the 2 MWth operational mode), yielding the nodal power distribution and the power peaking factor, in order to check if the power peaking constraint is satisfied.

4   The burnup calculation at a 2MWth power level, performed in a number of time steps and aimed at calculating the EOC configuration of the core.

5   The EOC 'clean core' calculation in which the effective multiplication factor of the clean core is calculated, in order to check whether the EOC reactivity constraint is satisfied.

Naturally, if during the course of performing these calculations it turns out that for a specific core configuration one of the constraints is violated, the evaluation of this specific pattern is immediately terminated. This is realized by the program COVIMO (Constraint Violation Monitor). The objective considered by us is to maximize $k_{eff}^{(uc)}(BOC)$ subject to the different safety and operational constraints. If $k_{eff}^{(uc)}(BOC)$ is maximal, the operation cycle length is maximal as well, which guarantees maximal discharge burnup of the fuel elements to be removed from the core.

6.3 Results

From the results obtained by us it turns out that, if one wishes to realize the target cycle length of three months, it seems indeed absolutely necessary to implement a center-to-outside loading. The constraints imposed by the physics of the problem appear in fact to leave very little space for combinatorial freedom in adjusting the core configuration. This is why a number of engineering constraints have been programmed which force the core configuration to be evaluated not to differ too much from a reference core configuration which was found to satisfy all operational and safety constraints. Within the constrained candidate space defined by these engineering constraints, a more local search could be performed in order to investigate whether better core configurations can be found. In Fig.6.4, it is indicated that, when no engineering constraints are used, the probability of

94

encountering worse patterns due to random permutations is much higher than the probability of finding improved patterns. In the right, dense part of the cloud in Fig.6.4, the results encountered in a pairwise interchange optimization (PIO) search [Van Geemert 1996] performed in this constrained candidate space are shown. The PIO procedure indeed manages to find a slightly better core configuration in terms of the objective function than the reference core configuration that was used in actual practice. In Figs.6.3a and 6.3b, both the reference core configuration and the improved core configuration are shown. The different burnup levels of the fuel elements are ordered in terms of raking numbers, starting with low burnup (1) up to the highest burnup (26). We note that the fuel elements in the control positions R1-4 were kept fixed.

			◯		
26	20	6	13	19	18
	21	R1	5	R2	12
	14	3	1	2	10
	15	R3	4	R4	17
25	16	7	8	9	24
		22	11	23	

			◯		
26	20	6	13	19	18
	21	R1	5	R2	12
	14	3	1	2	10
	15	R3	4	R4	17
25	16	7	8	9	24
		22	11	23	

Fig.6.3a The reference core configuration   Fig.6.3b The improved core configuration
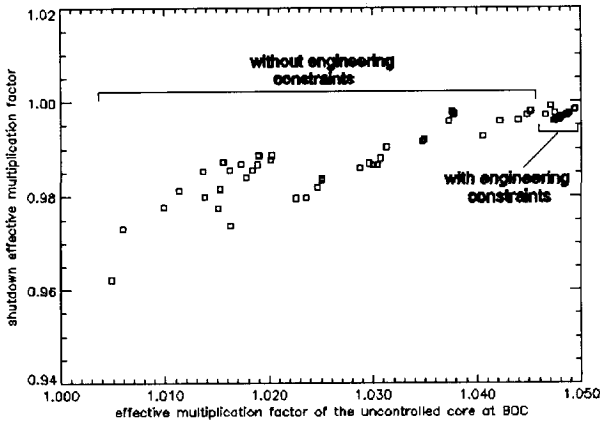
Fig. 6.4   Plot of evaluated core configurations in the perfor
mance plane spanned by the clean and shutdown
effective multiplication factors, respectively.

6.4 Conclusions

The operational and safety demands on the fuel cycle for the HOR more or less seem to dictate that a Center-to-Outside loading should be implemented, with only very limited combinatorial freedom allowed in choosing the core configuration. In spite of this, it has turned out to be possible to find a slightly better core configuration by using a heuristic search procedure than by application of a trial-and-error method. To this end, an automated design tool has been constructed in which the validated PSI nodal code SILWER is embedded as a black box simulator in a simple heuristic optimization shell. At IRI, the option is studied to condition the modular programs such that it will become possible to apply the optimization procedure in the design of future transitional cores containing both HEU (High-Enriched Uranium) and LEU (Low-Enriched Uranium) fuel elements, for which the optimization studies may be expected to yield more improvement.

References

[Paratte 1996] J.M. Paratte et al., ELCOS the PSI Code System for LWR Core Analysis, PSI Bericht Nr. 96-02, Villigen CH, January 1996.

[Leege 1997] P.F.A. de Leege, SSLINK : Linking a Nodal Code to the SCALE Code System, proceedings of the ANS Joint International Conference on Mathematical Methods and Supercomputing for Nuclear Applications, Vol.1, 220-223 (1997).

[Van Geemert 1997] R. van Geemert, A.J. Quist, J.E. Hoogenboom, H.P.M. Gibcus, Fuel Shuffling Optimization for the Delft Research Reactor, proceedings of the International Topical Meeting on Research Reactor Fuel Management, Bruges, Belgium (1997).

[Van Geemert 1996] R. van Geemert, A.J. Quist, J.E. Hoogenboom, Reload Pattern Optimization by Application of Multiple Cyclic Interchange Algorithms, proceedings of the International Conference on the Physics of Reactors, (PHYSOR'96), Mito, Japan (1996).

Chapter 7

General Conclusions and Recommendations

From a *practical* point of view, the reloading pattern optimization problem has been solved in the sense that heuristic procedures such as the ones presented or referred to in this thesis are capable of producing very good and economic reloading schemes without the necessity of inpractically large computational efforts. Perturbation theoretical techniques like described in chapters 4 and 5 can be applied for achieving considerable speed-up of the core burnup equations, thus further limiting the computational efforts or allowing for even more elaborate searches within the same computation time. In this thesis, a study is presented on how to use perturbation theory and heuristic search algorithms for optimization of *equilibrium cycles*. From the obtained results, it can be concluded that these formalisms and methods are very convenient tools in reload pattern design.

However, from a *theoretical* point of view, the reloading pattern optimization problem has *not* been adequately solved at all in the sense that no optimization method (other than the evaluation of all possibilities, which is computationally infeasible) -yet- exists which can eventually guarantee global optimality of its final result. From this theoretical point of view, it is to be feared that the reloading pattern optimization problem will never be really globally solved. As indicated in chapters 1 and 3, the main difficulty arises from the inherent property that no easily definable mathematical ordering principle exists. The purpose of such an ordering law is basically to map the solution space such that it will eventually consist of mathematically identifiable regions of approximately the same objective and constraint function values. In reload pattern optimization, both the objective and the constraint functions are known only in a very difficult, nonlinear and nonconvex form, which makes the acquisition of higher-order gradient information very difficult if not impossible. Actually, the perturbation methods discussed in chapters 4 and 5 do produce direct *first-order* derivative information. However, due to the discrete nature of the problem variable, the changes to be evaluated are far from infinitesimal, and generally much too large for their effects to be evaluated by first-order approximation only.

An approach in which first-order derivative information *is* very useful and can actually be used to guide the search process (although no global optimality of the final result can be guaranteed), is provided by the mixed-integer non-linear optimization methods [Quist 1999a] that are discussed and referred to in section 1.2.4. In this approach, the reload matrix X can be 'relaxed' (i.e. made continuous, with $0 \le X_{IJ} \le 1$ instead of $X_{IJ} = 0$ or 1) and thus subsequent small variations of the relaxed matrix can be estimated well using locally valid gradient information. Unfortunately however, the basic drawback of this methodology is that it seems limited to the use of simplified core and burnup models.

Thus, due to the fact that in heuristic search algorithms the discrete nature of the reload matrix is maintained, the first-order derivative information cannot be used to direct the search process. Although in the perturbation-theoretical framework described in section 4.1.2 of this thesis, a procedure emerges that can be applied for achieving higher-order accuracy and a considerable speed-up of the reload pattern evaluations, this can not

be used for indicating the appropriate local search direction, since this method is inherently iterative in nature. Further, generation of direct higher-order derivative information is probably extremely complicated if not impossible since more Lagrange multipliers would be needed and a larger number of coupled and (far) more complicated adjoint equations would have to be solved. In spite of this, heuristic algorithms like the ones described in this thesis have fortunately proven to be very appropriate tools for reload pattern optimization, featuring a lack of need for any gradient information, indifference with respect to the core model complexity and a high level of robustness.

It is a generally known fact that research is never really finished. Especially in computational research, it is never that difficult to come up with ideas and suggestions for improving the accuracy, efficiency and validity of computational models that have been studied. A useful (and inevitable) suggestion is to fully exploit the present-day potential of *parallel computing* for boosting the speed with which the methodology described in this thesis can be run on computers. Parallellization can be introduced in the implementations of both the heuristic search methods and the methods for solving the generalized adjoint equations in the GPT-formalism. Most of the heuristic search procedures described in this thesis can be very easily parallellized, such as the local cyclic interchange and global random chain search procedures discussed in section 3.2. Another example of an easily parallellizable optimization procedure, obviously, is the genetic algorithm [Axmann 1997]. It is interesting to note that the simulated annealing method and the PMA algorithm described in this study are inherently *sequential* optimization algorithms, as *annealing* basically boils down to generating one single Markov search chain that is supposed to eventually concentrate in one specific nearly-optimal cluster and end in the best pattern therein. Naturally, the generalized adjoint equations can be solved parallelly as well, since their number is directly proportional to the number of response (fuel) nodes in the core system.

Further, it is always possible to enhance the degree of sophistication and accuracy of a computational model to describe a system governed by the laws of physics, such as a nuclear reactor. The majority of the general computational methods described in this thesis (such as GPT) have been formulated such that they can also be applied to models featuring for example a more advanced nodal expansion approach, more energy groups, 3-D instead of 2-D calculations, a finer mesh (allowing for the consideration of *orientational degrees of freedom* in the positioning of the fuel assemblies), adding thermal hydraulics to the system equations, etc.

An interesting issue that has not been adressed in this thesis is the *burnable poison optimization problem*. Burnable poisons are materials with very high absorption cross sections that can be added to fresh, unburnt fuel assemblies in order to prevent discrepancies in the spatial power distribution and to serve as instruments for long-term reactivity control. These discrepancies can be prevented by simply designing the core configuration such that the power distribution is relatively uniform, but the use of burnable poisons is suspected to enhance the degrees of freedom in configuring the core while still satisfying the power peaking constraint. In cooperation with the Operations Research group of the Mathematics department of Delft University of Technology, some work has been done on studying whether the fuel assembly assignment problem and the burnable poison distribution optimization problem can be solved simultaneously (and thus in an integral way) [Quist 1999b]. Solution of the combined problem is complicated as the general variable

becomes a composition of a discrete quantity (the fuel assembly assignment or reload operator) and a continuously variable distribution vector indicating the concentrations of the burnable poisons in the various fuel elements. This complexity is the basic reason why in previous studies [Zavaljevski 1990] the two components of the problem have been *decoupled*. The approach adopted by the Operations Research group is based on the application of mixed-integer non-linear optimization solvers and a problem formulation in which the entire hyperspace of all state variables occurring in the system equations is treated as the solution space [Quist 1999a].

A very useful suggestion for adding an interesting search property to the stochastic optimization algorithms discussed in this thesis is to set up a *probabilistic engineering constraint approach*. In reload pattern optimization practise, the concept of engineering constraint utilization is broadly applied [Galperin 1989, Bruggink 1994, Van Geemert 1995]. Engineering constraints generally consist of knowledgde-based rules that serve to exclude some classes of reload patterns *a priori* from evaluation as candidates. As such, they are basically used to cut off a lot of combinatoric branches in setting up the search space, thus reducing the search space size and increasing the optimization convergence rate. Obviously, the formulation of reliable engineering constraints requires a lot of core design knowledge as well as some caution, since theoretically it will be possible that the set of logical rules may actually exclude patterns that should not be excluded based on their physical properties.

The idea of probabilistic engineering constraints is to allow the search process to gradually teach itself about the relation between fuel age distribution and fuel cycle performance, by simply archiving the distributions and their associated performances. For achieving this, we propose to incorporate the idea of stochastically accepting or rejecting mutated schemes based on their fuel age distributions. To this end, the following temperature dependent acceptance probability could be used :

$$P_m(T_i) = \prod_{I=1}^{N} e^{\dfrac{-\beta\, |k_{\infty,I}^{(m)} - k_{\infty,I}^{(best)}|}{N T_i^{\alpha}}} \tag{7.1}$$

relating the reactivity distribution $\{k_{\infty,I}^{(m)}, I=1,\dots,N\}$ to the distribution of the best pattern found sofar. T_i is the annealing temperature. Naturally, the probability distribution should feature a number of process parameters, indicated here with β and α, to be tuned to get optimal search characteristics. The actual implementation of the probabilistic engineering constraints by using random numbers and acceptance criteria can be done in conjunction with and analogous to the method described in section 3.3.1 of this thesis.

Obviously, one will obtain the expected behaviour of the search procedure that, at the start, no pattern will be stochastically rejected because of their fuel age distributions. As the temperature decreases further and further however, less and less patterns which are very dissimilar from the best patterns obtained sofar will be accepted as candidates. And of course, the powerful property is again that the age distribution that serves as input for the mutation can be completely different. Due to this, no undesired convergence to a fixed distribution structure associated with a local optimum will occur.

References

[Axmann 1997] J.K. Axmann, "Parallel Adaptive Evolutionary Algorithms for Pressurized Water Reactor Reload Pattern Optimizations", *Nuclear Technology* **119**, pp. 276-292 (1997).

[Bruggink 1994] J.C. Bruggink, private communication.

[Galperin 1989] A. Galperin, S. Kimhi, M. Segev, "A Knowledge-based System for Optimization of Fuel Reload Configurations", *Nuclear Science & Engineering* **102**, pp.43-53 (1989).

[Quist 1999a] A.J. Quist, R. van Geemert, J.E. Hoogenboom, T. Illés, C. Roos, T. Terlaky, "Application of Nonlinear Optimization to Reactor Core Fuel Reloading", *Annals of Nuclear Energy* **26**, 423-448 (1999).

[Quist 1999b] A.J. Quist et. al., to be published (1999).

[Van Geemert 1995] R. van Geemert, "Evaluation and Optimization of Fuel Assembly Shuffling Schemes for a Nuclear Reactor Core", IRI-131-95-016, Interfaculty Reactor Institute, Delft, 1995.

[Zavaljevski 1990] N. Zavaljevski, "A Model for Fuel Shufling and Burnable Absorbers Optimization in Low Leakage PWRs", *Annals of Nuclear Energy*, Vol.17., No.4, pp.217-220 (1990).

Appendix A

Numerical procedures for solution of the flux shape equations and determination of internodal diffusion probabilities

In this appendix, the numerical procedures utilized for solving the flux shape eigenvalue equations are briefly discussed. Further, the adjoint flux shape equation will be introduced, the solution of which plays an important role in standard perturbation theory and in solving the generalized adjoint flux shape equations discussed in chapter 4. Finally, the method used for numerical determination of the internodal diffusion probabilities for use in the kernel equation (2.39) is presented.

A.1. Numerical solution of the two-dimensional 1½-group diffusion equation for a quadrant core system

As discussed in chapter 2, the 1½-group diffusion eigenvalue equation is :

$$- \underline{\nabla} \cdot \left(D_1(\underline{r}) \underline{\nabla}\phi_1(\underline{r}) \right) + \left(\Sigma_{a1}(\underline{r}) + \Sigma_{1 \to 2}(\underline{r}) \right) \phi_1(\underline{r}) = \lambda \, \nu\Sigma_F(\underline{r}) \, \phi_1(\underline{r}) \qquad \text{(A-1)}$$

In the 1½-group diffusion approximation, the thermal flux distribution follows from $\phi_2 = \Sigma_{1 \to 2}/\Sigma_{a2}\phi_1$. This eigenvalue equation must be solved numerically for a two-dimensional quadrant core region such as the one depicted in Fig.A.1, in which each square node in the core region represents a fuel element position. Basically, each node has its own node-averaged material properties D_1, Σ_{a1}, Σ_{a2}, $\Sigma_{1 \to 2}$, $\nu\Sigma_{f1}$ and $\nu\Sigma_{f2}$ which are assumed homogeneous. It is assumed that the fuel loading, and thus the flux distribution in the system, is quadrant-symmetric. The numerical implementation adopted by us is such that each node consists of 10^2 meshpoints, so the system depicted in Fig.A.1 corresponds to a mesh field containing 130^2 meshpoints. In a two-dimensional geometry, the 1½-group diffusion lambda eigenvalue equation can be written as :
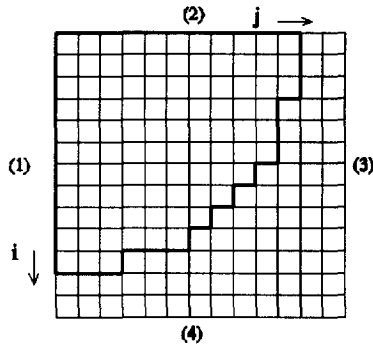
Fig.A.1 Quadrant core region

$$- D_1(x,y) \left(\frac{\partial^2 \phi_1(x,y)}{\partial x^2} + \frac{\partial^2 \phi_1(x,y)}{\partial y^2} \right) + \left(\Sigma_{a1}(x,y) + \Sigma_{1 \to 2}(x,y) \right) \phi_1(x,y)$$

$$= \lambda \ \nu \Sigma_F(x,y) \phi_1(x,y) \qquad (A-2)$$

The central difference formula can be used to approximate :

$$\left(\frac{\partial^2 \phi}{\partial x^2} \right)_{x_i, y_j} \approx \frac{\phi_{i-1,j} - 2 \phi_{i,j} + \phi_{i+1,j}}{(\Delta x)^2} \qquad (A-3)$$

$$\left(\frac{\partial^2 \phi}{\partial y^2} \right)_{x_i, y_j} \approx \frac{\phi_{i,j-1} - 2 \phi_{i,j} + \phi_{i,j+1}}{(\Delta y)^2} \qquad (A-4)$$

Using these expressions at the meshpoints (x_i, y_j), it is found that

$$- \frac{D_{1,i,j}}{(\Delta x)^2} \left[(\phi_{1,i+1,j} + \phi_{1,i-1,j}) + (\phi_{1,i,j+1} + \phi_{1,i,j-1}) \right]$$

$$+ \left[\Sigma_{a1,i,j} + \Sigma_{1-2,i,j} + 2D_{1,i,j} \left(\frac{1}{(\Delta x)^2} + \frac{1}{(\Delta y)^2} \right) \right] \phi_{1,i,j}$$

$$= \lambda \ \nu \Sigma_{F,i,j} \phi_{1,i,j} \qquad (A-5)$$

For boundaries (3) and (4) the following boundary conditions must be obeyed :

$$\phi_{i,N} = 0 \ , \quad \phi_{N,j} = 0 \ , \qquad (A-6)$$

and for boundaries (1) and (2) the 'reflected' boundary conditions must be implemented :

$$\phi_{1,j} = \phi_{2,j} \ , \quad \phi_{i,1} = \phi_{i,2} \qquad (A-7)$$

In the two-dimensional mesh, the mesh points (i,j) can be labelled as : $(i,j) \rightarrow k(i,j)$ with $k(i,j) = i + (j-1) \cdot N_{mesh}$, with N_{mesh} the number of meshpoints in the x- and y-direction (in our case, $N_{mesh} = 130$). Eventually, the system of equations can be written in matrix form as :

$$(L - \lambda F) \cdot \phi = 0 \qquad (A-8)$$

This eigenvalue equation features a large number of eigenvalues λ_n and corresponding eigenvectors or "modes" ϕ_n. Thus, basically, the diffusion eigenvalue equation should be written as :

$$(\mathbf{L} - \lambda_n \mathbf{F}) \cdot \underline{\phi}_n = \underline{0} \tag{A-9}$$

The eigenvalues are ordered such that $|\lambda_0| \leq |\lambda_1| \leq |\lambda_2| \leq |\lambda_3| \leq \ldots$. For the purpose of the work described in this thesis, we focus on how to obtain the fundamental mode, which is the mode corresponding to the smallest eigenvalue λ_0. We note here that, physically, $\lambda_0 = 1/k_{eff}$, with k_{eff} the effective multiplication factor of the system. We also stress beforehand the fact that all the different modes are orthogonal, i.e. $<\underline{\phi}_n | \underline{\phi}_m> = 0$ if $n \neq m$. In the finite difference picture, the inner product $<\underline{\phi}_n | \underline{\phi}_m>$ is defined as :

$$\left\langle \underline{\phi}_n | \underline{\phi}_m \right\rangle = \sum_i \sum_j \phi_{ij}^{(n)} \phi_{ij}^{(m)} \tag{A-10}$$

The iterative procedure is generally started with an initial "guess" for the spatial neutron flux distribution $\underline{\phi}_0^{(trial)}$. This "guess" will usually not equal the fundamental spatial mode $\underline{\phi}_0$ and, therefore, $\underline{\phi}_0^{(trial)}$ can theoretically be approximated retrospectively as a weighted sum of all spatial modes. Especially for large dimensions of $\mathbf{A}$, $\mathbf{F}$ and $\underline{\phi}$, such as is the case here $(\dim\{\mathbf{A}\} = 130^4, \dim\{\mathbf{F}\} = 130^4$ and $\dim\{\underline{\phi}\} = 130^2)$, this theoretical series expansion will almost perfectly match $\underline{\phi}_0^{(trial)}$:

$$\underline{\phi}_0^{(trial)} = \sum_{i=0}^{\infty} c_i \underline{\phi}_i \tag{A-11}$$

In solving the eigenvalue equation iteratively, obtaining the fundamental solution corresponding to the smallest value of λ (and, thus, the largest value of k_{eff}), the physical picture of simulating the nuclear chain reaction is adopted. In this method, successive neutron flux "generations" are calculated from their preceding generations, and the total neutron flux generations are kept stationary in an artificial way, by stepwise renormalisation of the total core power level. This implies that a distinction can be made between 'inner' and 'outer' iterations. In the inner iterative procedure, the solution is found of the equation

$$\mathbf{L} \cdot \underline{\phi}_0^{(m+1)} = \mathbf{F} \cdot \underline{\phi}_0^{(m)} \tag{A-12}$$

with $\underline{\phi}_0^{(m+1)}$ the neutron flux 'generation' succeeding $\underline{\phi}_0^{(m)}$. In order to solve this equation, one must realize that $\mathbf{F}$ is a diagonal matrix, but $\mathbf{L}$ is not. However, $\mathbf{L}$ can be written as the sum of its diagonal part $\mathbf{L_D}$ and non-diagonal part $\mathbf{L_{ND}}$:

$$\left(\mathbf{L_D} + \mathbf{L_{ND}}\right) \cdot \underline{\phi}_0^{(m+1)} = \mathbf{F} \cdot \underline{\phi}_0^{(m)} \tag{A-13}$$

Thus, Eq.(A-12) can be solved in the following iterative way :

$$\underline{\phi}_0^{(m+1),i+1} = \mathbf{L_D}^{-1} \cdot \left(\mathbf{F} \cdot \underline{\phi}_0^{(m)} - \mathbf{L_{ND}} \cdot \underline{\phi}_0^{(m+1),i} \right) \tag{A-14}$$

with $\underline{\phi}_0^{(m+1),i}$ the ith iterand for $\underline{\phi}_0^{(m+1)}$. This inner iteration procedure can be terminated if the convergence criterion

$$\text{abs}\left[\frac{\|\phi_0^{(m+1),i+1}\| - \|\phi_0^{(m+1),i}\|}{\|\phi_0^{(m+1),i}\|}\right] \leq \epsilon_{inner} \tag{A-15}$$

is satisfied. Subsequently, the $\phi_0^{(m+1)}$ is normalized such that the total power level constraint is obeyed :

$$\phi_0^{(m+1)} := \frac{P_{tot}}{w_f \left\langle \Sigma_F | \phi_0^{(m+1),i+1} \right\rangle} \phi_0^{(m+1),i+1} \tag{A-16}$$

Finally, it is checked if

$$\text{abs}\left[\frac{\|\phi_0^{(m+1)}\| - \|\phi_0^{(m+1)}\|}{\|\phi_0^{(m)}\|}\right] \leq \epsilon_{outer} . \tag{A-17}$$

If not, the value of m is incremented, and Eq.(A-12) is solved again until satisfactory convergence in the outer iteration procedure has been achieved. The eigenvalue λ_0 follows from

$$\lambda_0 = \frac{\left\langle \phi_0^{(m+1)} | L \phi_0^{(m+1)} \right\rangle}{\left\langle \phi_0^{(m+1)} | F \phi_0^{(m+1)} \right\rangle} \tag{A-18}$$

Several acceleration mechanisms [Duderstadt 1976] exist which can be implemented for achieving considerable speed-up of the convergence processes, for both the inner and the outer iterations. Well-known examples are the *successive overrelaxation (SOR) method* for acceleration of the inner iterations and the *source extrapolation method* for acceleration of the outer iterations, both of which have been implemented in the software developed in this study.

In analogous iterative procedures, each of the higher modes ϕ_n could be obtained by adding a filtering operation prior to each outer iteration m. In this filtering operation, all components present in $\phi_n^{(m)}$ of the modes $\phi_0, \phi_1, \phi_2, ..., \phi_{n-1}$ are removed from ϕ_n :

$$\text{Filt}\left\{\phi_n^{(m)}\right\} \to \phi_n^{(m)} - \sum_{i=0}^{n-1} c_i \phi_i \quad \text{with } c_i = \left\langle \phi_i | \phi_n^{(m)} \right\rangle \tag{A-19}$$

Thus eventually, since ϕ_n is the mode corresponding to the smallest eigenvalue λ_n of the subset $\{\lambda_n, \lambda_{n+1}, \lambda_{n+2}, ...\}$, this procedure yields ϕ_n as the dominant mode in the subset $\{\phi_n, \phi_{n+1}, \phi_{n+2}, ...\}$. Basically, the filtering procedure simply ensures that each of the outer iterates $\phi_0^{(m)}$ is orthogonal to each of the lower modes $\phi_0, \phi_1, \phi_2, ..., \phi_{n-1}$. The same procedures as described above could also be applied to obtain the eigenset $\{\lambda_n^*, \phi_n^*; n=0,1,2,...\}$ of the *adjoint* flux shape λ-eigenvalue equation :

Appendix A. Numerical procedures for solving the flux shape equations

$$\left(L^* - \lambda_n^* F^* \right) \cdot \phi_n^* = 0 \tag{A-20}$$

Generally, $\lambda_n^* = \lambda_n$. The fundamental adjoint flux shape ϕ_0^* is a very important quantity in the field of *generalized perturbation theory* (see chapter 4). The basic reason for this is the validity of a mathematical orthogonality property which can be proved in the following way : after premultiplication of Eq.(A-9) with λ_m^*, recalling the commutativity property $<\phi_m^* | L \phi_n > = <L^* \phi_m^* | \phi_n >$ and employing Eq.(A-20), we obtain

$$\lambda_m \left\langle \phi_m^* | F \phi_n \right\rangle = \lambda_n \left\langle \phi_m^* | F \phi_n \right\rangle \tag{A-21}$$

Hence, since $\lambda_n \neq \lambda_m$ if $m \neq n$, the inner product $<\phi_m^* | F \phi_n >$ should vanish for the case $m \neq n$. Thus, the validity of the property

$$\left\langle \phi_m^* | F \phi_n \right\rangle = c_n \delta_{nm} \tag{A-22}$$

has been established. The physical significance of this property is that, if some adjoint flux shape Γ^* is to be orthogonal to the fission rate distribution $F\phi_0$, it should not contain any component of ϕ_0^*, i.e., it should be orthogonal to ϕ_0^*. This is usually effected by the filtering operation

$$\Gamma^* := \Gamma^* - \frac{\left\langle \Gamma^* | F \phi_0 \right\rangle}{\left\langle \phi_0^* | F \phi_0 \right\rangle} \phi_0^* \tag{A-23}$$

Another convenient application of the fundamental adjoint flux shape is in a straightforward mathematical expression for the efficient calculation of the perturbation $\delta\lambda$ in the eigenvalue due to a perturbation in the operators L and F :

$$\delta\lambda = \frac{\left\langle \phi_0^* | \delta L - \lambda \delta F | \phi_0' \right\rangle}{\left\langle \phi_0^* | F \phi_0' \right\rangle} \tag{A-24}$$

When writing numerical procedures for solving the eigensystem, it is important to realize that the matrices L and F are very *sparse*, that is, most of the matrix elements are zero. In the case of the matrix F we are even dealing with a diagonal matrix in which all matrix elements off the diagonal are zero. In the diffusion matrix L, a meshpoint is directly coupled only with itself and (in the two-dimensional case) with its four nearest neighbours, such as indicated in Fig.2.2. Therefore, for each meshpoint (i,j) in the two-dimensional mesh, only diffusion coupling indicators are necessary. This means that the large sparse matrix L with $\dim\{L\} = 130^4$ can be compressed to the compact object $\tilde{L}$ with $\dim\{\tilde{L}\} = 130^2 \cdot 5$. The element $(L \cdot \phi)_{i,j}$ can be obtained as follows :

$$\left(L \cdot \phi \right)_{i,j} = \sum_{i',j'} L_{i,j;i',j'} \phi_{i',j'} = \tilde{L}_{i,j,1} \phi_{i-1,j} + \tilde{L}_{i,j,2} \phi_{i,j+1} + \tilde{L}_{i,j,3} \phi_{i+1,j}$$

$$+ \, \tilde{L}_{i,j,4} \, \phi_{i,j-1} \, + \, \tilde{L}_{i,j,5} \, \phi_{i,j} \tag{A-25}$$

Since the adjoint matrix $\mathbf{L}^*$ can be defined by

$$\mathbf{L}^*_{i,j;i',j'} = \mathbf{L}_{i',j';i,j} \tag{A-26}$$

the element $(\mathbf{L}^* \cdot \underline{\phi})_{i,j}$ can be obtained by application of

$$\left(\mathbf{L}^* \cdot \underline{\phi}\right)_{i,j} = \sum_{i',j'} \mathbf{L}_{i',j';i,j} \, \phi_{i',j'} = \tilde{L}_{i-1,j,3} \, \phi_{i-1,j} \, + \, \tilde{L}_{i+1,j,1} \, \phi_{i+1,j} \, + \, \tilde{L}_{i,j-1,2} \, \phi_{i,j-1}$$

$$+ \, \tilde{L}_{i,j+1,4} \, \phi_{i,j+1} \, + \, \tilde{L}_{i,j,5} \, \phi_{i,j} \tag{A-27}$$

The splendid computational power of the *kernel method* introduced in chapter 2 arises not only from the fantastic reduction of the dimensions of the system matrices, but also from the fact that, in the kernel equation, L is diagonal instead of $\mathbf{F}$, due to which *no inner iterations are needed*. The adjoint kernel equation is characterized mathematically by a simple exchange of the indices I and J with respect to the 'normal' kernel equation :

$$\Sigma_{R,I} \, \phi_I^* = \lambda \sum_{J=1}^{N} \, P_{JI} \nu \, \Sigma_{F,I} \, \phi_J^*$$

A.2   Solving the generalized adjoint flux shape equation

The equation to be solved here is

$$\left(\mathbf{L}^* - \lambda_0 \, \mathbf{F}^*\right) \cdot \underline{\Gamma}^* = \underline{Q}^* \tag{A-28}$$

with λ_0 and $\underline{Q}^*$ known (as well as, of course, $\mathbf{L}^*$ and $\mathbf{F}^*$). This equation is a fixed source equation with the peculiarity that the operator on the left side is *singular*. We hereby recall that, when the criticality calculations are based on λ-reset processes, the solution $\underline{\Gamma}^*$ of Eq.(A-28) must satisfy the orthogonality requirement

$$\left\langle \underline{\Gamma}^* \mid \mathbf{F} \, \underline{\phi}_0 \right\rangle = 0 \tag{A-29}$$

in conformity with what is argued on page 64 in chapter 4.

In developing the iterative solution procedure for the *finite difference treatment* of Eq.(A-28), we have to cope with the unfortunate property in the finite difference treatment of the adjoint diffusion operator $\mathbf{L}^*$ that it is not a diagonal matrix, and should therefore be split into its diagonal part $\mathbf{L}_D$ and non-diagonal part $\mathbf{L}_{ND}$ matrix. After writing $\mathbf{L}^*$ as the sum of its diagonal part and its non-diagonal part, Eq.(A-28) can be rewritten as :

$$\underline{\Gamma}^* = \mathbf{L}_D^{*-1} \cdot \left(\underline{Q}^* + (\lambda_0 \, \mathbf{F}^* - \mathbf{L}_{ND}) \cdot \underline{\Gamma}^*\right) \tag{A-30}$$

Thus, the iterative scheme to be adopted in case of a finite difference treatment is :

$$\Gamma_{i+1}^{*} = L_{D}^{*-1} \cdot \left(Q^{*} + (\lambda_{0} F^{*} - L_{ND}) \cdot \Gamma_{i}^{*} \right) \tag{A-31}$$

In the case of the nodal kernel approach, the operator L will be diagonal, so $L_{ND}=0$.

The orthogonality requirement (A-29), combined with the general orthogonality relation (A-22), requires that Γ^{*} has no component of the fundamental adjoint mode ϕ_{0}^{*} (in the case that the criticality calculations are based on λ-reset processes). Therefore, prior to each iterative step i, a filtering operation is to be applied in which the component of the mode ϕ_{0}^{*} is removed from Γ_{i}^{*} :

$$\text{Filt}\left\{ \Gamma_{I}^{*} \right\} \rightarrow \Gamma_{I}^{*} - c_{0} \phi_{0}^{*} \quad \text{with } c_{0} = \left\langle \phi_{0}^{*} \mid \Gamma_{I}^{*} \right\rangle \tag{A-32}$$

Naturally, the iteration can be terminated when a certain convergence criterion is satisfied, for example :

$$\text{abs}\left[\frac{\| \Gamma_{i}^{*} \| - \| \Gamma_{i-1}^{*} \|}{\| \Gamma_{i-1}^{*} \|} \right] \le \epsilon_{\Gamma} . \tag{A.33}$$

A.3   Numerical determination of the internodal diffusion kernel coupling coefficients.

As derived in chapter 2, the formal mathematical expression of the internodal coupling coefficients T_{IJ} occurring in the kernel is

$$T_{IJ} = \frac{\int_{V_{I}} \int_{V_{J}} G(r,r') \phi_{1}(r') d^{3}r' d^{3}r}{\int_{V_{I}} \phi_{1}(r') d^{3}r'} \tag{A.34}$$

with $G(r,r')$ the Green's function or kernel satisfying

$$\left[-\nabla \cdot D_{1}(r) \nabla G(r,r') + \Sigma_{a1}(r) + \Sigma_{1-2}(r) \right] G(r,r') = \delta(r-r') \tag{A-35}$$

In the nodal mesh field picture depicted in Fig.A.1, T_{IJ} can be calculated numerically as

$$T_{IJ} = \frac{\sum_{(i,j) \in I} \sum_{(k,l) \in J} G_{i,j;k,l} \phi_{kl}}{\sum_{(i,j) \in I} \phi_{ij}} \tag{A-36}$$

with the numerical kernel G_{ij} defined as the solution of

$$L \underline{G}_{i,j} = \underline{\delta}_{i,j} \tag{A-37}$$

which can be written in more numerical detail as the solution of

$$\sum_{i',j'} L_{k,l;i',j'} G_{i',j';k,l} = \delta_{k,l;i,j} = \begin{cases} 1 \ , \ (k,l) = (i,j) \\ 0 \ , \ \text{otherwise} \end{cases} \tag{A-38}$$

In the iterative solution algorithm for Eq.(A-38), we have to cope with the unfortunate property in the finite difference treatment of the adjoint diffusion operator L^* that it is not a diagonal matrix, and should therefore be split into its diagonal part L_D and non-diagonal part L_{ND} matrix. After writing L^* as the sum of its diagonal part and its non-diagonal part, Eq.(A-28) can be rewritten as :

$$\underline{G}_{ij}^{(i+1)} := L_D^{*^{-1}} \cdot \left(\underline{\delta}_{ij} - L_{ND} \cdot \underline{G}_{ij}^{(i)} \right) \tag{A-39}$$

Appendix B

A few comments on the compact inner product notations used in chapters 4 and 5

In the chapters 4 and 5, the nature of the equations, their detailed contents and the nature of the results of the defined inner products are generally not mentioned strictly or explicitly, though the surrounding text does describe what these equations and inner products represent. In this appendix, a few examples of the most important types of these equations and compact inner product notations will be treated in more detail, in order to give a more elaborate picture of their actual contents.

B.1 A few notes on the most important types of compact equations and inner product notations

For the sake of simplicity and convenience, the equations and inner products in the chapters 4 and 5, relating different vectors and matrices, have been written in a rather compact way, such that the actual contents of the various equations is not revealed or highlighted in too much detail. This serves to indicate the generality of the presented formalisms -that is, to show that the general mathematical shape of the equations is more essential than their small-scale details. Further, this helps to prevent the distracting presence of an abundant amount of summation symbols and indices in the equations and definitions. In this appendix, a few examples of the most important types of compact inner product notations adopted in chapters 4 and 5 will be mentioned and analysed in more detail.

The most important point that should be indicated here is that an *implicit product in the nuclide type space* occurs when the operators $\hat{\sigma}$ and $\hat{D}$ occur in combination with the nuclide density field $\underline{N}(t)$. A good example is Eq.(4.22) :

$$\frac{\partial}{\partial t} \underline{N}(t) = \left(\hat{\sigma} \, \Phi(t) \, \underline{\psi}(t) + \hat{D} \right) \underline{N}(t) \tag{4.22}$$

which is a compact way of writing

$$\frac{\partial}{\partial t} N_{I,q}(t) = \Phi(t) \, \underline{\psi}(t) \sum_{q'=1}^{(nn)} \left(\sigma_{qq'} + D_{qq'} \right) N_{Iq'}(t) \tag{B.1}$$

for all fuel nodes I and nuclide types q (We note that the subscript qq' serves to indicates

processes in which nuclide type q' is converted into nuclide type q). With this information it is not very difficult to write the full expression for the product $< \underline{N}^*(t) | \hat{\sigma} \psi_i \underline{N}(t) >$, appearing in Eq.(4.27) :

$$\left\langle \underline{N}^*(t) \middle| \hat{\sigma} \psi_i \underline{N}(t) \right\rangle = \sum_{I=1}^{N} \psi_{I,i} \sum_{q=1}^{(nn)} N_{I,q}(t) \sum_{q'=1}^{(nn)} \sigma_{qq'} N_{Iq'}(t) \qquad (4.27)$$

Apparently, this inner product yields a *scalar*. However, there are cases (notably when the nuclide density distribution is missing in the ket of the inner product, and the implicit product in the nuclide type space is absent) when the inner product can actually be a *vector*. For example, $< \Gamma_i^* | (\partial F_i / \partial \underline{N}_i) \psi_i >$, appearing in Eq.(4.34), can be written in more detail as

$$\left\langle \Gamma_i^* \middle| \frac{\partial F_i}{\partial \underline{N}_i} \psi_i \right\rangle = \sum_{I=1}^{N} \Gamma_{I,i}^* \sum_{J=1}^{N} \frac{\partial F_{IJ}^{(i)}}{\partial N_I^{(i)}} \psi_{J,i} = \sum_{I=1}^{N} \Gamma_{I,i}^* \sum_{J=1}^{N} \begin{pmatrix} \dfrac{\partial F_{IJ}^{(i)}}{\partial N_{1,I}} \\ \vdots \\ \vdots \\ \vdots \\ \dfrac{\partial F_{IJ}^{(i)}}{\partial N_{(nn),I}} \end{pmatrix} \psi_{J,i} \qquad (B.2)$$

In Eq.(4.34), this vector is used in an explicit product with the perturbation in the nuclide density distribution for time step i, $\delta \underline{N}_i$, in order to obtain a scalar term contributing to the scalar change $\delta \Re[\delta \underline{N}(t)]$ in the response functional value.

Nomenclature

I. List of most important symbols

$\mathbf{I}$	unity operator
$\underline{1}$	vector containing nothing but unity elements
a	Lagrange multiplier with respect to flux normalization
A	response quantity (dimension : not fixed)
$\mathbf{B}$	transmutation operator (s^{-1})
c_n	fourier coefficient corresponding to n^{th} eigenstate
$\hat{\mathbf{D}}$	decay matrix (s^{-1})
$\hat{\mathbf{D}}^T$	transposed decay matrix (s^{-1})
D_1	diffusion coefficient for the fast group (cm)
D_2	diffusion coefficient for the thermal group (cm)
D_{XY}	degree of dissimilarity for two patterns $\mathbf{X}$ and $\mathbf{Y}$
$F(x)$	general notation for a function with vector x (dimension : not fixed)
f_{lim}	power peaking factor limit
$\mathbf{F}$	neutron production matrix (cm^{-1})
$\mathbf{F}^*$	adjoint neutron production matrix (cm^{-1})
$G(\underline{r}-\underline{r}')$	diffusion kernel or Green's function (cm^{-2})
H_C	reactor core height (cm)
$H_R(i)$	reference pattern i (trajectory notation)
(I,q)	node I, nuclide type q
$\underline{J}(\underline{r})$	neutron current density ($cm^{-2}s^{-1}$)
k_I	node-averaged infinite multiplication factor of node I
k_{eff}	effective multiplication factor
k_B	Boltzmann's constant ($J\,K^{-1}$)
$\mathbf{L}$	neutron loss matrix (cm^{-1})
$\mathbf{L}^*$	adjoint neutron loss matrix (cm^{-1})
$\mathbf{L}_D$	diagonal part of neutron loss matrix (cm^{-1})
$\mathbf{L}_{ND}$	non-diagonal part of neutron loss matrix (cm^{-1})
$\mathscr{L}$	search chain length
N	number of fuel elements in the system
$N(r,t)$	space- and time-dependent nuclide density vector (cm^{-3})
$\underline{N}_F$	nuclide density vector for fresh fuel element (cm^{-3})
$\underline{N}(t)$	time-dependent nuclide density distribution (cm^{-3})
$\underline{N}^*(t)$	adjoint nuclide density distribution (dimension : not fixed)

111

Nomenclature

n	number of fuel age groups or fuel batches
(nn)	number of nuclides under consideration
N	number of fuel elements involved in a permutation
p	power peaking factor
P^*	adjoint power normalization factor (dimension : not fixed)
P(N)	probability that N fuel elements are involved in the permutation
P_I	node-averaged power density in node I (W cm^{-3})
$P^{(n)}$	n-fold permutator
P_m	probability that pattern m is selected in PMA
Q^*	adjoint source (dimension : not fixed)
$\underline{r}$	spatial position vector (cm)
r_i	ith random number
$\mathfrak{R}$	response functional (dimension : not fixed)
$\mathfrak{R}_{red}$	reduced response functional (dimension : not fixed)
S	sensitivity matrix (dimension : not fixed)
t	time (s)
Δt	duration with time interval (s)
T_i	annealing temperature for ith step of the annealing process
T_0	initial annealing temperature
T_{IJ}	coupling coefficient that couples the node-averaged neutron flux in node J to the node-averaged neutron flux in node I.
t_T^-	t : t↑t$_T$ (time moment infinitesimally prior to t$_T$) (s)
t_T^+	t : t↓t$_T$ (time moment infinitesimally after to t$_T$) (s)
U	number of possible reload operations
v_1	fast group neutron velocity (cm s^{-1})
v_2	thermal group neutron velocity (cm s^{-1})
w_f	energy released per fission (J)
X	reload operator or matrix
X_{IJ}	element of reload matrix (see definition on page 30)
z_m	objective function value associated with reload pattern m (dimension : not fixed)

Greek

α	cooling parameter
$\underline{\Gamma}^*$	generalized adjoint flux (solution of Eqs.(4.9),(4.30)) (dimension : not fixed)
γ_q	yield factor from fission for nuclide q

Nomenclature

$\delta(\underline{r}-\underline{r}')$	spatial delta function representing a unit point source at $\underline{r}'$ (cm^{-3})
$\delta^\cdot(t-t_a)$	special time delta function selecting function values at $t\uparrow t_a$ (s^{-1})
$\underline{\delta}_{Jq}$	Kronecker delta (see Eq.(4.40))
ϵ	convergence criterion
ζ_m	penalty function value associated with reload pattern m
λ	lambda eigenvalue (reciprocal of k_{eff})
λ_q	time-decay factor for nuclide q (s^{-1})
ν	neutron multiplication factor
$\hat\sigma$	microscopic absorption cross sections matrix (cm^2)
$\hat\sigma^T$	transposed microscopic absorption cross sections matrix (cm^2)
σ_{a1}	microscopic absorption cross section for the fast group (cm^2)
σ_{a2}	microscopic absorption cross section for the thermal group (cm^2)
σ_{f1}	microscopic fission cross section for the fast group (cm^2)
σ_{f2}	microscopic fission cross section for the thermal group (cm^2)
$\sigma_{1\to2}$	microscopic scattering cross section for downscattering from the fast group to the thermal group (cm^2)
Σ_{a1}	macroscopic absorption cross section for the fast group (cm^{-1})
Σ_{a2}	macroscopic absorption cross section for the thermal group (cm^{-1})
Σ_{f1}	macroscopic fission cross section for the fast group (cm^{-1})
Σ_{f2}	macroscopic fission cross section for the thermal group (cm^{-1})
$\Sigma_{1\to2}$	macroscopic scattering cross section for downscattering from the fast group to the thermal group (cm^{-1})
Φ	power normalization factor (dimension : not fixed)
$\phi(r,E,t)$	energy-, space- and time dependent neutron flux (cm^{-2}s^{-1})
ϕ_1	fast neutron flux (cm^{-2}s^{-1})
ϕ_2	thermal neutron flux (cm^{-2}s^{-1})
$\underline{\psi}$	normalized neutron flux
$\underline{\psi}^*$	adjoint flux (solution of Eq.(4.11)) (cm^{-2}s^{-1})

II. List of abbreviations

^{241}Am	Americium-241
BOC	Begin of Cycle
BP	Burnable Poison
BWR	Boiling Water Reactor
COL	Centre-to-Outside Loading
CORCOD	Correlation Code
COVIMO	Constraint Violation Monitor

CPU	Central Processing Unit
DEC	Digital Equipment Corporation (TM)
DPT	Depletion Perturbation Theory
ELCOS	Eir LWR Code System (Eir : former name of PSI)
EOC	End of Cycle
FE	Feed Enrichment
GA	Genetic Algorithms
GPT	Generalized Perturbation Theory
HEU	High-Enriched Uranium
HOR	Hoger Onderwijs Reactor
^{135}I	Iodium-135
IRI	Interfaculty Reactor Institute
LEU	Low-Enriched Uranium
LWCR	Light Water Cooled Reactor
MCHFR	Maximum Critical Heat Flux Ratio
MCPR	Maximum Critical Power Ratio
MRFE	Minimal Required Feed Enrichment
NEM	Nodal Expansion Method
OCL	Outside-to-Center Loading
PIO	Pairwise Interchange Optimization
PMA	Population Mutation Annealing
PPC	Power Peaking Constraint
PPF	Power Peaking Factor
PSI	Paul Scherrer Institute (Switzerland)
PT	Perturbation Theory
^{239}Pu	Plutonium-239
^{240}Pu	Plutonium-240
^{241}Pu	Plutonium-241
^{242}Pu	Plutonium-242
PWR	Pressurized Water Reactor
SA	Simulated Annealing
SCALE	Standardized Computer Analysis for Licensing Evaluation
SILWER	LWR Simulation Code
SINFIG	SILWER input file generator
^{149}Sm	Samarium-149
SOR	Successive Overrelaxation
SSLINK	SCALE-SILWER-LINK
^{135}Te	Tellurium-135
^{235}U	Uranium-235
^{238}U	Uranium-238

Summary

A nuclear reactor core generally consists of a population of nuclear fuel elements that can be divided into fuel age or burnup level groups. At the end of the core operation cycle (which normally lasts from 12 up to 18 months), the oldest group is discharged from the core, and the remaining fuel elements are given a new position in the core grid. After this, the remaining vacant positions are filled with new, unburnt fuel elements. This is the description of a process generally referred to as *reloading*, and a popular name for the fuel element assignment scheme is *reload pattern*. The work described in this thesis has been aimed at the development of calculational methods for optimization of reload patterns for batch-refuelled nuclear reactors.

Basically, the goal has been the methods development for an algorithm that is efficient, flexible with respect to the choice of the objective function, capable of supplying the user with a very well performing reload scheme and not requiring enormous computational efforts. In the work that has been done, two important research subjects can be distinguished :

1) The development and application of a number of heuristic search strategies capable of generating high-quality candidate patterns with limited computational effort and relatively insensitive to the lack of an easily definable mathematical ordering principle for reload patterns. These strategies generally comply with the 'Multiple Cyclic Interchange' search concept, according to which the hunt for the best reload pattern can be divided into multiple stages. The transition from the initial stage to the final stage is characterized by an increase in the degree of locality in the search procedure. The general idea is that, during the first stages, the "elite" cluster of the best candidates must be identified, after which the solution space can be sampled more and more locally in order to locate the best pattern in this cluster. The transition from 'global' to 'local' search behaviour can be either prompt, by defining strictly separated search regimes, or gradual by introducing stochastic acceptance tests.

Application of the heuristic search methods as described here allows for a *black box* approach in which gradient information is not required, and in which the system equations governing the behaviour of the reactor core system do not have to be implemented in the optimization procedure. In these search procedures, the system equations are simply isolated in an external simulator module which generally simply returns the objective function value and informs the optimization shell whether or not any reactor physics constraints are violated.

From the results obtained in this study, it can be concluded that the proposed search procedures are indeed relatively insensitive to the lack of a well-defined ordering principle for reload operators, and therefore constitute a reliable and robust method for finding high-quality reload patterns for a reactor core.

It should be noted that none of the heuristic search procedures is capable of guaranteeing global optimality and, in general, the patterns produced by these procedures are unlikely to be the global optimum. However, the results of different types of these

heuristic search procedures seem to indicate that the solution space contains elite 'families' of patterns which are all very close to one another in terms of their (top) performances, though they may be very dissimilar in terms of the fuel assignments in the core. In other words, it is suspected that the optimum is quite 'flat', due to which the (theoretically present but untrackable) global optimum is not expected to be more than only marginally superior to the best result of the heuristic search algorithms.

2) The other important part of this study has been dedicated to the development and implementation of a general higher-order perturbation theoretical formalism for realizing the availability of higher-order gradient information. Especially for large reactor cores, the use of perturbation theory is absolutely necessary if one wants to evaluate the effects of thousands of fuel element permutations within a practical calculational time frame. For fast evaluation of a new reload pattern, this pattern can be split into the original, unperturbed reference reload pattern and the perturbation in the reference pattern which yields this new pattern. A variational technique, in which Lagrange multipliers are utilized, can be applied for calculating the first-order estimate of the perturbation effect on any response quantity of interest. Explicit consideration of the higher-order terms in the development of the response functional results in a very rapidly-converging iterative scheme with which an accurate, higher-order estimate of the perturbation effect in the response quantity can be obtained within very short CPU-time. In addition, a Depletion Perturbation Theoretical (DPT) formalism has been implemented with which burnup sensitivity information can be generated for first-order accurate calculation of the change in the End-Of-Cycle nuclide density distribution due to a change in the Begin-Of-Cycle nuclide density distribution.
   In particular, it has been studied how the first-order gradient information can be utilized in fuel management optimization for the *cyclic mode* or *equilibrium cycle*. For the application of perturbation theory in equilibrium cycle reload pattern optimization, it is necessary to consider perturbations in the most abstract equilibrium cycle parameter, which is the reload pattern itself. In this, it is very important to realize that, for the cyclic mode, a permutation in the reload scheme perturbs the *entire* time-dependent nuclide density field in the core. From the mathematical reload operation invariance condition, very rapidly converging iterative schemes have been developed (incorporating the DPT sensitivity information) with which the perturbed equilibrium cycle solutions could be reconstructed very well and within relatively short CPU-time.

   Further, an automated design tool has been developed for the Hoger Onderwijs Reactor (HOR) in Delft, the Netherlands. As a black box evaluator, the 3-D nodal code SILWER, previously used only for evaluation of pre-determined core designs, was integrated in the core optimization procedure. SILWER is a part of the Swiss Paul Scherrer Institute's ELCOS package and features optional additional thermal-hydraulic, control rods and xenon poisoning calculations. This allowed for relatively fast and accurate evaluation of different core designs during the optimization search. Special attention has been paid to handling the input- and outputfiles for SILWER such that hardly any adjustment of the code itself was required for its integration in the optimization programme.

Samenvatting

Een reactorkern is in het algemeen opgebouwd uit een populatie van splijtstofelementen die verdeeld kan worden in leeftijds- ofwel opbrandgroepen. Aan het einde van de reactorbedrijfscyclus (normaliter 12 à 18 maanden) wordt de oudste groep uit de kern verwijderd, waarna de overige splijtstofelementen een nieuwe positie in het kernrooster krijgen. De dan overblijvende vacatures worden met verse, nog ongebruikte splijtstofelementen gevuld. De handeling van het (her)rangschikken wordt *herladen* genoemd, en een populaire benaming voor het splijtstofelementtoewijzingsschema is *herlaadpatroon*.

Het werk beschreven in dit proefschrift is gericht geweest op de ontwikkeling van rekenmethoden voor optimalisatie van herlaadpatronen voor lichtwaterreactoren. De te ontwikkelingen zoekalgoritmen dienden efficiënt en flexibel met betrekking tot de doelfunctiekeuze te zijn, en in staat om voor de gebruiker een zeer goed herlaadpatroon te genereren zonder daarbij van extreme rekenkracht gebruik te moeten maken. De kern van het onderzoek is te onderscheiden geweest in de volgende zwaartepunten :

1)   De ontwikkeling en toepassing van enkele alternatieve heuristische zoekstrategieën die in staat zijn binnen beperkte hoeveelheden rekentijd kandidaatpatronen van hoge kwaliteit te genereren en die relatief ongevoelig zijn voor de afwezigheid van een mathematisch definieerbaar ordeningsprincipe voor de herlaadpatronen. Het belangrijkste voorbeeld hiervan is het zogenaamde 'Multiple Cyclic Interchange' concept, waarin de jacht op het beste herlaadpatroon verdeeld kan worden gedacht in meerdere fasen. De overgang van de startfase naar de eindfase wordt gekenmerkt door een toename in de mate van lokaliteit in de zoekprocedure. Het algemene idee is dat, gedurende de eerste fasen, het "elite" cluster van beste kandidaten moet worden geïdentificeerd, waarna de oplossingsruimte steeds lokaler wordt afgezocht om in dit cluster het beste patroon te vinden. De overgang van 'globaal' zoekgedrag naar 'lokaal' zoekgedrag kan prompt zijn, door de definitie van strikt gescheiden zoekregimes, of geleidelijk door de introductie van stochastische acceptatietests.

Toepassing van de heuristische zoekalgoritmen zoals beschreven in dit proefschrift staat een *black box* benadering toe waarin gradientinformatie niet vereist is, en waarin de systeemverge- lijkingen die het gedrag van de reactorkern dicteren niet in de optimalisatie procedure geïmplementeerd hoeven worden. De systeemvergelijkingen zijn geïsoleerd in een externe simulator module die in het algemeen simpelweg de doelfunctiewaarde van het te beschouwen patroon geeft en de optimalisatie-shell informeert over eventuele schending van veiligheids- of bedrijfsconstraints. Gezien de resultaten verkregen in deze studie kan geconcludeerd worden dat de voorgestelde zoekprocedures inderdaad relatief ongevoelig zijn voor de afwezigheid van een goedgedefinieerde ordeningswetmatigheid en daarom een betrouwbare en robuuste methode representeren voor het vinden van goede herlaadpatronen.

Het moet opgemerkt worden dat geen van de heuristische zoekprocedures in staat is globale optimaliteit te garanderen and dat in het algemeen de patronen die door deze procedures worden gegenereerd worden niet het globale optimum zullen zijn. Echter de resultaten van verschillende typen zoekprocedures lijken aan te duiden dat de zoekruimte 'elite families' in zich heeft die elkaar in doelfunctiewaarde erg dicht benaderen hoewel zij, wat betreft de ruimtelijke splijtstofburnupverdeling, behoorlijk verschillend kunnen zijn. Met

andere woorden, we vermoeden dat het optimum tamelijk 'vlak' is. Hierdoor zal verwachtingsgewijs het (theoretisch aanwezige maar praktisch niet localiseerbare) globale optimum niet meer dan slechts marginaal beter zijn dan het beste resultaat van het beste zoekalgoritme.

2) Het andere belangrijke deel van het onderzoek is gericht geweest op de ontwikkeling en toepassing van een algemeen hogere-orde verstoringstheoretisch formalisme om de beschikbaar- heid van hogere-orde gradiëntinformatie te realiseren. In het bijzonder voor grote reactorkernen is het gebruik van verstoringstheorie absoluut noodzakelijk indien men de effecten van duizenden splijtstofelementpermutaties wil berekenen binnen normale rekentijdproporties. Voor snelle evaluatie van een nieuw te onderzoeken herlaadpatroon kan dit patroon worden gesplitst in het originele, onverstoorde referentiepatroon en de verstoring in het referentiepatroon die het nieuwe patroon oplevert. Een variationele techniek, waarin gebruikt wordt gemaakt van Lagrange multiplicatoren, kan dan worden toegepast voor eerste orde schatting van het effect van de verstoring op een willekeurige te beschouwen responsgrootheid. De theorie waarop de variationele techniek is gebaseerd worden in het algemeen aangeduid met *gegeneraliseerde verstoringstheorie*. Expliciete beschouwing van de hogere-orde termen in de ontwikkeling van de responsfunctionaal resulteert in een zeer snel convergerend iteratief schema met behulp waarvan een nauwkeurige, hogere-orde schatting van het verstoringseffect in de responsgrootheid kan worden verkregen binnen zeer korte rekentijd.

In het bijzonder is bekeken hoe de eerste-orde gradiëntinformatie kan worden gebruikt in fuel management optimalisatie voor de cyclische mode ofwel *evenwichtscyclus*. De evenwichtscyclus geassocieerd met een herlaadpatroon is gedefinieerd als de limiet bedrijfscyclus die uiteindelijk tevoorschijn komt na meerdere successievelijke implementaties van hetzelfde herlaadpatroon. De interesse voor de evenwichtscyclus stamt voort uit het idee dat, daar splijtstofeconomie een multicycli-aangelegenheid is, herlaadschema's het best te evalueren zijn door te kijken naar het gedrag waartoe ze aanleiding geven in het geval van een evenwichtscyclus. Voor toepassing van verstoringstheorie in evenwichtscyclusoptimalisatie is het noodzakelijk om verstoringen te beschouwen in de meest abstracte evenwichtscyclusparameter, namelijk het herlaadpatroon zelf. Hierbij is het van belang te bedenken dat een permutatie in het herlaadschema het gehele nuclidendichthedenveld in de reactorkern verstoort. Gedurende dit onderzoek zijn vanuit de mathematische herlaadoperatie-invariantieconditie met behulp van verstoringstheoretische benaderingen zeer snel convergerende iteratieve stelsels ontwikkeld waarmee de verstoorde evenwichtsoplossingen heel goed en binnen korte tijd kunnen worden gereconstrueerd.

Verder is gewerkt aan een geautomatiseerde ontwerptool voor de Hoger Onderwijs Reactor (HOR) te Delft, Nederland. Als 'black box' evaluator is de gevalideerde 3D-nodale diffusiecode SILWER toegepast. SILWER is een deel van het ELCOS pakket van het Zwitserse Paul Scherrer Instituut (PSI) en biedt opties om thermo-hydraulische, regelstaaf-en xenongifberekeningen te doen. Met SILWER kunnen relatief snelle en nauwkeurige evaluaties worden gedaan van verschillende kernontwerpen gedurende de optimalisatieprocedure. In het construeren van de ontwerptool is speciale aandacht geschonken aan het omgaan met input- en outputfiles zodanig dat de code zelf voor integratie in de optimalisatieroutine niet hoefde worden aangepast.

List of Publications

I. JOURNAL PUBLICATIONS

R. van Geemert, P.F.A. De Leege, A.J. Quist, J.E. Hoogenboom and H.P.M. Gibcus, "Research Reactor In-Core Fuel Managament Optimization by Application of Multiple Cyclic Interchange Algorithms", *Nuclear Engineering & Design* **186**, 369-377 (1998).

P.C.M. Gubbens, R. van Geemert and K.H.J. Buschow, "Magnetic Behaviour of the Quasi Ground State Doublet in TmCuAl", *Journal of Magnetism and Magnetic Materials* 177-181 (1998) 1149-1150.

A.J. Quist, R. van Geemert, J.E. Hoogenboom, T. Illés, C. Roos and T. Terlaky, "Application of Nonlinear Optimization to Reactor Core Fuel Reloading", *Annals of Nuclear Energy* **26**, 423-448 (1999).

A.J. Quist, E. de Klerk, C. Roos, T. Terlaky, R. van Geemert, J.E. Hoogenboom, T. Illés, "Finding Optimal Reactor Core Reloading Patterns using Nonlinear Optimization and Search Heuristics", accepted for publication in *Optimization Engineering*.

E.J.M. Wallerbos, R. van Geemert, "Academic Nuclear Engineering Education : The Dutch Way", *Nuclear Europe Worldscan*, Vol. XVII, no. 9-10, Sept-Oct, p. 43 (1997).

II. CONFERENCE PROCEEDINGS

R. van Geemert and J.E. Hoogenboom, "A Two-Dimensional Analytical Nodal Core Model for Use in a Reload Pattern Optimization Procedure", *Proc. of the 9th Topical Meeting*, Moscow, MEPhI, h/c "Volga", Volume 1, 197-199, September 4-8, 1995.

R. van Geemert, A.J. Quist and J.E. Hoogenboom, "Reload Pattern Optimization by Application of Multiple Cyclic Interchange Algorithms", *Proc. Inter. Conf. on the Physics of Reactors PHYSOR96*, I38-I47, Mito, Japan, 1996.

R. van Geemert, A.J. Quist and J.E. Hoogenboom, "Fuel Shuffling Optimization for the Delft Research Reactor", *Proceedings of the International Topical Meeting on Research Reactor Fuel Management*, 65-69, Bruges, Belgium, 1997.

R. van Geemert, A.J. Quist and J.E. Hoogenboom, "Application of Depletion Perturbation Theory and Sensitivity Analysis for Minimizing the Required Feed Enrichment for an Equilibrium Cycle", *Proceedings of the ANS Topical Meeting "Advances in Nuclear Fuel Management-II"*, 15.1-15.9 Myrtle Beach, USA, 1997.

R. van Geemert, P.F.A. de Leege, A.J. Quist and J.E. Hoogenboom, "Research Reactor In-Core Fuel Management by Incorporation of a 3D Nodal Diffusion Code in a Heuristic Search Procedure", *Proceedings of the International Topical Meeting on Research Reactor Fuel Management*, Bruges, 195-199, Belgium, 1998.

R. van Geemert, J.E. Hoogenboom, A.J. Quist, "Application of Higher-Order Generalized Perturbation Theory for Fast Core Calculations in Reload Pattern Optimization", *Proceedings of the Annual Meeting on Nuclear Technology 1998*, 11-14, Germany, 1998.

R. van Geemert, J.E. Hoogenboom, A.J. Quist, "In-Core Fuel Management Optimization by Incorporation of a Higher-Order Generalized Perturbation Theoretical Approach in a Heuristic Search Procedure", *Proceedings of the International Conference on the Physics of Nuclear Reactors (PHYSOR'98)*, V1.91-101, Long Island, New York (1998).

III. REPORTS

R. van Geemert, "^{169}Tm Mössbauer spectroscopy on TmCuAl", IRI-132-94-12, Interfaculty Reactor Institute, Delft, 1994.

R. van Geemert, "Evaluation and Optimization of Fuel Assembly Shuffling Schemes for a Nuclear Reactor Core", IRI-131-95-016, Interfaculty Reactor Institute, Delft, 1995.

A.J. Quist, E. de Klerk, C. Roos, T. Terlaky, R. van Geemert, J.E. Hoogenboom, T. Illés, "Finding Optimal Nuclear Reactor Core Reloading Patterns using Nonlinear Optimization and Search Heuristics", TWI-report 98-04, Delft University of Technology, 1998.

Curriculum Vitae

The author of this thesis attended high school at the 'Develsteincollege' in his home-town Zwijndrecht, where he was born on the third of August, 1971. After obtaining his VWO diploma in 1989 he started his study of Applied Physics at Delft University of Technology. He performed his graduation work in the Mössbauer spectrometry group of the Department of Radiation Physics, located in the Interfaculty Reactor Institute of Delft University of Technology. In cooperation with Dr. P.C.M. Gubbens he used the Möss-bauer spectrometry technique for investigation of the interesting hyperfine structure of the rare earth intermetallic compound TmCuAl. In addition to the experimental work he wrote a simulation program based on stochastic theory with which the temperature depen-dence in the shapes of the Mössbauer spectra could be reconstructed.

Directly after obtaining his Master of Science degree in September 1994, he started working as a PhD-student in the Nuclear Reactor Physics Department of the Interfaculty Reactor Institute, under supervision of prof.dr.ir. H. van Dam and dr.ir. J.E. Hoogen-boom. His PhD research was focussed on methods development for nuclear reactor core reload pattern optimization and resulted in this thesis. The research principally consisted of work on stochastic optimization strategies, Green's function theory, nodal core neutro-nics and depletion calculations, and the development and implementation of generalized perturbation theoretical techniques to be applied in reload pattern optimization.

Since June 1998 he is employed as a Research Associate in the Physical, Mathematical and Space Geodesy group of the Faculty of Civil Engineering and Geosciences of Delft University of Technology.
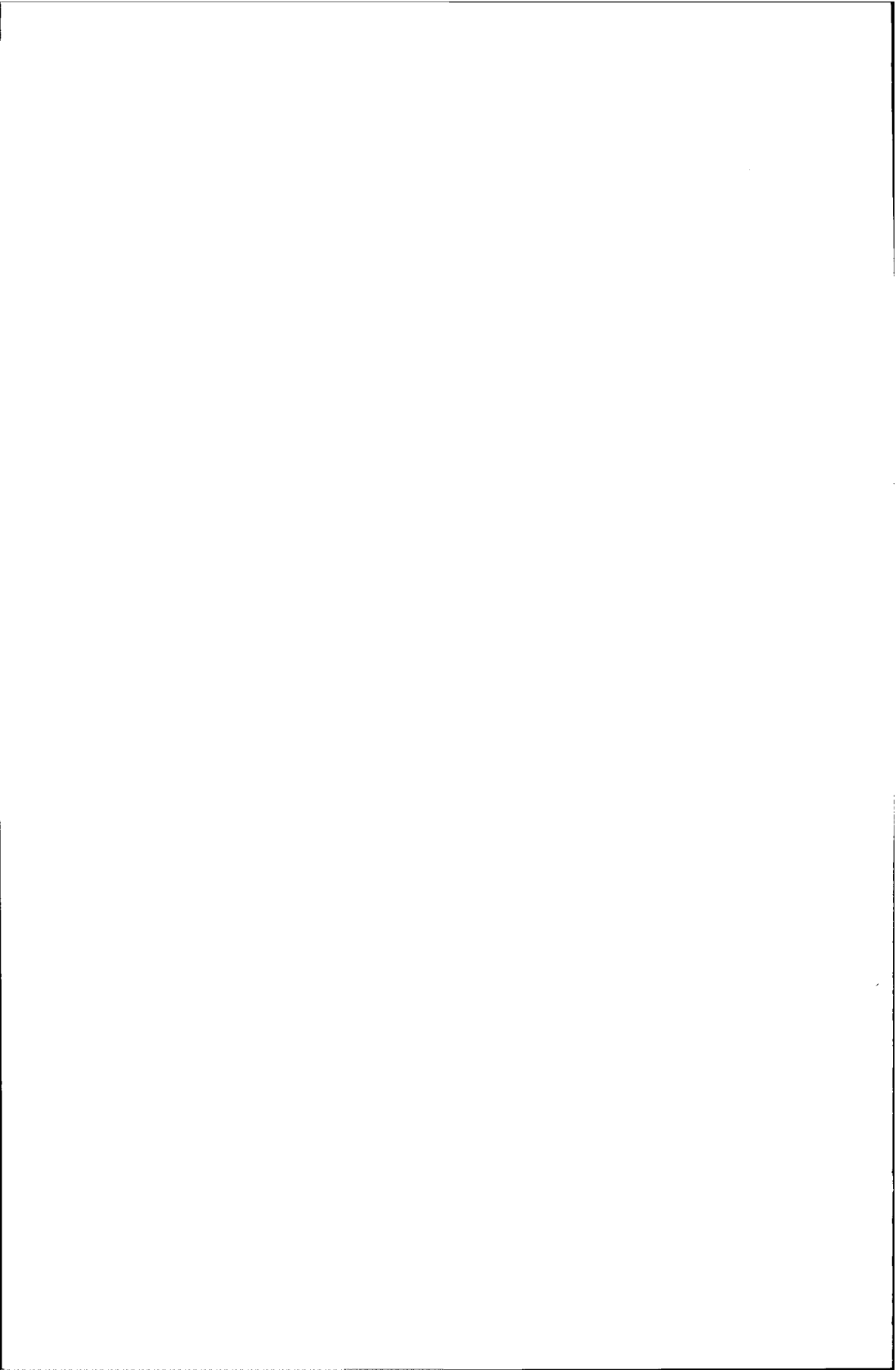
Acknowledgements

On this final page, I would like to thank all the people who in some way made a contribution to the realization of this thesis. In particular, I would like to mention :

- Prof.dr.ir. H. van Dam for the opportunity to perform the research described in this thesis and for the excellent educational program that was offered.

- Dr.ir. J.E. Hoogenboom for the solid supervision he offered to me.

- Ir. A.J. Quist, Dr. T. Terlaky, prof.dr.ir. C. Roos, dr. E. de Klerk, dr. T. Illés, ir. A.J. de Jong and dr. J. Valkó for the fruitful discussions and collaborations of the past years.

- Ir. P.F.A. de Leege and ing. A. Hersman for their numerous useful programming recommendations.

- My 'fellow barak-C inhabitants' Erik Wallerbos, David van Bragt, Todd Adams, Viktor Golovko, AnnaLisa Manera and Robert Zboray, for the nice company they offered me during the past years.

- Dr. T. Šmuc for his interest in my work and for his friendship.

Finally, I would like to use this opportunity to thank my parents for all the support and encouragements I received from them throughout the years.

René